UNIVERSITY OF CALIFORNIA SAN DIEGO

Synthesis, structure, and reactivity of μ_3-Sn capped trinuclear nickel clusters

A Dissertation submitted in partial satisfaction of the requirements
for the degree Doctor of Philosophy

in

Chemistry

by

Nicole Torquato

Committee in charge:

Professor Clifford P. Kubiak, Chair
Professor Guy Bertrand
Professor Darren J. Lipomi
Professor Valerie A. Schmidt
Professor Alina M. Schimpf

2023

The Dissertation of Nicole A. Torquato is approved, and it is acceptable in quality and form for publication on microfilm and electronically.

University of California San Diego

2023

DEDICATION

To my parents, John, and Nick.

TABLE OF CONTENTS

LIST OF FIGURES

LIST OF TABLES

LIST OF ABBREVIATIONS

dppm	bis(diphenylphosphino)methane
NMR	Nuclear Magnetic Resonance
VT	Variable Temperature
DFT	Density Functional Theory
NBO	Natural bond order
XRD	X-ray diffraction
CV	Cyclic voltammetry
NSF	National Science Foundation
CCDC	Cambridge Crystallographic Data Centre
Cp	Cyclopentadiene
Cp*	1,2,3,4,5-pentamethylcyclopentadiene
UV-Vis	Ultraviolet-visible

ACKNOWLEDGEMENTS

First and foremost, I would like to thank my advisor Cliff Kubiak for his support throughout my PhD. I am forever grateful for the freedom he gave me to pursue my own path in research, develop my own ideas, and become an independent researcher.

Next, I would like to thank my lab mates at UCSD, both past and present. Specifically, I would like to thank Thomas Chan, his friendship and support made my PhD possible. His bubbly personality, can-do attitude, and kindhearted disposition, led to a lighthearted lab atmosphere filled with laughter and positivity. I already miss being your lab mate and hope for a future where we can work together again. I want to give a special thanks for my wonderful undergraduate mentees, Quentin Bertrand and Jaden Lara. In addition, I would like to thank Liana Alves, a fellow colleague in Alina Schimpf's lab, roommate, and close friend. I will miss our movie nights, afternoon tea sessions, beach days and your famous carrot cake.

I want to give a special thanks to my PI at Sandia National Laboratories, Mitch Anstey. Thank you for taking a chance on me. You laid out a foundation for me in chemistry that enabled me to thrive. I am so grateful for your patience, kindness, and guidance. You are a role model of the mentor and manager that I hope to become.

I want to express my deepest gratitude to my undergraduate mentor, Micah Ziegler. You are a natural teacher! I loved working for you and looked forward to coming into lab every day. Your teachings in organometallic chemistry laid the groundwork for my graduate studies and enabled me to become an independent researcher. I am so grateful for your mentorship and advice throughout the years.

To Nick, I am so lucky to have you in my life. Your love and support made my PhD possible. You are such a brilliant scientist, and I am so appreciative to be able to bounce ideas

off you and talk chemistry over the past 5 years. I have loved our San Diego surf sessions, adventures in Joshua tree, and the incredible ice cream, pastry, and fish taco shops throughout La Jolla. It has been wonderful having you visit me for extended periods of time throughout my PhD and I am excited for what our future holds for us.

Finally, I would like to thank my parents and brother for their love and support throughout my studies.

Chapter 2, in full, is a reprint of the material as it appears in Torquato, N.A.; Palasz, J.M.; Bertrand, Q.C.; Brunner, F.M.; Chan, T; Gembicky, M.; Mrse, A.A.; Kubiak, C.P. "Synthesis, structure and reactivity of μ_3-SnH capped trinuclear nickel cluster," *Chem. Sci.*, 2022, 13, 11382-11387. N. A. T. acknowledges Micah Ziegler for invaluable discussions. N. A. T. acknowledges support from NSF for a Graduate Research Fellowship. Financial support from NSF is also gratefully acknowledged (CHE-1853908). The authors thank Theresa Block, Aylin Koldemir, and Rainer Pöttgen for Mössbauer investigations. The dissertation author was the primary investigator and author of this paper.

Chapter 3, in full, is being prepared for submission for publication of the material entitled Torquato, N.A.; Palasz, J.M.; Mrse, A.A.; Kubiak, C.P. "H_2/D_2 Exchange by a μ_3-SnH, μ_3-H capped trinuclear Nickel Cluster," *Manuscript in Preparation*. The authors thank Dee-Hua Huang and Laura Pasternack at Scripps Research for VT NMR investigations. N.A.T. acknowledges Nick Myllenbeck for invaluable discussions. N.A.T acknowledges support from NSF for a Graduate Research Fellowship. Research support from NSF is also gratefully acknowledged (CHE-1853908). The dissertation author was the primary investigator and author of this paper.

Chapter 4, in full, is a reprint of the material as it appears in Torquato, N.A.; Lara, J.K.; Bertrand, Q.C.; Mrse, A.A.; Gembicky, M.; Kubiak, C.P. "Electronic structural studies of μ_3-$Sn(OR)_3$ capped trinuclear nickel clusters," *Polyhedron*, 2022, 224, 116000. N.A.T acknowledges support from NSF for a Graduate Research Fellowship. Research support from the National Science Foundation (CHE-1853908) is gratefully acknowledged. The dissertation author was the primary investigator and author of this paper.

Chapter 5 contains unpublished material describing future directions in this field. The dissertation author was the primary author of this chapter.

VITA

2017 Bachelor of Science in Chemistry, University of California San Diego

2023 Doctor of Philosophy in Chemistry, University of California San Diego

PUBLICATIONS

Torquato, N.A.; Palasz, J.M.; Mrse, A.A.; Kubiak, C.P. H_2/D_2 Exchange by a μ_3-SnH, μ_3-H capped trinuclear Nickel Cluster, *Manuscript in Preparation*.

Torquato, N.A.; Palasz, J.M.; Bertrand, Q.C.; Brunner, F.M.; Chan, T; Gembicky, M.; Mrse, A.A.; Kubiak, C.P. Synthesis, structure and reactivity of μ_3-SnH capped trinuclear nickel cluster, *Chem. Sci.*, **2022**, 13, 11382-11387.

Torquato, N.A.; Lara, J.K.; Bertrand, Q.C.; Mrse, A.A.; Gembicky, M.; Kubiak, C.P. Electronic structural studies of μ_3-$Sn(OR)_3$ capped trinuclear nickel clusters, *Polyhedron*, **2022**, 224, 116000.

Miller, C.J.; Brunner, F.M.; Kelly, H.R.; Cheung, P.L.; **Torquato, N.A.** ;Gembicky, M.; Okuno, S.; Chan, T.; Bastista, V.S.; Kubiak, C.P. PM-IRRAS and DFT investigation of the surface orientation of new Ir piano-stool complexes attached to Au (111). *Dalton Trans.*, **2022**, 51, 17688-17699

ABSTRACT OF THE DISSERTATION

Synthesis, structure, and reactivity of μ_3-Sn capped trinuclear nickel clusters

by

Nicole A. Torquato

Doctor of Philosophy in Chemistry

University of California San Diego, 2023

Professor Clifford P. Kubiak, Chair

Chapter 1. This section presents an overview of literature pertaining to low-valent/low-oxidation state tin hydrides, transition metal coordinated tin hydrides, and group 10 trinuclear metal cluster synthesis, characterization, and reactivity.

Chapter 2. Treatment of the trichlorotin-capped trinuclear nickel cluster, $[Ni_3(dppm)_3(\mu_3\text{-}Cl)(\mu_3\text{-}SnCl_3)]$, **1**, with 4 eq. $NaHB(Et)_3$ yields a μ_3-SnH capped trinuclear nickel cluster, $[Ni_3(dppm)_3(\mu_3\text{-}H)(\mu_3\text{-}SnH)]$, **2** [dppm = bis(diphenylphosphino)methane]. Single-crystal X-ray diffraction, nuclear magnetic resonance (NMR) spectroscopy, and computational studies together support that cluster **2** is a divalent tin hydride. Complex **2** displays a wide range of reactivity including oxidative addition of bromoethane across the Sn center. Addition of 1 eq. iodoethane to complex **2** releases H_2 (g) and generates an ethyltin-capped nickel cluster with a μ_3-iodide, $[Ni_3(dppm)_3(\mu_3\text{-}I)(\mu_3\text{-}Sn(CH_2CH_3))]$, **4**. Notably, insertion of alkynes into the Sn–H bond of **2** can be achieved *via* addition of 1 eq. **1**-hexyne to generate the 1-hexen-2-yl-tin-capped nickel cluster, $[Ni_3(dppm)_3(\mu_3H)(\mu_3\text{-}Sn(C_6H_{11}))]$, **5**. Addition of H_2 (g) to **5** regenerates the starting material, **2**, and hexane. The formally 44-electron cluster **2** also displays significant redox chemistry with two reversible one-electron oxidations ($E = -1.3$ V, -0.8 V *vs.* $Fc^{0/+}$) and one-electron reduction process ($E = -2.7$ V *vs.* $Fc^{0/+}$) observed by cyclic voltammetry.

Chapter 3. H_2 and D_2 exchange by a μ_3-SnH, μ_3-H capped trinuclear nickel cluster, $[Ni_3(dppm)_3(\mu_3\text{-}H)(\mu_3\text{-}SnH)]$, **1**, (dppm = bis(diphenylphosphino)methane) was investigated through a variety of nuclear magnetic resonance (NMR) spectroscopy studies. Mechanistic studies reveal reversible exchange upon addition of D_2/H_2 between **1** and the deuteride species, $[Ni_3(dppm)_3(\mu_3\text{-}D)(\mu_3\text{-}SnD)]$, **1D**. Furthermore, these studies suggest a conformational change at the Ni-H functionality upon addition of H_2. Variable temperature (VT) NMR studies of **1** demonstrate a temperature dependence of the Sn-H and the Ni-H resonances, with the Ni-H experiencing the largest perturbation in chemical shift. Further mechanistic insights were obtained with VT NMR studies performed under an atmosphere H_2 and HD. Overall, these

studies provide evidence of H_2/D_2 exchange by complex **1** and suggest a novel mechanism for hydrogen activation and exchange processes.

Chapter 4. Spectroscopic and structural comparisons are made between a series of $(OR)_3Sn$ capped trinuclear nickel clusters. The synthesis of the $(OEt)_3Sn$ and $(OPh)_3Sn$ capped nickel clusters, $[Ni_3(dppm)_3(\mu_3\text{-}Cl)(\mu_3\text{-}Sn(OEt)_3)]$ (**1**), $[Ni_3(dppm)_3(\mu_3\text{-}Cl)(\mu_3\text{-}Sn(OPh)_3)]$ (**2**), was realized by the treatment of $[Ni_3(dppm)_3(\mu_3\text{-}Cl)(\mu_3\text{-}SnCl_3]$ with 6 eq. of KOEt or NaOPh, respectively. Treatment of complex **1** with 10 eq. glycerol results in the synthesis of the $(C_3H_5O_3)Sn$ capped trinuclear nickel cluster, $[Ni_3(dppm)_3(\mu_3\text{-}Cl)(\mu_3\text{-}Sn(C_3H_5O_3))]$ (**3**). The crystallographic studies of these clusters allow a detailed structural comparison. In addition, cyclic voltammetric data were obtained for complexes **1**, **2**, and **3** and their electrochemical properties are compared. Complex **1** and **3** exhibit reversible oxidation and reduction events. Complex **2** displays a reversible oxidation and a pseudo-reversible reduction.

Chapter 5. The focus of this chapter is to briefly describe project ideas based on main group coordinated polynuclear clusters that future researchers may find worthwhile.

CHAPTER 1. A Brief Review: Low-valent/Low-oxidation state Tin Hydrides, Transition Metal Coordinated Tin Hydrides, and Multinuclear Cluster Chemistry

1.1 Introduction

Over the past few decades, significant advancements in group 14 chemistry have led to the discovery of an abundance of main group compounds behaving similarily to transition metal complexes.[1, 2] These advancements originate with the design and synthesis of low valent/low oxidation state group 14 species, whose structural features lead to the activation of small molecules, such as, H_2, CO_2, and NH_3, or unsaturated organic molecules, including alkenes, alkynes, ketones, and aldehydes.[2, 3] One exemplar is low-valent/low oxidation state tin hydrides, which have demonstrated new reactivity modes attributed to the reduced nature/open coordination site on tin.[3, 4] Past research in the field of tin hydride chemistry has largely focused on free-radical reactions and hydrometallation of unsaturated substrates.[5-7] However, new structural motifs for low-valent/low-oxidation state tin hyrides have led to increased reduction chemistry and catalysis.[3] The known structural and reaction chemistry of tin hydrides has been expanded to include coordination to transition metals.[8-12] There are comparatively few reports of tin hydrides coordinated to transition metal clusters.[13, 14] Leveraging experience with transition metal cluster synthesis and characterization, we sought to investigate fundamental properties of tin hydride capped trinuclear nickel clusters. This research is influenced by three related topics, to be discussed in more detail in this chapter: 1) low-valent/low-oxidation state tin hydrides, 2) transition metal coordinated tin hydrides, 3) group 10 trinuclear metal cluster synthesis, characterization, and reactivity, with an emphasis on tin coordination and trinuclear nickel cluster chemistry.

1.2 Organic Low-valent/Low-oxidation State Tin Hydrides

Back in the early 2000s, the first divalent tin (II) hydride, $[Ar^{iPr6}Sn(u\text{-}H)]_2$, was discovered by Power and Eicher.[15] Since then, several other tin (II) hydrides supported by a variety of aryl, *N*-heterocyclic carbenes (NHC)s, Nacnac, amido, boryl, and phosphine groups have been reported.[3] The major structural modifications of these tin hydride species have been a result of the donor capacity and sterics of the ligand on tin leading to reactivity modes unusual for tin hydride complexes.[3]

1.2.1 Reactivity of organic low-valent/Low-oxidation state tin hydrides

Low-valent/low-oxidation state tin hydrides have demonstrated a rich reaction profile.[3] First, a variety of low-valent stannylyne species are known to activate H_2 to form dimeric tin (II) hydrides. In one case, Power and coworkers reported H_2 activation by $Ar^{iPr4}SnSnAr^{iPr4}$ forming $[Ar^{iPr4}Sn(\mu\text{-}H)]_2$.[16] This study demonstrated that the hydrogenation of $Ar^{iPr4}SnSnAr^{iPr4}$ is reversible and under mild heat the tin hydride dimer, $[Ar^{iPr4}Sn(\mu\text{-}H)]_2$, dehydrogenates regenerating the stannylyne species, $Ar^{iPr4}SnSnAr^{iPr4}$.[16] Furthermore, they show that the tin hydride dimer, $[Ar^{iPr4}Sn(\mu\text{-}H)]_2$, undergoes deuterium exchange with excess D_2 gas forming the deuterium isotopologue, $[Ar^{iPr4}Sn(\mu\text{-}D)]_2$. While previous research in tin hydride dehydrogenation has focused mostly on base-induced dehydrocoupling of alkylstannanes[3], this study depicted one of the first examples of hydrogenation and dehydrogenation by a main group species effected under mild conditions.

Various studies involving aryl tin (II) hydrides have demonstrated olefin and alkyne insertion resulting in the corresponding hydrostannylation product.[3] In 2006, Roesky and coworkers generated the first monomeric Sn (II) hydride, (^{Dipp}Nacnac)SnH.[17] This species had a wide range of reported Sn-H insertion reactions involving C═O, C═N, and C≡C bonds (Figure

1.1).[2, 18] In addition, ([Dipp]Nacnac)SnH was reported to participate in aromatic C-F activation and metathesis.[19]

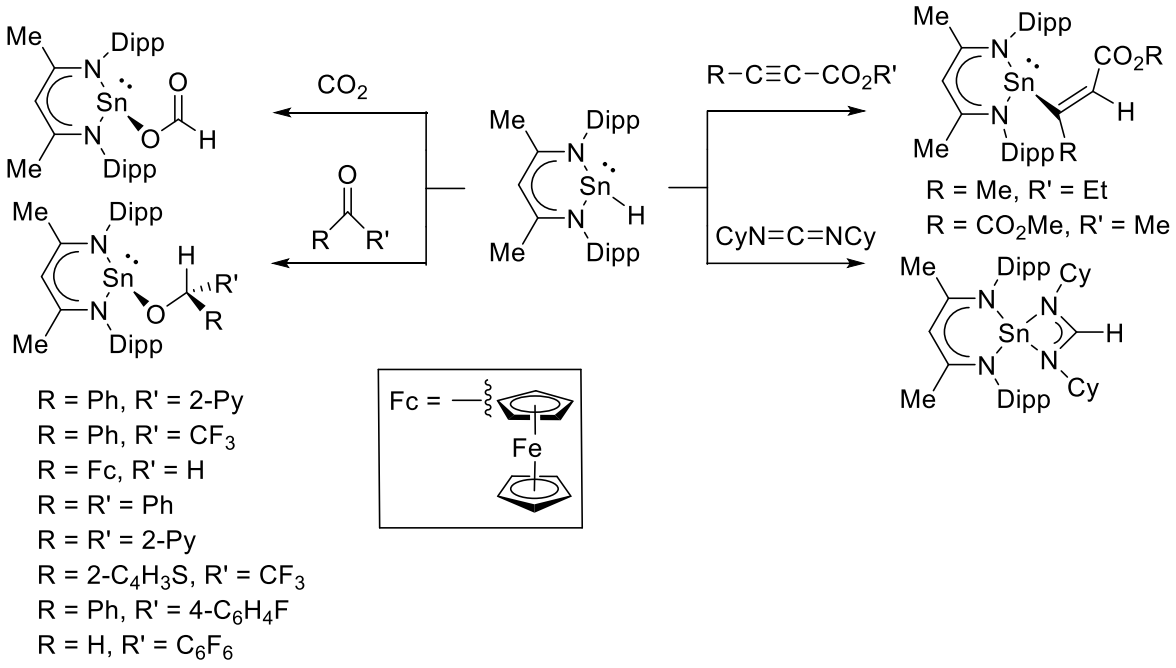

Figure 1.1. Sn-H insertion reactions involving ([Dipp]Nacnac)SnH.[2, 18]

Catalytic studies involving low-valent tin hydride species are mainly focused on hydroboration of carbonyls and CO_2.[3, 20, 21] Furthermore, Powers and coworkers demonstrate catalytic dehydrocoupling of amines and boranes by a tin (II) hydride species.[22]

1.3 Transition Metal Coordinated Tin-Hydrides

In an effort to change the electronic, structural and reaction profile for tin hydride complexes and further probe their direct interaction with transition metals, recent studied have focused on understanding the reaction dynamics of tin hydride complexes coordinated to transition metals.[3] For organizational purposes studies in this field are broken up according to research group.

1.3.1 Tilley and Coworkers

Early work by Tilley and coworkers involved the synthesis of a hafnium hydrostannyl complex, CpCp*Hf($SnHMes_2$)Cl (Cp* = η^5-C_5Me_5).[23] Mechanistic studies with these complexes

point towards α-elimination being a key step in early metal-mediated dehydrocoupling (Figure 1.2).[23] Follow-up studies, involving a hydrogen substituted stannylene complex, Cp*(^{i}Pr$_3$P)(H)Os═SnH(trip) (trip = 2,4,6-triisopropylphenyl), show unusual α-migration of the hydride on tin to osmium.[24] Mechanistic studies implicate a radical-mediated process resulting in the catalytic isomerization described.

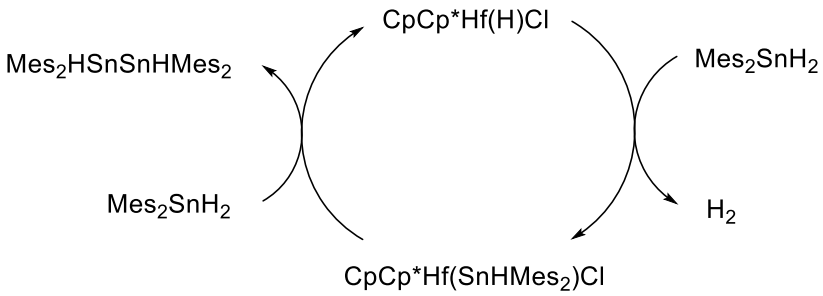

Figure 1.2. Proposed mechanism of dehydrocoupling by CpCp*Hf(SnHMes$_2$)Cl.[23]

1.3.2 Zandaro and Coworkers

Zandaro and coworkers focused on the synthesis, structure and reactivity of trihydrido tin coordinated transition metal complexes.[25-27] Reactivity studies of tin trihydride osmium complexes, Os(SnH$_3$)(Tp)L(PPh$_3$) [L = P(OMe)$_3$, P(OEt)$_3$], describe insertion of CO_2 into the Sn-H bond.[25] A similar reactivity profile is reported for the analogous SnH$_3$ coordinated Re and Mn complexes.[26]

1.3.3 Wesemann and Coworkers

Coordination of NHCs to low valent tin species were initially studied by this group.[3] Recent studies have involved the synthesis, characterization and reactivity of tin coordinated transition metal complexes. This includes the production of a dimeric platinum-stannylene complex and a rhodium dihydride complex.[28, 29] Reactivity studies involving the rhodium dihydride complex, [(Ph$_3$P)$_2$RhH$_2$SnAr*] (Ar*=2,6-Trip$_2$C$_6$H$_3$, Trip=2,4,6-triisopropylphenyl), demonstrate dehydrogenation to the corresponding tetrylidyne [(Me$_3$P)$_2$(Ph$_3$P)Rh≡SnAr*].[29]

1.3.4 Rivard and Coworkers

Stabilization of tin (II) hydrides through the utilization of Lewis base/acid pairs was investigated by this group.[8-10, 30] Additionally, trapping of a highly unstable SnH_2 adduct through the use of electron accepting $W(CO)_5$ was shown. The tin (II) dihydride, $IPr{\cdot}SnH_2{\cdot}W(CO)_5$ (IPr = $[(HCNAr')_2C{:}]$; Ar′ = 2,6-$^{i}Pr_2C_6H_3$), reacts with aldehydes to make the corresponding hydrostannylation product.[9] Further work by this group demonstrates the trapping of inorganic ethylene species, H_2SiGeH_2 and H_2SiSnH_2, through similar push-pull and Lewis acid/base synthetic strategies.[10]

1.4 Group 10 transition metal clusters

Metal clusters are of particular interest in the academic community for their structural and catalytic properties, electrochemical behavior, and ability to mimic catalyst metal surfaces.[31] This brief review focuses in on the chemistry of group 10 trinuclear metal clusters.

1.4.1 Platinum and Palladium clusters

Most examples of the group 10 triuclear metal clusters in literature pertain to Pd and Pt. A wide variety of ligands have been used to generate and stabilize these clusters, including, silyenes, carbonyls, isocyanides, phosphines, and diphosphines.[32-35] Puddephatt and coworkers published much of the early work in this area, first synthesizing triplatinum and tripladium with carbonyl ligands and later generating trinuclear clusters employing stabilizing diphosphine ligands.[33, 34, 36-38] To date, there are only two groups in literature, Puddephatt and coworkers and Figueroa and coworkers, who have generated tin coordinated trinuclear platinum clusters.[39, 40] In Puddephatt and coworkers study an open face triplatinum cluster was used to activate small molecules including, Ph_3SnH, SnF_2-NaF, $SnCl_2$-NaCl leading to the synthesis of a variety of trihalide tin-capped triplatinum clusters (Figure 1.3).[39] Furthermore, this study showed that the open face triplatinum

cluster can activate Me_2SnH_2 resulting in the formation of a μ_3-$SnMe_2H$, μ_3-H capped triplatinum cluster.

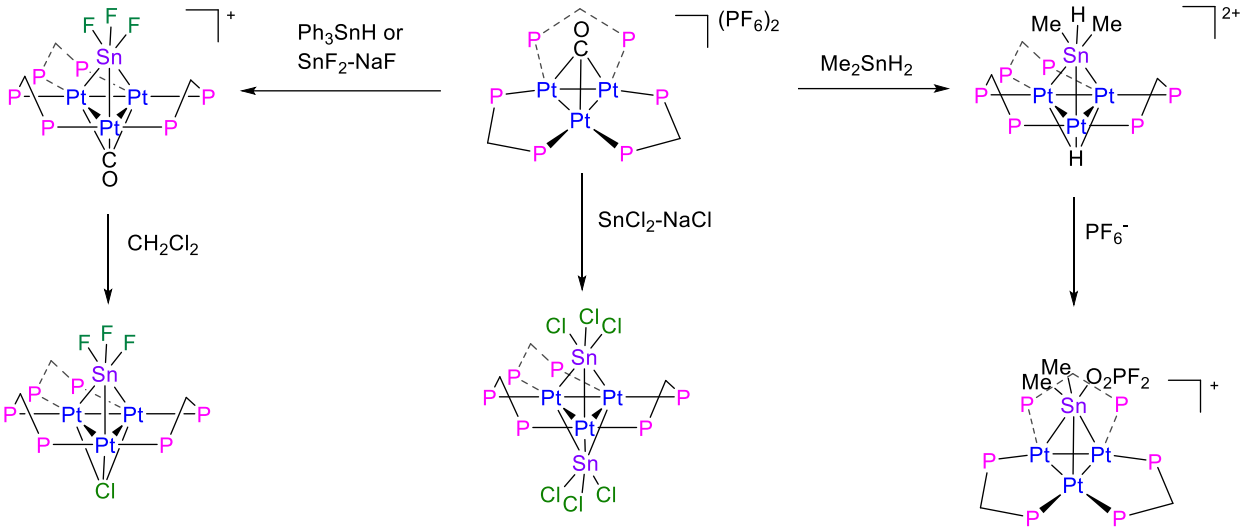

Figure 1.3. Reactivity of $[Pt_3(dppm)_3(\mu_3\text{-}CO)](PF_6)_2$ with various small molecule substrates. The phenyl rings attached to the phosphorous atoms were omitted for clarity.[39]

In 2016, the Figueroa group generated an analogue to Chini's $[Pt_3(CO)_6]^{2-}$ dianion stabilized by the steric bulk of m-terphenyl isocyanides, resulting in the synthesis of $[Pt_3(\mu\text{-}CO)_3(CNAr^{Dipp2})_3]^{2-}$.[40] In this study they investigated the reactivity properties of the title compound and found that it reacted with 1–2 eq. $ClAu(PPh_3)$ generating the mono- and di-$Au(PPh_3)$ capped trinuclear platinum clusters, $K(Et_2O)_2[Pt_3(\mu_3\text{-}AuPPh_3)(\mu\text{-}CO)_3(CNAr^{Dipp2})_3]$, and $Pt_3(\mu_3\text{-}AuPPh_3)_2(\mu\text{-}CO)_3(CNAr^{Dipp2})_3$, respectively. Furthermore, upon addition of 1 eq. $ClSnPh_3$, an open faced $SnPh_3$ capped trinuclear platinum cluster, $K[Pt_3(\mu_3\text{-}SnPh_3)(\mu\text{-}CO)_3(CNAr^{Dipp2})_3]$, was generated.

1.4.2 Nickel Clusters

Several reports detail the use ofsulfides, cyclopentadienes (CP), CP*, phosphines, and diphosphines to synthesize an array of trinuclear nickel clusters.[41-43] Given the breadth of contributions in this field, the discussion will focus on diphosphine stabilized trinuclear nickel clusters.

1.4.3 Trinuclear Nickel Clusters with Bridging Diphosphine Ligands

In 1990, Kubiak and coworkers generated a μ_3-CNMe, μ_3-I capped trinuclear nickel cluster, $[Ni_3(\mu_3\text{-}CNMe)(\mu_3\text{-}I)(CNMe)_2(dppm)_2][I]$, (dppm = bis(diphenylphosphino) methane), representing the first triply-bridged methyl isocyanide. [44] Shortly after, an analogous species, $[Ni_3(\mu_3\text{-}CNMe)(\mu_3\text{-}I)(dppm)_3]$, was synthesized which proved to be a competent electrocatalyst in the 2-electron disproportionation of CO_2 to CO and CO_3^{2-}.[45] Furthermore, it was found that $[Ni_3(\mu_3\text{-}I)_2(dppm)_3]$, can be used in the photochemical production of the radical anion of carbon dioxide, $CO_2^{\bullet-}$, which can subsequently be used in the formation of dicarboxylic acids from olefins.[46] To refine the structural and electronic description of compounds in this class, in 1996, Kubiak and coworkers describe the synthesis, characterization, and electronic studies of a family of clusters, $[Ni_3(\mu_3\text{-}L)(\mu_3\text{-}X)(dppm)_3]$.[47] This study utilized a variety of electronically and sterically unique isocyanides to understand the effects that the capping substituent has on the electronics of the trinuclear nickel core. They determined that the physical, spectroscopic, and electrochemical properties are similar for this class of compound regardless of the electronics of the capping isocyanide. Cyclic voltammetry of these species featured a single-electron reduction at ca. -1.1 vs. SCE. Later that same year, a Tellurium-phosphine adduct was used to make a telluride capped trinuclear nickel cluster $[Ni_3(\mu_3\text{-}Te)_2(\mu\text{-}dppm)_3]$.[48] This cluster contains 50e- and shows multiple reversible 1e- processes in cyclic voltammetry experiments, corresponding to the generation of the 48e-, 49e- and 51e- clusters. Finally, in an effort to obtain an open-faced trinuclear nickel cluster, thallium (I) was added to $[Ni_3(\mu_3\text{-}I)_2(dppm)_3]$, which resulted in the insertion product $[Ni_3(\mu_3\text{-}TlI)(\mu_3\text{-}I)(\mu\text{-}dppm)_3]^+$.[49]

1.4.4 Tin-capped Trinuclear Nickel Clusters with Bridging Diphosphine Ligands

In 2002, Breedlove and Kubiak developed the first *triangulo*-nickel clusters capped by tin, $[Ni_3(dppm)_3(\mu_3\text{-}I)(\mu_3\text{-}SnCl_x)]^{n+}$ ($x = 2$, $n = 1$; $x = 3$, $n = 0$).[50] Cyclic voltammetry of the

trichlorostannyl-capped cluster demonstrates dissociation of a chloride ligand upon reduction (Figure 1.4). This process is reversible, and upon oxidation of the cluster, the chloride re-inserts. This demonstrates that electrochemical reduction of these clusters weakens the Sn-ligand bond.

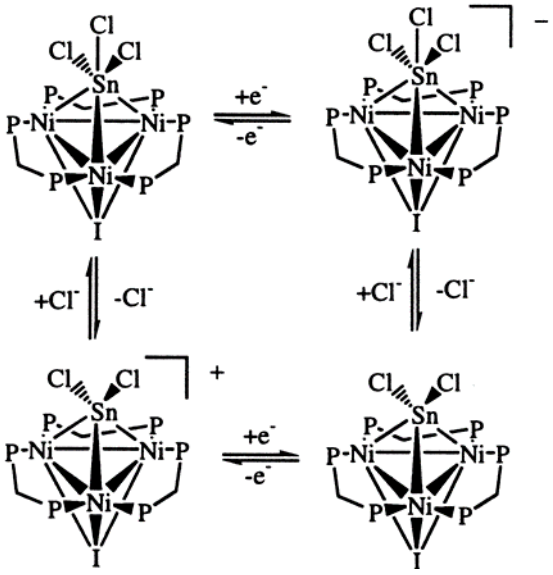

Figure 1.4. Chloride Dissociation and Redox Equilibria of Trichlorostannyl-capped Nickel Cluster, $[Ni_3(dppm)_3(\mu_3\text{-}I)(\mu_3\text{-}SnClx)]^{n+}$ (x = 2, n = 1; x = 3, n = 0).[50]

In addition, in 2005, Simon-Manso and Kubiak reported a trihydroxytin-capped nickel cluster that reversibly inserted CO_2 into the Sn-O bond at 1 atm (Figure 1.5).[51] This unprecedented selectivity for CO_2 at low pressures, along with the ability of the tin-capped cluster to dissociate ligands upon electrochemical reduction has led us to pursue variation of the tin substituents in organometallic nickel clusters to explore a wider reactivity scope.

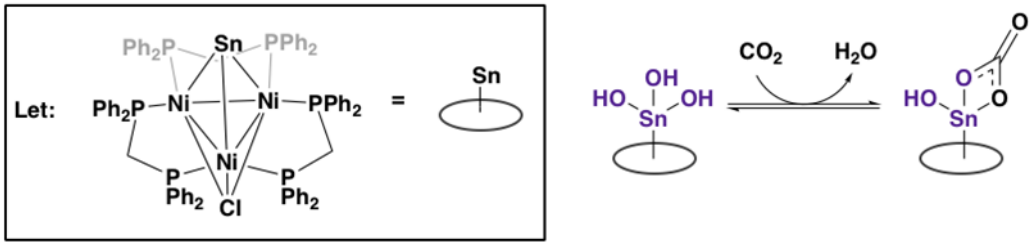

Figure 1.5. μ_2, η_3-CO_2 insertion into Sn hydroxide cluster. [51]

1.5 Conclusion

Many examples of low-valent/low-oxidation state tin hydrides, transition metal coordinated tin hydrides, and group 10 trinuclear metal clusters have been reported. Previous work from our group reported a wide array of trinuclear nickel clusters, capped by a variety of L and X type ligands.[45-47, 50-52] Many of these clusters display extensive redox chemistry, interesting electronic structures, and applications as electrocatalysts. The structural motifs exhibited by these clusters and their electronic properties inspired us to explore the synthesis and characterization of low valent tin hydride–capped trinuclear nickel clusters. The results reported in the thesis focus on 1) the expansion of the library of capping ligands for nickel trimers, 2) enabling new structural and reactivity modes for tin hydrides by varying the electronics of the trinuclear nickel core, 3) investigating cooperative effects between the tin hydride species and the trinuclear nickel core in small molecule activation reactions

1.6 References

1. P. P. Power, Nature, 2010, 463, 171-177.

2. S. K. Mandal and H. W. Roesky, Acc. Chem. Res., 2012, 45, 298-307.

3. M. M. D. Roy, A. A. Omaña, A. S. S. Wilson, M. S. Hill, S. Aldridge and E. Rivard, Chem. Rev., 2021, 121, 12784-12965.

4. T. J. Hadlington, M. Driess and C. Jones, Chem. Soc. Rev., 2018, 47, 4176-4197.

5. N. D. Smith, J. Mancuso and M. Lautens, Chem. Rev., 2000, 100, 3257-3282.

6. I. Yoshifumi, O. Hiroji, O. Koichiro and U. Kiitiro, Bull. Chem. Soc. Jpn., 1987, 60, 3468-3470.

7. H. G. Kuivila, Acc. Chem. Res., 1968, 1, 299-305.

8. S. M. I. Al-Rafia, O. Shynkaruk, S. M. McDonald, S. K. Liew, M. J. Ferguson, R. McDonald, R. H. Herber and E. Rivard, Inorg. Chem., 2013, 52, 5581-5589.

9. S. M. I. Al-Rafia, A. C. Malcolm, S. K. Liew, M. J. Ferguson and E. Rivard, Journal of the American Chemical Society, 2011, 133, 777-779.

10. S. M. I. Al-Rafia, A. C. Malcolm, R. McDonald, M. J. Ferguson and E. Rivard, Angew. Chem. Int. Ed., 2011, 50, 8354-8357.

11. J.-J. Maudrich, M. Widemann, F. Diab, R. H. Kern, P. Sirsch, C. P. Sindlinger, H. Schubert and L. Wesemann, Eur. J. Chem., 2019, 25, 16081-16087.

12. Q. Zhu, J. C. Fettinger and P. P. Power, Dalton Trans., 2021, 50, 12555-12562.

13. M. M. M. Khan, S. Ghosh, G. Hogarth, D. A. Tocher, M. G. Richmond, S. E. Kabir and H. W. Roesky, J. Organomet. Chem., 2017, 840, 47-55.

14. C. J. Cardin, D. J. Cardin, H. E. Parge and J. M. Power, J. Chem. Soc., Chem. commun., 1984, DOI: 10.1039/C39840000609, 609-610.

15. B. E. Eichler and P. P. Power, J. Am. Chem. Soc., 2000, 122, 8785-8786.

16. S. Wang, T. J. Sherbow, L. A. Berben and P. P. Power, J. Am. Chem. Soc., 2018, 140, 590-593.

17. L. W. Pineda, V. Jancik, K. Starke, R. B. Oswald and H. W. Roesky, Angew. Chem. Int. Ed., 2006, 45, 2602-2605.

18. A. Jana, H. W. Roesky, C. Schulzke and A. Döring, Angew. Chem. Int. Ed., 2009, 48, 1106-1109.

19. A. Jana, H. W. Roesky, C. Schulzke and P. P. Samuel, Organometallics, 2010, 29, 4837-4841.

20. T. J. Hadlington, M. Hermann, G. Frenking and C. Jones, J. Am. Chem. Soc., 2014, 136, 3028-3031.

21. T. J. Hadlington, C. E. Kefalidis, L. Maron and C. Jones, ACS Catal., 2017, 7, 1853-1859.

22. J. D. Erickson, T. Y. Lai, D. J. Liptrot, M. M. Olmstead and P. P. Power, Chem. comm., 2016, 52, 13656-13659.

23. N. R. Neale and T. D. Tilley, J. Am. Chem. Soc., 2002, 124, 3802-3803.

24. P. G. Hayes, C. W. Gribble, R. Waterman and T. D. Tilley, J. Am. Chem. Soc., 2009, 131, 4606-4607.

25. G. Albertin, S. Antoniutti, A. Bacchi, M. Bortoluzzi, G. Pelizzi and G. Zanardo, Organometallics, 2006, 25, 4235-4237.

26. G. Albertin, S. Antoniutti, J. Castro, S. García-Fontán and G. Zanardo, Organometallics, 2007, 26, 2918-2930.

27. G. Albertin, S. Antoniutti, J. Castro and G. Zanardo, Inorganica Chim. Acta, 2010, 363, 605-616.

28. C. P. Sindlinger and L. Wesemann, Chem. comm., 2015, 51, 11421-11424.

29. M. Widemann, K. Eichele, H. Schubert, C. P. Sindlinger, S. Klenner, R. Pöttgen and L. Wesemann, Angew. Chem. Int. Ed., 2021, 60, 5882-5889.

30. A. K. Swarnakar, S. M. McDonald, K. C. Deutsch, P. Choi, M. J. Ferguson, R. McDonald and E. Rivard, Inorg. Chem., 2014, 53, 8662-8671.

31. E. L. Muetterties, T. N. Rhodin, E. Band, C. F. Brucker and W. R. Pretzer, Chem. Rev., 1979, 79, 91-137.

32. K. Tanaka, M. Kamono, M. Tanabe and K. Osakada, Organometallics, 2015, 34, 2985-2990.

33. G. Ferguson, B. R. Lloyd and R. J. Puddephatt, Organometallics, 1986, 5, 344-348.

34. R. J. Puddephatt, L. Manojlovic-Muir and K. W. Muir, Polyhedron, 1990, 9, 2767-2802.

35. D. Imhof and L. M. Venazi, Chem. Soc. Rev., 1994, 23, 185-193.

36. S. S. M. Ling and R. J. Puddephatt, J. Chem. Soc., Chem. commun., 1982, DOI: 10.1039/C39820000412, 412-413.

37. G. Ferguson, B. R. Lloyd, L. Manojlovic-Muir, K. W. Muir and R. J. Puddephatt, Inorg. Chem., 1986, 25, 4190-4197.

38. S. S. M. Ling, N. Hadj-Bagheri, L. Manojlovic-Muir, K. W. Muir and R. J. Puddephatt, Inorg. Chem., 1987, 26, 231-235.

39. M. C. Jennings, G. Schoettel, S. Roy and R. J. Puddephatt, Organometallics, 1991, 10, 580-586.

40. B. R. Barnett, A. L. Rheingold and J. S. Figueroa, Angew. Chem. Int. Ed., 2016, 55, 9253-9258.

41. J. J. Maj, A. D. Rae and L. F. Dahl, J. Am. Chem. Soc., 1982, 104, 3054-3063.

42. W. Tremel, B. Krebs and G. Henkel, Inorganica Chim. Acta, 1983, 80, L31-L32.

43. J. H. J. Berthel, M. W. Kuntze-Fechner and U. Radius, Eur. J. Inorg. Chem, 2019, 2019, 2618-2623.

44. K. S. Ratliff, G. K. Broeker, P. E. Fanwick and C. P. Kubiak, Angew. Chem. Int. Ed., 1990, 29, 395-396.

45. K. S. Ratliff, R. E. Lentz and C. P. Kubiak, Organometallics, 1992, 11, 1986-1988.

46. D. A. Morgenstern, R. E. Wittrig, P. E. Fanwick and C. P. Kubiak, J. Am. Chem. Soc., 1993, 115, 6470-6471.

47. D. A. Morgenstern, G. M. Ferrence, J. Washington, J. I. Henderson, L. Rosenhein, J. D. Heise, P. E. Fanwick and C. P. Kubiak, J. Am. Chem. Soc., 1996, 118, 2198-2207.

48. G. M. Ferrence, P. E. Fanwick and C. P. Kubiak, Chem. comm., 1996, DOI: 10.1039/CC9960001575, 1575-1576.

49. M. J. A. Johnson, P. K. Gantzel and C. P. Kubiak, Organometallics, 2002, 21, 3831-3832.

50. B. K. Breedlove, P. E. Fanwick and C. P. Kubiak, Inorg. Chem., 2002, 41, 4306-4308.

51. E. Simón-Manso and C. P. Kubiak, Angew. Chem. Int. Ed., 2005, 44, 1125-1128.

52. R. E. Wittrig, G. M. Ferrence, J. Washington and C. P. Kubiak, Inorganica Chem. Acta, 1998, 270, 111-117.

CHAPTER 2. Synthesis, structure and reactivity of μ3-SnH capped trinuclear nickel cluster

2.1 Introduction

Tin hydrides have been widely employed in stoichiometric and catalytic hydrogen atom transfer to a diverse range of substrates.[1, 2] Industrially relevant tin hydrides predominately feature tin in the +4 oxidation state. However, recent advances in group 14 hydride chemistry have introduced a range of tin hydride species formally in the +2 oxidation state that enable new reactivity profiles and pathways.[1, 3] Over the past 20 years, seminal studies by Power and co-workers have demonstrated the synthesis, isolation, and structural characterization of low-valent Sn, Ge, and Pb hydrides.[4-8] These studies have led to multiple advances in main group reactivity, such as aromatic C-F activation, C-H activation, hydrostannylation chemistry, and catalytic hydroboration.[9-13] Furthermore, recent studies have revealed new functionalities for tin (II) species including reversible coordination of H_2, coordination of NH_3 and N-H activation, and oxidative addition of H_2, H_2O, and silyl and boryl Sn^{IV} species. [14, 15] In an effort to change the electronics and structural platform for tin hydride complexes, there have been reports of tin hydride complexes coordinated to transition metals, featuring tin in the +2 oxidation state, utilizing Lewis base/Lewis acid pairs for stabilization. [16-21] Overall, these advancements in the tin chemistry platform specifically regarding the production of low valent and highly reduced tin species have led to the observation of transition-metal like reactivity of tin, including activation of small and unsaturated molecules.[22] In an effort to expand on the known structural and reaction chemistry of tin, we sought to investigate the impacts of supporting different tin functional groups on polynuclear transition metal clusters.[23-25] Herein, we describe the synthesis, structure, and reactivity of a divalent Sn hydride capped trinuclear nickel cluster, $[Ni_3(dppm)_3(\mu_3\text{-}H)(\mu_3\text{-}SnH)]$, **2** [dppm =

bis(diphenylphosphino)methane]. Complex **2**, displays a wide range of reactivity, including oxidative addition of alkyl halides and alkyne insertion with subsequent hydrogenation.

2.2 Results and Discussion

The synthesis and structural determination of a trichlorostannyl-capped cluster, $[Ni_3(dppm)_3(\mu_3\text{-}Cl)(\mu_3\text{-}SnCl_3)]$ (**1**) has been reported previously.[26] Treatment of **1** with 4 eq. $NaB(Et)_3H$ at room temperature liberates H_2 (g) and affords **2** in 88% yield (Figure 2.1). This complex was characterized by X-ray crystallography, nuclear magnetic resonance (NMR) spectroscopy, and cyclic voltammetry. DFT calculations were also used to investigate the electronic structure.

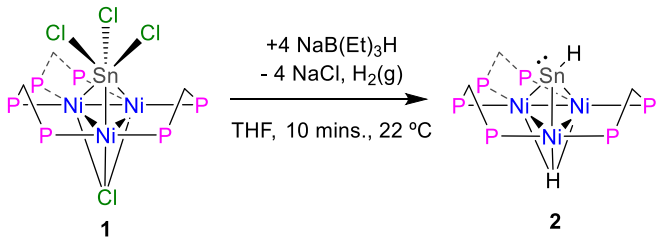

Figure 2.1. Synthesis of $[Ni_3(dppm)_3(\mu_3\text{-}H)(\mu_3\text{-}SnH)]$, **2**.

Vapor diffusion of diethyl ether into a THF solution of **2** at -35°C resulted in brownish-red X-ray quality crystals. X-ray diffraction revealed that cluster **2** crystallized in the triclinic space group $P\bar{1}$and features a μ_3-Sn atom capping a triangular face consisting of three nickel atoms supported by three bridging dppm ligands (Figure 2.2). Although the Sn-H hydrogen atom in **2** could not be precisely located in the difference electron-density map, the Sn-H linkage was unequivocally confirmed by ^{1}H and ^{119}Sn NMR spectroscopy (*vide infra*). Density functional theory (DFT) calculations and natural bond orbital (NBO) analysis also support this structural assignment (see Appendix A for details).

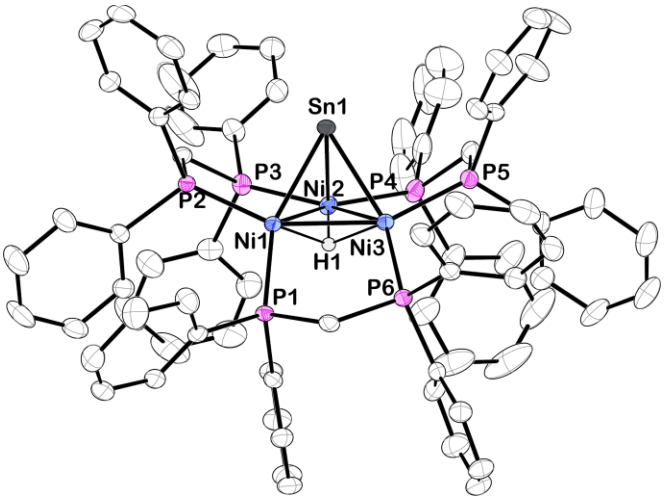

Figure 2.2. Solid-state structure of **2** as determined by single-crystal X-ray diffraction. Thermal ellipsoids were set at the 50% probability level. A diethyl ether molecule and carbon bound hydrogens were omitted for clarity. The hydride attached to Sn was not precisely located.

Compared to **1**, **2** exhibits substantially shorter Sn–Ni bond distances and considerably longer Ni–Ni bond distances (Table 2.1). While many low-valent Sn-hydrides form dimers [3, 4, 9], **2** does not, likely as a result of the trinuclear $Ni_3(dppm)_3$ framework providing considerable steric bulk, an effect seen in other monomeric Sn-H complexes.[27, 28] The structure of **2** shows slight variations in Ni–Sn bond distances. Additionally, the Ni_1–Ni_3 bond distance is significantly shortened in comparison to the other Ni–Ni bonds (Figure 2.2 and Table 2.1). This implies that, in the solid-state, the μ_3 binding of the Sn–H is not entirely symmetric, and the interactions of Sn-H may be more localized on one nickel center. Similar variations in Ni–Sn bond distances are seen in the starting material, **1**.[25, 26] These structural features are also observed in the results of DFT calculations. DFT and natural bond order (NBO) analysis for complex **2** (B3LYP/LANL2DZ) reveal that the Sn-H interacts principally with one nickel atom (Figure 2.3, see also Appendix A).

Table 2.1. Selected bond distances and Angles of **1**, **2**, **3**, **4** and **5**.

Bond Length [Å]/ Angle [°]	1	2	3	4	5
Ni1-Ni2	2.4593(18)	2.7445(6)	2.4104(9)	2.6840(5)	2.5011(10)
Ni1-Ni3	2.4829(18)	2.4449(5)	2.4020(9)	2.8886(5)	2.5285(10)
Ni2-Ni3	2.4825(16)	2.7315(6)	2.3858(9)	2.8227(5)	2.6655(11)
Sn1-Ni1	2.6118(14)	2.5187(5)	2.7261(8)	2.4423(4)	2.4324(8)
Sn1-Ni2	2.5960(16)	2.5502(5)	2.5716(7)	2.4419(4)	2.5282(8)
Sn1-Ni3	2.6185(16)	2.5348(5)	2.7447(7)	2.4607(4)	2.4724(8)
∠C-Sn-Ni1				143.57(8)	162.02(16)
∠C-Sn-Ni2				140.24(8)	136.59(17)
∠C-Sn-Ni3				132.11(8)	125.91(16)

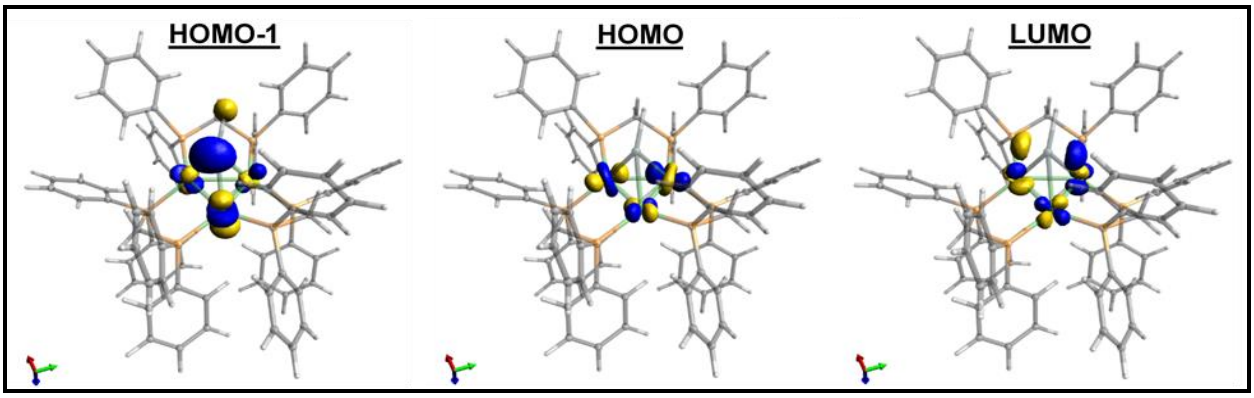

Figure 2.3. Computed molecular orbitals of **2**, utilizing a B3LYP basis set and LANL2DZ functional showing the two highest energy occupied orbitals (HOMO -1 and HOMO) and the lowest energy unoccupied orbital (LUMO).

Further details of the molecular and electronic structure were elucidated by ^{31}P, ^{1}H, and ^{119}Sn NMR spectroscopy. The ^{31}P NMR spectroscopy of **2** in benzene-d_6 revealed symmetrical binding of the μ_3-SnH and μ_3-H capping groups on the NMR timescale as demonstrated by an isolated sharp singlet resonance at 23.4 ppm. The Ni–H resonance was located in the ^{1}H NMR at -0.86 ppm and it appears as a heptet, featuring significant two-bond coupling ($^{2}J_{P-H}$) to the six phosphorus atoms coordinated to the nickel atoms. In addition, the Sn–H ^{1}H NMR resonance was located at –0.42 ppm and it appears as a singlet. The assignment of this resonance as that belonging to the hydrogen-bound Sn was evidenced by the proton-coupled ^{119}Sn NMR spectrum which, at room temperature, features a doublet at 2939.4 ppm (see Appendix A: Figure 2.10). The ^{1}H decoupled ^{119}Sn NMR spectrum contained a singlet resonance, indicating that there is one

hydrogen atom bound to Sn, which is also further confirmed by integration of the peaks in the ^{1}H NMR spectrum.

Satellite peaks arising from coupling of hydrogen to the ^{117}Sn and ^{119}Sn nuclei with $^{1}J_{(Sn–H)}$ values near 1900 Hz are normally observed for tetravalent Sn(IV) hydrides. [3, 29, 30] In contrast, divalent Sn(II) hydride complexes typically exhibit much smaller coupling constants ($^{1}J_{(Sn-H)}$ *ca.* 100 Hz) because in these Sn(II) hydrides most of the s-orbital electron density is localized to the lone pair on Sn.[4, 31-33] The $^{1}J_{(117/119Sn-1H)}$ coupling constant of **2** was found to be 360 Hz, consistent with a divalent Sn center. This assignment is corroborated by NBO analysis, which predicts that the Sn hybridization used to form the Sn–H linkage in **2** has about 20% s-character at Sn. Furthermore, DFT analysis indicates the presence of a lone pair on Sn in the HOMO-1 (Figure 2.3). In addition, preliminary Mössbauer results on **2** depict a +2 oxidation state Sn center. Overall, NMR. computational studies, and preliminary Mössbauer results suggest that the Sn can be considered as sp^2 hybridized with most of the s-orbital density localized on a lone pair on Sn.

To support experimentally the assignment of **2** as a Sn (II) hydride with a lone pair, we performed reactivity studies. Alkyl halides are known to undergo oxidative addition to Sn (II) complexes that feature a lone pair.[34] Addition of 1 eq. $BrCH_2CH_3$ to **2** in THF at –20 °C, results in the oxidative addition of $BrCH_2CH_3$ at the Sn center and formation of $[Ni_3(dppm)_3(\mu_3\text{-}H)(\mu_3\text{-}Sn((Br)(H)(CH_2CH_3))]$, **3** in 75% yield (Figure 2.4).

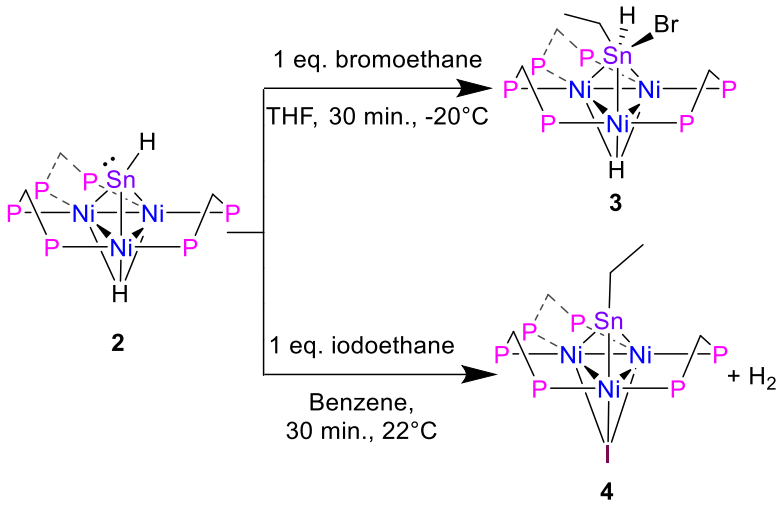

Figure 2.4. Synthesis of **3** and **4**.

The formation of **3** is characterized by a significant upfield shift in the ^{31}P NMR spectrum compared to **2**, with a resonance located at 4.2 ppm in benzene-d_6. As for the ^{1}H NMR signals, the Ni-H resonance shifts upfield to -4.70 appearing as a heptet, and the Sn-H resonance shifts downfield to 8.78 ppm, presumably a result of the close proximity to the Sn-Br bond. There is significant broadening in the ^{31}P and ^{1}H NMR spectra due to the break in symmetry from the three different functional groups attached to Sn. In comparison to **2**, the proton-coupled ^{119}Sn NMR of **3** depicts an upshifted doublet with a resonance located at 247.8 ppm and a $^{1}J_{(Sn–H)}$ = 993.6 Hz, suggesting a larger s orbital contribution from the Sn into the H atom bond (Table 2.2, also see Appendix A: Figure 2.15). The $^{1}J_{(Sn–H)}$ value of **3** is comparable to that reported by the Rivard group for a Sn (II) dihydride transition metal coordinated complex, IPr-SnH_2-$W(CO)_5$ (IPr = [(HCNAr′)$_2$C:]; Ar′ = 2,6-^{i}Pr$_2$C$_6$H$_3$). [16]

Table 2.2. Selected chemical shifts and $^{1}J_{(Sn–H)}$ in benzene-d_6 of **2**,**3**,**4**, and **5**.

	^{31}P δ (ppm)	Ni-H δ (ppm)	Sn-H δ (ppm)	^{119}Sn δ (ppm)	$^{1}J_{(Sn–H)}$ (Hz)
2	23.4	-0.86	-0.42	2939.4	346.7
3	4.2	-4.80	8.77	248.0	993.6
4	34.1			2115.1	
5	31.0	3.54-3.62		1837.8	

Vapor diffusion of pentane into a THF solution of **3** at -20°C resulted in red X-ray quality crystals (Figure 2.5). The hydride attached to Sn was not precisely located. There appears to be significant asymmetry of the μ_3-SnHBr(CH_2CH_3) binding to the trinuclear nickel core, suggested by the significant elongation of the Sn-Ni1 and Sn-Ni3 bonds versus the Sn-Ni2 bond (Table 2.1). Furthermore, the data indicates an overall shortening of the Ni-Ni bond distances more closely resembling that of cluster **1** than **2** (Table 2.1).

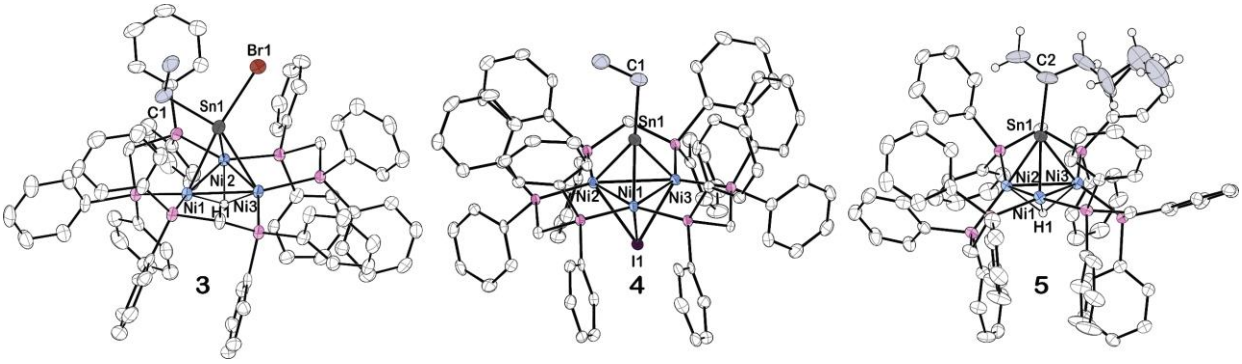

Figure 2.5. Solid-state structure of **3**, **4** and **5** as determined by single-crystal X-ray diffraction. Thermal ellipsoids were set at the 50% probability level. A solvent molecule and carbon bound hydrogens were omitted for clarity. The hydride attached to tin was not precisely located in complex **3**.

Suprisingly, in an analogous reaction to forming cluster **3**, treatment of **2** with 1 eq. ICH_2CH_3, releases H_2 and generates an CH_3CH_2Sn-capped, nickel cluster with a μ_3 iodide, [Ni_3(dppm)$_3$(μ_3-I)(μ_3-Sn(CH_2CH_3)], **4**, in 94% yield (Figure 2.4). The formation of **4**, is characterized by a significant downfield shift from the starting material in the ^{31}P NMR to 34.1 ppm in benzene-d_6, which is flanked by satellites arising from 2-bond coupling to the ^{119}Sn nuclei ($^2J_{(Sn,P)}$ = 98.8 Hz), while the ^{119}Sn NMR shifts upfield to 2115.14 ppm (Table 2.2, See Appendix A: Figure 2.20).

Layering of pentane over a benzene solution of **4** at 22°C resulted in brownish-red X-ray quality crystals (Figure 2.5). The Sn-Ni bond distances and the C-Sn-Ni bond angles reveal an almost linear binding orientation of the μ_3-SnCH_2CH_3 to the center of the trinuclear nickel core.

Furthermore, the shortened Sn-Ni bond distances: 2.4423(4), 2.4419(4), and 2.4607(4), are of similar length to other transition metal coordinated stannylyne complexes in the literature, which primarily exhibit a linear arrangement unless there are considerable steric demands due to the ligand environment.[35-40] We will report separately results of Mössbauer spectroscopy and computational studies to support this assignment.

Hydrostannylation is a well-known transformation in organic chemistry.[41] Hydrostannylation utilizing tin (II) species has been demonstrated. These reactions feature transition metal and radical catalyst-free cis-hydrostannylation of the alkynes under mild conditions.[42-44] Therefore, it was of interest to evaluate the reactivity of complex **2** with alkynes. 1 eq. of 1-hexyne was added to **2** in a benzene solution, which resulted in insertion to yield 1-hexen-2-yl-Sn-capped nickel cluster, [Ni_3(dppm)$_3$(μ_3-H)(μ_3-Sn(C_6H_{11})], **5**, in 98% yield. (Figure 2.6). A study from the Power group demonstrated Sn (II) hydrostannylation of primary alkynes resulted in Sn binding to the terminal position.[42] However, complex **5** exhibits a distinct preference to bind to the secondary position.

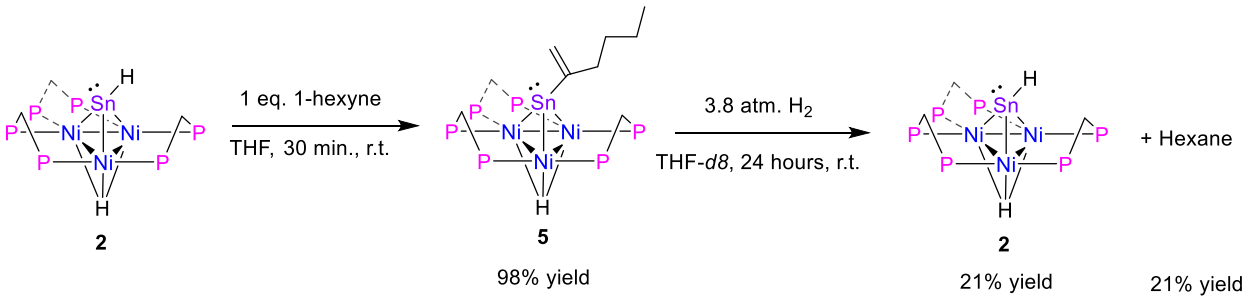

Figure 2.6. Synthesis of [Ni_3(dppm)$_3$(μ_3-H)(μ_3-Sn(C_6H_{11})], **5**, and hydrogenation to [Ni_3(dppm)$_3$(μ_3-H)(μ_3-SnH)], **2.**

The formation of **5**, is characterized by an upfield shift in the ^{31}P NMR to 31.0 ppm from the starting material, **2**. In comparison to **2**, we see an upshifted Ni-H resonance, at -3.54 – -3.62 ppm, while the ^{119}Sn NMR shifts upfield to 1837.8 ppm. Vapor diffusion of pentane into a diethyl ether solution of **5** at -20°C results in brown X-ray quality crystals. (Figure 2.5). The μ_3-Sn(C_6H_{11})

features a significant bend from a 180-degree angle to the center of the three nickel clusters, suggesting the presence of a lone pair on the Sn, similar to cluster **2** (Table 2.1). This is supported by variations in the Sn-Ni bond distances in complex **5**, in contrast to **4**. Additionally, the Sn-Ni and Ni-Ni bond distances in **5** is similar to those of complex **2** (Table 2.1).

After isolating complex **5**, hydrogenation of the 1-hexen-2-yl fragment and regeneration of **2** was attempted. Upon addition of H_2 (g) to complex **5**, complex **2** and hexane are formed in 21% yield by ^{1}H NMR. In this process, an intermediate species is formed at -4.5 ppm via ^{31}P NMR and there is a shift in the Ni-H resonance to -6.2 ppm *via* ^{1}H NMR, before the regeneration of complex **2** (See Appendix A: Figures 2.25-2.27). Thus far, this intermediate has proved elusive due to the chemical instability in solution. NMR stability studies of **5** in THF-d_8 at 22°C found that 92% of the initial integration of ^{1}H NMR features were lost over 24 hours, leading to a variety of unidentified species (See Appendix A: Figures 2.28, 2.29). Repeat studies in benzene-d_6 yielded similar conclusions. This is an unexpected result, as previous studies demonstrating tin (II) hydrostannylation of alkynes only studied the formation of stable tin alkene species and have not shown the hydrogenation chemistry of these products.[42-44] The literature indicates that, Sn has primarly been utilized as a stochiometric reagent, however, this study demonstrates a platform that may lead to catalytic application of alkyne reduction by Sn-H utilizing H_2 (g).[41]

Finally, the oxidative addition chemistry revealed by the novel low valent μ_3-SnH capped trinuclear nickel cluster **2** raises the question of electronics pertaining to this species. Cyclic voltammetry (CV) of a solution of **2** in THF revealed two reversible, one-electron oxidations (at E = -0.8, -1.3 V *vs.* $[Cp_2Fe]^{0/+}$) and one partially-reversible one electron reduction process (E = -2.7 V) *vs.* $[Cp_2Fe]^{0/+}$ (See Appendix A for CV: Figures 2.32-2.36). Complex **2** is a formally 44-electron trinuclear cluster of the *closo* structural class and is therefore electronically deficient in

accordance with Wade's rules.[45, 46] To elucidate the nature of these oxidation events, we computed molecular orbitals of **2** (Figure 2.3). Analysis of the computed MOs suggests that the oxidation events involve depleting electron density from the d-orbital based Ni–Ni antibonding interactions, thereby providing relief from antibonding instability. The reduction process is best described as the introduction of electron density into the LUMO, which features electron density shared between the Ni_3 core and Sn and d-orbital based Ni-Ni antibonding interations. This is expected to increase Ni–Ni antibonding instability in the complex, which is consistent with the partial irreversibility observed for the redox process observed in the CV. Together, the electrochemical and DFT results of **2** suggest frontier d-orbitals interactions centered at the Ni_3 core. Given that the coordination environment around the Ni_3 cluster does not allow for activation by the Ni_3 center, we propose these charge states may be mediated through the Sn center, potentially enabling the oxidative addition and unique hydrogenation chemistry displayed here.

2.3 Conclusion

In summary, this report describes the synthesis and structural analysis of a divalent Sn–H capped trinuclear nickel cluster. This cluster features three chemically reversible redox processes and may represent an example of a general and useful platform for isolating Sn–H species to investigate their electronic properties and chemical reactivity in greater detail. Cluster **2** displays a breadth of reactivity, including oxidative addition of alkyl halides and insertion of alkynes. Furthermore, the alkyne insertion product, **5**, was found to undergo hydrogenation chemistry with H_2 (g) to reform the starting material, **2**, and hexane in 21% yield. While these reactivity studies are comparable to other tin (II) species that feature insertion of alkynes and oxidative addition at Sn; to our knowledge, we report the first example of tin (II) hydrogenation of the hydrostannylated alkyne.[34, 42-44] This demonstrates a platform that may lead to catalytic applications for the Sn-H mediated hydrogenation of unsaturated organic molecules. Ongoing studies of **2**, **3**, **4** and **5** are

focused on Mössbauer characterization, DFT modeling and further chemical reactivity experiments. Results will be reported separately.

2.4 Acknowledgments

Chapter 2, in full, is a reprint of the material as it appears in Torquato, N.A.; Palasz, J.M.; Bertrand, Q.C.; Brunner, F.M.; Chan, T; Gembicky, M.; Mrse, A.A.; Kubiak, C.P. "Synthesis, structure and reactivity of μ_3-SnH capped trinuclear nickel cluster," *Chem. Sci.*, 2022, 13, 11382-11387. N. A. T. acknowledges Micah Ziegler for invaluable discussions. N. A. T. acknowledges support from NSF for a Graduate Research Fellowship. Financial support from NSF is also gratefully acknowledged (CHE-1853908). The authors thank Theresa Block, Aylin Koldemir, and Rainer Pöttgen for Mössbauer investigations. The dissertation author was the primary investigator and author of this paper.

2.5 References

1. A. G. Davies, Organotin chemistry, John Wiley & Sons, 2006.

2. M. Pereyre, J.-P. Quintard and A. Rahm, Tin in organic synthesis, Butterworth-Heinemann, 2013.

3. E. Rivard, R. C. Fischer, R. Wolf, Y. Peng, W. A. Merrill, N. D. Schley, Z. Zhu, L. Pu, J. C. Fettinger, S. J. Teat, I. Nowik, R. H. Herber, N. Takagi, S. Nagase and P. P. Power, J. Am. Chem. Soc., 2007, 129, 16197-16208.

4. B. E. Eichler and P. P. Power, J. Am. Chem. Soc., 2000, 122, 8785-8786.

5. Y. Peng, B. D. Ellis, X. Wang and P. P. Power, J. Am. Chem. Soc., 2008, 130, 12268-12269.

6. S. Wang, M. L. McCrea-Hendrick, C. M. Weinstein, C. A. Caputo, E. Hoppe, J. C. Fettinger, M. M. Olmstead and P. P. Power, J. Am. Chem. Soc., 2017, 139, 6586-6595.

7. S. Wang, M. L. McCrea-Hendrick, C. M. Weinstein, C. A. Caputo, E. Hoppe, J. C. Fettinger, M. M. Olmstead and P. P. Power, J. Am. Chem. Soc., 2017, 139, 6596-6604.

8. J. Schneider, C. P. Sindlinger, K. Eichele, H. Schubert and L. Wesemann, J. Am. Chem. Soc., 2017, 139, 6542-6545.

9. E. Rivard and P. P. Power, Dalton Trans., 2008, 4336-4343.

10. A. Jana, H. W. Roesky, C. Schulzke and P. P. Samuel, Organometallics, 2010, 29, 4837-4841.

11. A. Jana, H. W. Roesky, C. Schulzke and A. Döring, Angew. Chem. Int. Ed., 2009, 48, 1106-1109.

12. T. J. Hadlington, M. Hermann, G. Frenking and C. Jones, J. Am. Chem. Soc., 2014, 136, 3028-3031.

13. O. T. Summerscales, C. A. Caputo, C. E. Knapp, J. C. Fettinger and P. P. Power, J. Am. Chem. Soc., 2012, 134, 14595-14603.

14. S. Wang, T. J. Sherbow, L. A. Berben and P. P. Power, J. Am. Chem. Soc., 2018, 140, 590-593.

15. A. V. Protchenko, J. I. Bates, L. M. A. Saleh, M. P. Blake, A. D. Schwarz, E. L. Kolychev, A. L. Thompson, C. Jones, P. Mountford and S. Aldridge, J. Am. Chem. Soc., 2016, 138, 4555-4564.

16. S. M. I. Al-Rafia, A. C. Malcolm, S. K. Liew, M. J. Ferguson and E. Rivard, J. Am. Chem. Soc., 2011, 133, 777-779.

17. S. M. I. Al-Rafia, O. Shynkaruk, S. M. McDonald, S. K. Liew, M. J. Ferguson, R. McDonald, R. H. Herber and E. Rivard, Inorg. Chem., 2013, 52, 5581-5589.

18. J.-J. Maudrich, M. Widemann, F. Diab, R. H. Kern, P. Sirsch, C. P. Sindlinger, H. Schubert and L. Wesemann, Eur. J. Chem., 2019, 25, 16081-16087.

19. Q. Zhu, J. C. Fettinger and P. P. Power, Dalton Trans., 2021, 50, 12555-12562.

20. M. M. D. Roy, A. A. Omaña, A. S. S. Wilson, M. S. Hill, S. Aldridge and E. Rivard, Chem. Rev., 2021, 121, 12784-12965.

21. S. M. I. Al-Rafia, A. C. Malcolm, R. McDonald, M. J. Ferguson and E. Rivard, Angew. Chem. Int. Ed., 2011, 50, 8354-8357.

22. P. P. Power, Nature, 2010, 463, 171-177.

23. Q. Zhao, T. D. Harris and T. A. Betley, J. Am. Chem. Soc., 2011, 133, 8293-8306.

24. E. V. Eames and T. A. Betley, Inorg. Chem., 2012, 51, 10274-10278.

25. B. K. Breedlove, P. E. Fanwick and C. P. Kubiak, Inorg. Chem., 2002, 41, 4306-4308.

26. E. Simón-Manso and C. P. Kubiak, Angew. Chem. Int. Ed., 2005, 44, 1125-1128.

27. A. R. Leverett, V. Diachenko, M. L. Cole and A. I. McKay, Dalton Trans., 2019, 48, 13197-13204.

28. T. J. Hadlington, M. Hermann, J. Li, G. Frenking and C. Jones, Angew. Chem. Int. Ed., 2013, 52, 10199-10203.

29. V. M. S. Gil and W. Von Philipsborn, Magn. Reson. Chem., 1989, 27, 409-430.

30. B. Wrackmeyer, in Annual Reports on NMR Spectroscopy, ed. G. A. Webb, Academic Press, 1999, vol. 38, pp. 203-264.

31. R. E. Wasylishen and N. Burford, Can. J. Chem., 1987, 65, 2707-2712.

32. C. P. Sindlinger and L. Wesemann, *Chem. Sci.*, 2014, **5**, 2739-2746.

33. L. W. Pineda, V. Jancik, K. Starke, R. B. Oswald and H. W. Roesky, *Angew. Chem. Int. Ed.*, 2006, **45**, 2602-2605.

34. M. J. S. Gynane, M. F. Lappert, S. J. Miles and P. P. Power, *J. Chem. Soc., Chem. Comm.*, 1976, 256-257.

35. A. C. Filippou, A. I. Philippopoulos and G. Schnakenburg, *Organometallics*, 2003, **22**, 3339-3341.

36. A. C. Filippou, D. Hoffmann and G. Schnakenburg, *Chem. Sci.*, 2017, **8**, 6290-6299.

37. J. D. Queen, A. C. Phung, C. A. Caputo, J. C. Fettinger and P. P. Power, *J. Am. Chem. Soc.*, 2020, **142**, 2233-2237.

38. M. Widemann, K. Eichele, H. Schubert, C. P. Sindlinger, S. Klenner, R. Pöttgen and L. Wesemann, *Angew. Chem. Int. Ed.*, 2021, **60**, 5882-5889.

39. A. C. Filippou, P. Ghana, U. Chakraborty and G. Schnakenburg, *J. Am. Chem. Soc.*, 2013, **135**, 11525-11528.

40. A. C. Filippou, P. Portius, A. I. Philippopoulos and H. Rohde, *Angew. Chem. Int. Ed.*, 2003, **42**, 445-447.

41. M. Alami, A. Hamze and O. Provot, *ACS Catal.*, 2019, **9**, 3437-3466.

42. M. L. McCrea-Hendrick, S. Wang, K. L. Gullett, J. C. Fettinger and P. P. Power, *Organometallics*, 2017, **36**, 3799-3805.

43. T. J. Hadlington, M. Hermann, G. Frenking and C. Jones, *Chem. Sci.*, 2015, **6**, 7249-7257.

44. S. K. Mandal and H. W. Roesky, *Acc. Chem. Res.*, 2012, **45**, 298-307.

45. K. Wade, *Chem. Commun.*, 1971, 792-793.

46. D. M. P. Mingos, *Nat. Phys. Sci.*, 1972, **236**, 99-102.

2.6. Appendix A

2.6.1 Experimental General Considerations

General considerations

All reactions and manipulations were carried out under an atmosphere of nitrogen using either Schlenk line techniques or VAC glovebox. Solvents were sparged with nitrogen, dried on a custom dry solvent system over alumina columns, and stored over molecular sieves before use. $SnCl_2$ (anhydrous), $Ni(COD)_2$, bis(diphenylphosphino)methane (dppm), $Ni(acac)_2$, $NaB(Et)_3H$ (1.0 M solution in THF) were obtained from commercial suppliers and used without further purification. Benzene-d_6 and THF-d_8 was stored under nitrogen over 3Å molecular sieves. $Cl_3SnNi_3(dppm)_3Cl$, **1**, was prepared according to literature procedures.[1]

Analytical methods.

Carbon, hydrogen, and nitrogen elemental analyses were performed by Midwest Microlab and Robertson Microlit Laboratories.

NMR Spectroscopy.

^{1}H and ^{31}P were recorded on a Jeol 500 MHz spectrometer. ^{13}C and ^{119}Sn NMR spectra were recorded on a Jeol 400 MHz and Varian 500 MHz Spectrometers. ^{1}H chemical shifts are reported relative to the residual hydrogen atoms in benzene-d_6 solvent. ^{31}P chemical shifts are reported relative to 85% H_3PO_4.^{119}Sn NMR was referenced externally to $SnBu_4$ in benzene-d_6 {-11.7ppm}.

X-ray Crystallography.

Single crystal X-ray diffraction of complex **2** was performed using Bruker APEX-II Ultra CCD diffractometer equipped with Mo Kα radiation (λ= 0.71073 Å). Single crystal X-ray diffraction of complex **3** and **4** was performed using Bruker X8-ApexII CCD Sealed Tube equipped with Mo Kα radiation (λ= 0.71073 Å). Finally, single crystal X-ray diffraction of complex **5** was performed using Bruker/Nonius Microstar 592 equipped with Cu Kα radiation (λ= 1.54 Å). Crystals were

mounted on a Cryoloop with Paratone oil. Data were collected in a nitrogen gas stream at 100(2) K using f and v scans. The data were integrated using the Bruker SAINT software program and scaled using the SADABS software program. Solution by direct methods (SHELXT[2]) produced a complete phasing model consistent with the proposed structure. All nonhydrogen atoms were refined anisotropically by full-matrix least-squares (SHELXL-2014).[2] For highly disordered diethyl ether and pentane molecules, the PLATON routine SQUEEZE[3] or a solvent mask was used to account for the corresponding electrons as a diffuse contribution to the overall scattering without specific atom positions. To stabilize the disorder present in these molecule RIGU and SADI commands were used accordingly.

Electrochemistry.

All electrochemical experiments were performed inside a VAC glovebox. These experiments were performed in 0.3 M [$^{n}Bu_4N$][PF_6] solution in THF using BASi Epislon potentiostat. A single-compartment cell was used for cyclic voltammetry experiments with a glassy carbon working electron (3 mm in diameter, Bioanalytical Systems, Inc.), glassy carbon counter electrode, and Ag/AgCl pseudo-reference electrode. All potentials are referenced to the $Fc^{+/0}$ couple using ferrocene as an internal reference.

UV-Vis Spectroscopy

UV-visible spectra were collected on a Shimadzu UV-3600 UV/vis/NIR spectrometer. Samples for determination were taken in 1 cm path length quartz cuvettes.

Density Function Theory (DFT) Calculations.

Calculations of geometry optimization, frequency, and energy were performed using Gaussian software suite (version g16.B01). The B3LYP functional with default spin parameters and the LANL2DZ basis set were used. Geometry optimizations were performed starting from XYZ

coordinates adapted from the reported crystal structure of the $HSnNi_3(dppm)_3H$ cluster. Optimizations were done with tight convergence criteria, and no restrictions or constraints were places on any of the calculated structures. NBO analyses were done with the built in NBO suites of Gaussian.

2.6.2 Synthesis

Synthesis of [$Ni_3(dppm)_3(\mu_3\text{-}H)(\mu_3\text{-}SnH)$], 2: A solution $NaBEt_3H$ (1.26 mL, 1.25 mmol, 1.0 M in THF) was added dropwise to a solution of **1** (500.0 mg, 0.3145 mmol) dissolved in THF (10 mL) at 22 °C. After 1 h. the complete conversion of starting material was observed by $^{31}P\{^1H\}$ NMR spectroscopy. Volatile compounds were removed *in vacuo* to afford a brown residue, which was then dissolved in benzene and filtered over a Celite plug to remove undissolved solids (presumably including NaCl). The solution was then concentrated to 2 mL and then layered with pentane (approx. 18 mL). After 2 days at 22 °C, a dark brown solid formed, and the yellowish-orange supernatant was carefully decanted. The solid was triturated with pentane (3 x 5 mL). After the solid was allowed to settle, the supernatant was carefully decanted; residual volatile compounds were removed *in vacuo* to yield **2** as a brown powder (400.7 mg, 0.2763 mmol, 88% yield). Vapor diffusion of diethyl ether into a THF solution of **2** at -20 °C afforded X-ray quality crystals. ^1H NMR (500.16 MHz, C_6D_6, 298 K) δ 7.53 (d, J = 7.1 Hz, 12H, ArH), 7.15 (m, 12H, ArH), 6.95 – 6.83 (m, 24H, ArH), 6.77 (t, J = 7.5 Hz, 12H, ArH), 3.61 (d, J = 13.9 Hz, 3H, $P(CH_2)P$), 3.41 (d, J = 15.2 Hz, 3H, $P(CH_2)P$)), -0.42 (s, $J_{(119/117Sn)}$ = 341.8 Hz, 1H, SnH), -0.86 (h, J = 8.5 Hz, 1H, NiH). ^{13}C NMR (100.56 MHz, C_6D_6) δ 141.5 (Ar), 139.1 (Ar), 133.9 (Ar), 132.4 (Ar), 127.6 (Ar), 45.3 ($P(CH_2)P$). $^{31}P\{^1H\}$ NMR (202.47 MHz, C_6D_6, 298 K): δ 23.4. ^{119}Sn NMR (149.13 MHz, C_6D_6, 298 K) δ 2939.4 (d, J = 346.7 Hz) $^{119}Sn\{^1H\}$ NMR (C_6D_6, 149.13 MHz, 298 K): δ 2939.4 (s). Elemental analysis (%) calcd for $C_{75}H_{68}Ni_3P_6Sn$: C 62.12, H 4.72; found: C 60.35, H 4.87. Repeated attempts did not provide a more satisfactory combustion analysis. We attribute

this to this complex being highly air sensitive. Although **2** did not meet the 0.4% journal requirement for elemental analysis, quantitative ^{1}H NMR was used to describe the purity of **2**. Integration of the dppm resonances on **2** against the methyl resonance on tetramethylbenzene depict 96.9% purity (S24).

Synthesis of [Ni$_3$(dppm)$_3$(μ$_3$-H)(μ$_3$-Sn((Br)(H)(CH$_2$CH$_3$))], 3:

Bromoethane (3.0 ul, 0.040 mmol) in 2 ml THF at -20°C was added dropwise to a solution of **2** (60.0 mg, 0.0414 mmol) dissolved in THF (3 mL) at -20°C. After 30 min. the complete conversion of starting material was observed by ^{31}P{^{1}H} NMR spectroscopy. The red solution was vacuumed down to 2 mL and then layered with pentane (approx. 18 mL). After 2 days at -20°C, dark red crystals formed, and the brown supernatant was carefully decanted. The solid was triturated with pentane (3 x 3 mL). After the solid was allowed to settle, the supernatant was carefully decanted; residual volatile compounds were removed *in vacuo* to yield **3** as a dark red powder (48.5 mg, 0.0311 mmol, 75% yield). Layering of pentane over a THF solution of **3** at -20 °C afforded X-ray quality crystals. ^{1}H NMR (500.16 MHz, C_6D_6, 298 K) δ 8.78 (s, 1H, SnH), 7.74 (s, 6H, ArH), 7.55 (s, 6H, ArH), 7.18 (s, 8H, ArH), 6.95 – 6.70 (m, 40H, ArH), 5.14 (s, 3H, P(CH$_2$)P), 3.80 (d, *J* = 13.0 Hz, 3H, P(CH$_2$)P), 2.14 (t, *J* = 7.5 Hz, 3H, CH$_3$CH$_2$Sn),1.54 (s, 1H, CH$_3$CH$_2$Sn), 0.79 (s, 1H, CH$_3$CH$_2$Sn), -4.79 (h, *J* = 9.4 Hz, 1H, NiH). ^{13}C NMR (100.56 MHz, C_6D_6)) δ 136.1 (Ar), 135.6 (Ar), 132.2 (Ar), 132.1 (Ar), 129.1 (Ar), 128.8 (Ar), 127.6 (Ar), 127.0 (Ar), 51.3 (P(CH$_2$)P), 22.7 (CH$_3$CH$_2$Sn), 17.0 (CH$_3$CH$_2$Sn). ^{31}P{^{1}H} NMR (202.47 MHz, C_6D_6, 298 K): δ 4.2. ^{119}Sn NMR (149.13 MHz, C_6D_6, 298 K): δ 248.0 (d, *J* = 993.6 Hz)^{119}Sn{^{1}H} NMR (C_6D_6, 149.13 MHz, 298 K): δ 247.8. (s). UV-Vis λmax (benzene)/nm 734 and 497 (ε/dm^3 mol^{-1} cm^{-1} 7110, 7380. Elemental analysis (%) calcd for $C_{77}H_{73}BrNi_3P_6Sn$: C 59.33 H 4.72; found: C 56.78, H 4.33. Repeated attempts did not provide a more satisfactory combustion analysis. We attribute this to this complex

being highly air sensitive. Although **3** did not meet the 0.4% journal requirement for elemental analysis, quantitative ^{1}H NMR was used to describe the purity of **3**. Integration of the Ni-H resonance on **3** against the methyl resonance on tetramethylbenzene depict 95.0% purity (S25).

Synthesis of [Ni$_3$(dppm)$_3$(μ$_3$-I)(μ$_3$-Sn(CH$_2$CH$_3$)], 4:

Iodoethane (7.0 ul, 0.087 mmol) was added to a solution of **2** (128.8 mg, 0.08883 mmol) dissolved in benzene (2 mL) at 22°C. After 30 min. the complete conversion of starting material was observed by ^{31}P{^{1}H} NMR spectroscopy. The brownish-red solution was then layered with pentane (approx. 18 mL). After 2 days at 22°C, dark brownish-red crystals formed, and the reddish-brown supernatant was carefully decanted. The solid was triturated with pentane (3 x 5 mL). After the solid was allowed to settle, the supernatant was carefully decanted; residual volatile compounds were removed *in vacuo* to yield **4** as a brownish red powder (133.3 mg, 0.08311 mmol, 94% yield). Layering of pentane over a benzene solution of **4** at 22°C afforded X-ray quality crystals. ^{1}H NMR (500.16 MHz, C_6D_6, 298 K) δ 7.36 (d, *J* = 7.3 Hz, 12H, ArH), 7.30 (d, *J* = 7.2 Hz, 12H, ArH), 6.85 (q, *J* = 7.2 Hz, 8H, ArH), 6.80 (t, *J* = 7.2 Hz, 16H, ArH), 6.75 (t, *J* = 7.8 Hz, 12H, ArH), 3.02 (d, *J* = 13.3 Hz, 3H, P(CH$_2$)P), 2.82 (d, *J* = 13.4 Hz, 3H, P(CH$_2$)P), 2.17 (t, *J* = 8.0 Hz, 3H, SnCH$_2$CH$_3$), 1.29 (q, *J* = 8.4 Hz, 2H, SnCH$_2$CH$_3$).^{13}C NMR (100.56 MHz, C_6D_6) δ 139.1 (Ar), 138.1 (Ar), 133.6 (Ar), 132.6 (Ar), 128.6 (Ar), 127.5 (Ar), 127.3 (Ar), 39.0 (P(CH$_2$)P), 35.6 (SnCH$_2$CH$_3$), 9.6 (SnCH$_2$CH$_3$). ^{31}P{^{1}H} NMR (202.47 MHz, C_6D_6, 298 K): δ 34.1. ^{119}Sn NMR (149.13 MHz, C_6D_6, 298 K) δ 2115.1 (s). Elemental analysis (%) calcd for $C_{83}H_{77}INi_3P_6Sn$ (**4**·C_6H_6): C 59.26, H 4.61; found: C 59.38, H 4.91. One molecule of benzene is shown in cif of complex **4**.

Synthesis of [$Ni_3(dppm)_3(\mu_3\text{-}H)(\mu_3\text{-}Sn(C_6H_{11})$], 5:

1-hexene (10.0 ul, 0.0877) was added to a solution of **2** (128.8 mg, 0.08883 mmol) dissolved in benzene (3 mL) at 22°C. After 30 min. the complete conversion of starting material was observed by $^{31}P\{^1H\}$ NMR spectroscopy. Volatile compounds were removed *in vacuo* to afford a brown residue, which was then dissolved in diethyl ether (2 mL), filtered, and then layered with pentane (approx. 18 mL). After 2 days at -20°C, dark brown crystals formed, and the brown supernatant was carefully decanted. The solid was triturated with pentane (3 x 5 mL). After the solid was allowed to settle, the supernatant was carefully decanted; residual volatile compounds were removed *in vacuo* to yield **5** as a brown powder (133.4 mg, 0.08707 mmol, 98% yield). Vapor diffusion of pentane into a diethyl ether solution of **2** at -20 °C afforded X-ray quality crystals. ^1H NMR (500.16 MHz, C_6D_6, 298 K) δ 7.48 (d, *J* = 6.6 Hz, 12H, ArH), 7.38 (d, *J* = 7.3 Hz, 12H, ArH), 6.95 – 6.86 (m, 24H, ArH), 6.79 (t, *J* = 7.5 Hz, 12H, ArH), 6.04 (s, 1H, CH_2CSn), 5.43 (s, 1H, CH_2CSn), 3.82 – 3.34 (m, 6H, $P(CH_2)P$), 2.24 (t, *J* = 7.8 Hz, 2H, CCH_2CH_2), 1.40 (q, *J* = 7.7 Hz, 2H, $CH_2CH_2CH_2$), 1.23-1.16 (m, 2H $CH_2CH_2CH_3$), 0.88 (t, *J* = 7.4 Hz, 3H, CH_2CH_3), -3.54 – -3.62 (m, 1H, NiH). ^{13}C NMR (100.56 MHz, C_6D_6) δ 180.3 (CH_2CSn), 141.7 (Ar), 139.4 (Ar), 133.9 (Ar), 132.9 (Ar), 127.4 (Ar), 119.7 (CH_2CSn), 43.6 ($P(CH_2)P$), 41.3 (CCH_2CH_2), 32.5 ($CH_2CH_2CH_2$), 23.0 ($CH_2CH_2CH_3$), 14.5 (CH_2CH_3). $^{31}P\{^1H\}$ NMR (202.47 MHz, C_6D_6, 298 K): δ 31.0. ^{119}Sn NMR (149.13 MHz, C_6D_6, 298 K) δ 1837.8 (s). Elemental analysis (%) calcd for $C_{82}H_{80}Ni_3P_6Sn$ (**5**·(1/6)C_5H_{12}) : C 64.38, H 5.65; found: C 63.78, H 5.22. (1/6 of a pentane molecule was observed in ^1H NMR of the material sent out for EA. We observed difficulties removing pentane even after drying overnight.)

Hydrogenation of 5 to 2.

A thick-walled NMR tube was charged with complex **5** (10.4 mg, 0.00679 mmol), an internal reference, tetramethylbenzene (1.4 mg, 0.010 mmol), and 0.1 ml THF-d_8. The tube was cycled onto the Schlenk line, freeze-pump-thawed 3x, and cooled to liquid nitrogen temperatures, -196°C. H_2 (g) was added to the NMR tube at -196°C, resulting in the addition of 3.8 atm of H_2 (g). This was allowed to warm up to 22°C and tracked via ^{1}H and ^{31}P NMR spectroscopy over time. Over the course of 24 hours, complex **5** converted to complex **2** and hexane in 21% yield, as determined by ^{1}H NMR integration of the P(CH_2)P, SnH and NiH resonances against tetramethylbenzene.

Decomposition of 5 in THF-d_8.

A thick-walled NMR tube was charged with complex **5** (10.4 mg, 0.00679 mmol), an internal reference, tetramethylbenzene (1.4 mg, 0.010 mmol), and 0.1 ml THF-d_8. Over the course of 24 hours, complex **5** decomposed by 92% as determined by ^{1}H NMR integration of the P(CH_2)P, SnH and NiH resonances against tetramethylbenzene.

Procedure for Quantitative ^{1}H NMR Analysis. A known mass of internal reference (tetramethylbenzene) and a known mass of compound (**2**, **3**, or **5**) was obtained. The corresponding masses yield the mol ratio of reference to compound in solution. The integration of the corresponding peaks of the reference and compound in ^{1}H NMR yield the mol ratio of these species. The division of the mol ratio using the mol ratio of the integration values over the known mol ratio (given by mass) multiplied by 100 gives the percent purity. General Comments on Assessing Purity of the Compounds in this Study. Quantitative ^{1}H NMR (qHNMR) provides a powerful methodology for the determination of purity of novel compounds. qHNMR allows for the determination of purity of chemical compounds containing NMR active protons, providing a

coupled assessment of molecular structure and purity, with sensitivity and precision rivalling and often surpassing traditional techniques such as elemental analysis. The power of the technique comes from the ability to not just calculate the mass percentage of detectable protons, but to do so with structurally meaningful spectra, verifying both the quantity and character of protons within the sample simultaneously. The technique is both reliable and sensitive, with reported relative standard deviations typically under 1% for concentrations of analyte in the 1-10 millimolar range.1 The technique has been successfully leveraged to analyze purity of pharmaceutical compound libraries and natural products with good success,[2-4] and thus we have begun incorporating this technique into our array of purity analysis protocols. A qHNMR experiment can be carried out by careful inclusion of an internal standard which is chemically innocent and well resolved from the analyte and can be dissolved in the choice NMR solvent. In many cases, it's feasible to do this assay using the NMR solvent as the internal standard, however it becomes vital to ensure no H/D exchange occurs with the solvent and the analyte, and that the H/D ratio of the carrying solvent is known with good precision. When successfully executed, this technique can have much better precision than elemental analysis, with the largest source of error deriving from the limitations of the laboratory mass balance, rather than the sensitivity of the NMR experiment. This has led the technique to become a competitive metrological technique for purity certification of chemical compounds, as well as the benchmarking of other analytical methods.[5] Within this work we often rely on qHNMR measurements to ensure the purity of our compounds as we believe it is a powerful and convenient methodology compared to elemental analysis, which has come under scrutiny as a modern analytical technique. 6 Several key experimental points need to be noted to ensure the successful employment of the technique. Most importantly, the analyte must be completely soluble at the prepared concentration. Any undissolved compound will lead to a dramatically

underestimated purity compared to the true value. The relaxation delays used in the NMR experiment must be sufficiently long to ensure accurate integration of the resulting spectra. This is typically only an issue in purely organic samples containing no heteroatoms but it is critical to the successful implementation of this technique. A much more detailed account on this technique has been prepared by Schoenberger.[5] In situations where extremely small quantities of material are studied, determination of purity using mass-spectrometry is still the most sensitive technique available, however for most synthetic scale applications qHNMR can prove one of the best options for assessing the purity of prepared compounds. Especially in the study of highly sensitive compounds, elemental analysis has often proven difficult to obtain for even wellbehaved samples where purity was not a serious question, and thus we believe it's appropriate to "pass the torch" to more reliable and informative methodologies such as qHNMR.

References to Section on Assessing Purity

1. Espina, R.; Yu, L.; Wang, J.; Tong, Z.; Vashishtha, S.; Talaat, R.; Scatina, J.; Mutlib, A., Nuclear Magnetic Resonance Spectroscopy as a Quantitative Tool To Determine the Concentrations of Biologically Produced Metabolites: Implications in Metabolites in Safety Testing. Chemical Research in Toxicology 2009, 22 (2), 299-310.

2. Liu, X.; Kolpak, M. X.; Wu, J.; Leo, G. C., Automatic Analysis of Quantitative NMR Data of Pharmaceutical Compound Libraries. Analytical Chemistry 2012, 84 (15), 6914-6918.

3. Gödecke, T.; Napolitano, J. G.; Rodríguez-Brasco, M. F.; Chen, S.-N.; Jaki, B. U.; Lankin, D. C.; Pauli, G. F., Validation of a Generic Quantitative 1H NMR Method for Natural Products Analysis. Phytochemical Analysis 2013, 24 (6), 581-597.

4. Nogueira, R.; Garrido, B. C.; Borges, R. M.; Silva, G. E. B.; Queiroz, S. M.; Cunha, V. S., Development of a new sodium diclofenac certified reference material using the mass balance

approach and 1H qNMR to determine the certified property value. European Journal of Pharmaceutical Sciences 2013, 48 (3), 502-513.

5. Schoenberger, T., Determination of standard sample purity using the high-precision 1HNMR process. Analytical and Bioanalytical Chemistry 2012, 403 (1), 247-254.

2.6.3 NMR Spectra

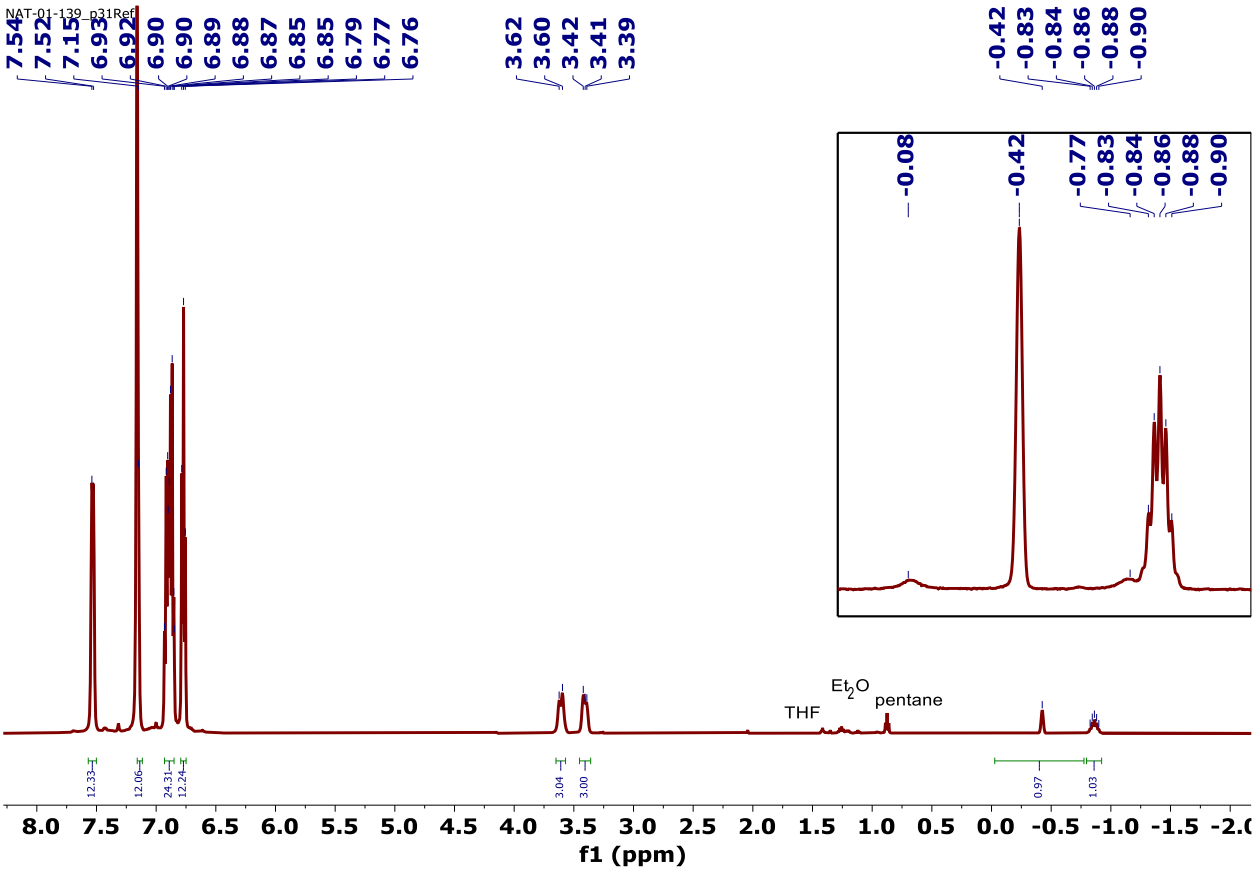

Figure 2.7. ^{1}H NMR spectrum of $[Ni_3(dppm)_3(\mu_3\text{-}H)(\mu_3\text{-}SnH)]$, **2**, in C_6D_6. There is an overlap of the residual hydrogen peak in C_6D_6 with a phenyl peak in **2**.

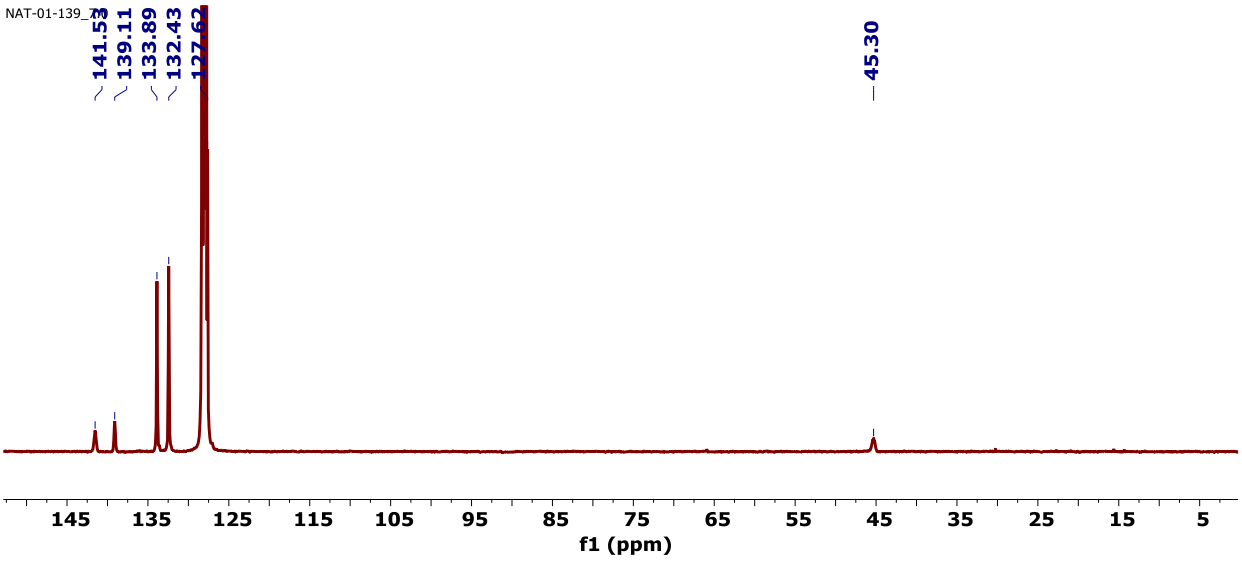

Figure 2.8. ^{13}C NMR spectrum of $[Ni_3(dppm)_3(\mu_3\text{-}H)(\mu_3\text{-}SnH)]$, **2**, in C_6D_6. There is an overlap of the residual hydrogen peak in C_6D_6 with phenyl peaks in **2**.

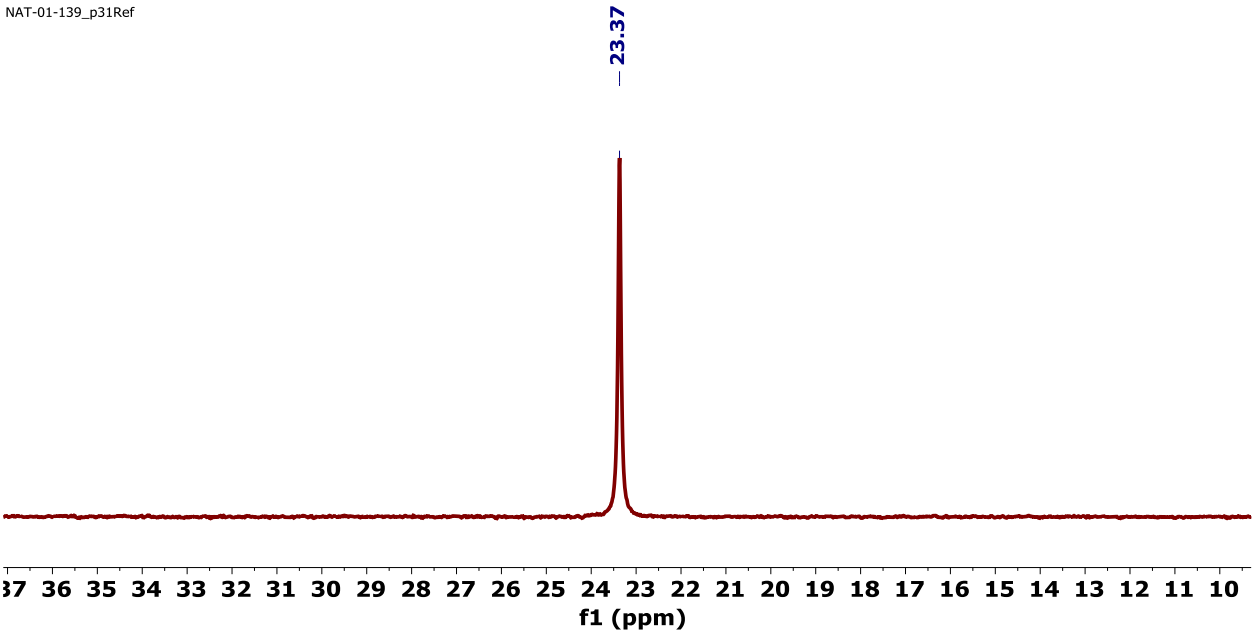

Figure 2.9. ^{31}P NMR spectrum of $[Ni_3(dppm)_3(\mu_3\text{-}H)(\mu_3\text{-}SnH)]$, **2**, in C_6D_6.

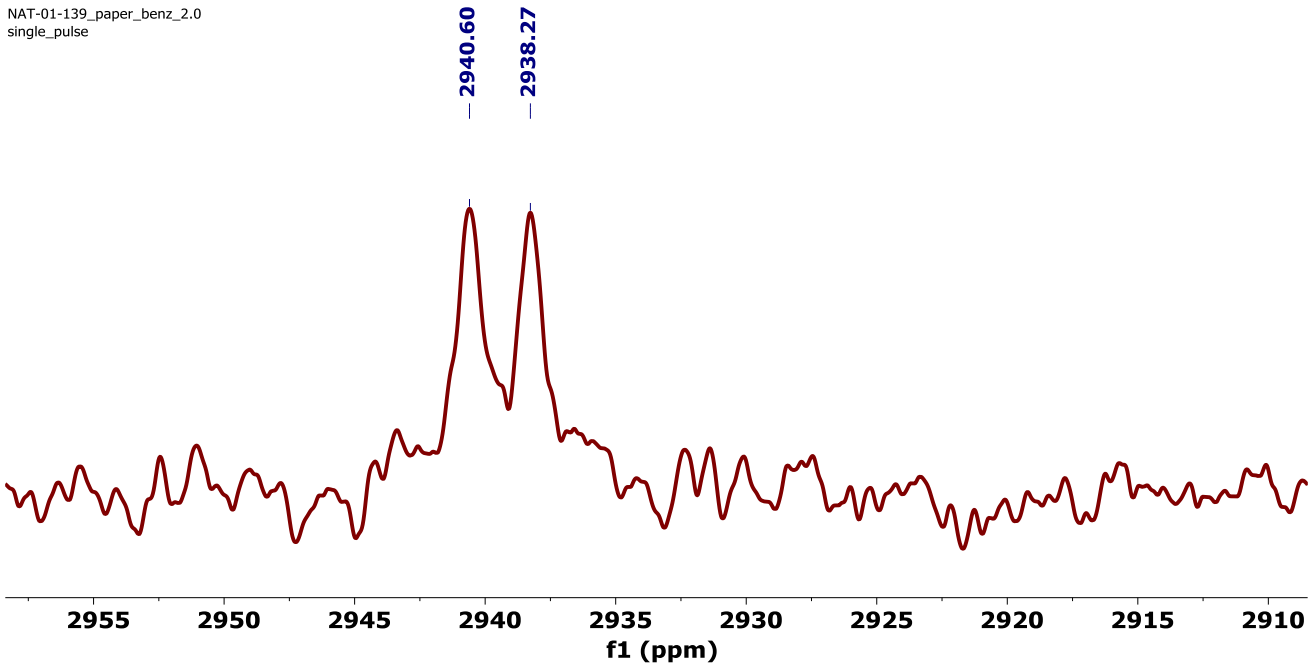

Figure 2.10. ^{119}Sn NMR spectrum of [Ni_3(dppm)$_3$(μ_3-H)(μ_3-SnH)], **2**, in C_6D_6.

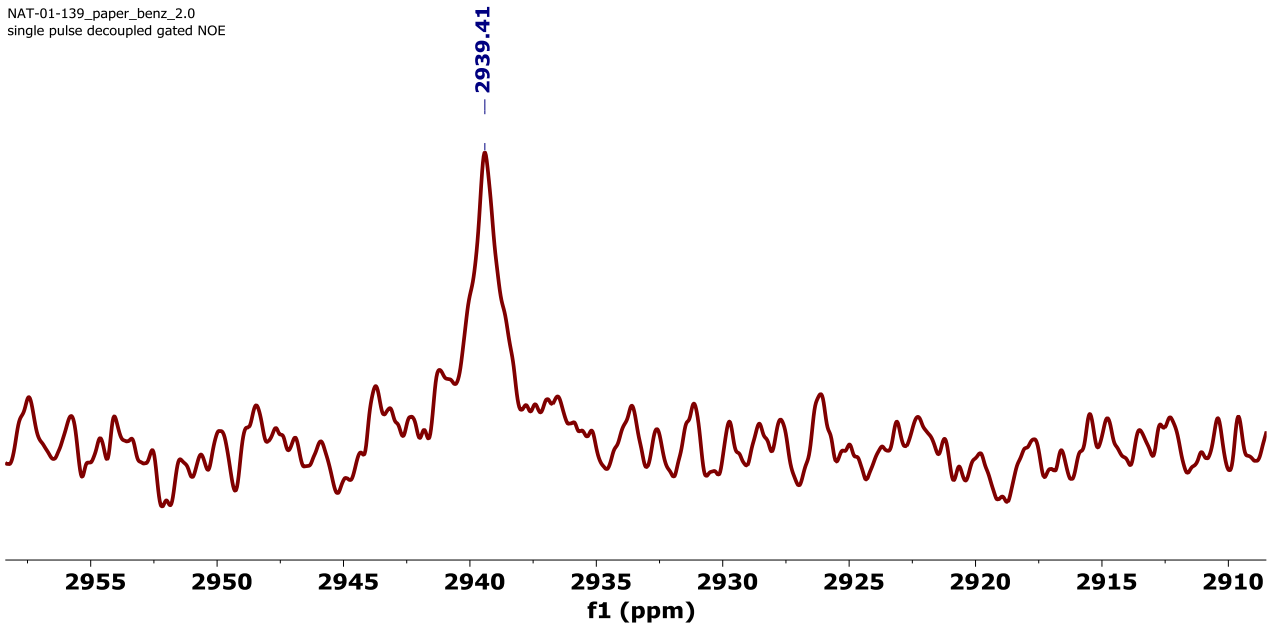

Figure 2.11. ^{119}Sn{^{1}H} NMR spectrum of [Ni_3(dppm)$_3$(μ_3-H)(μ_3-SnH)], **2**, in C_6D_6.

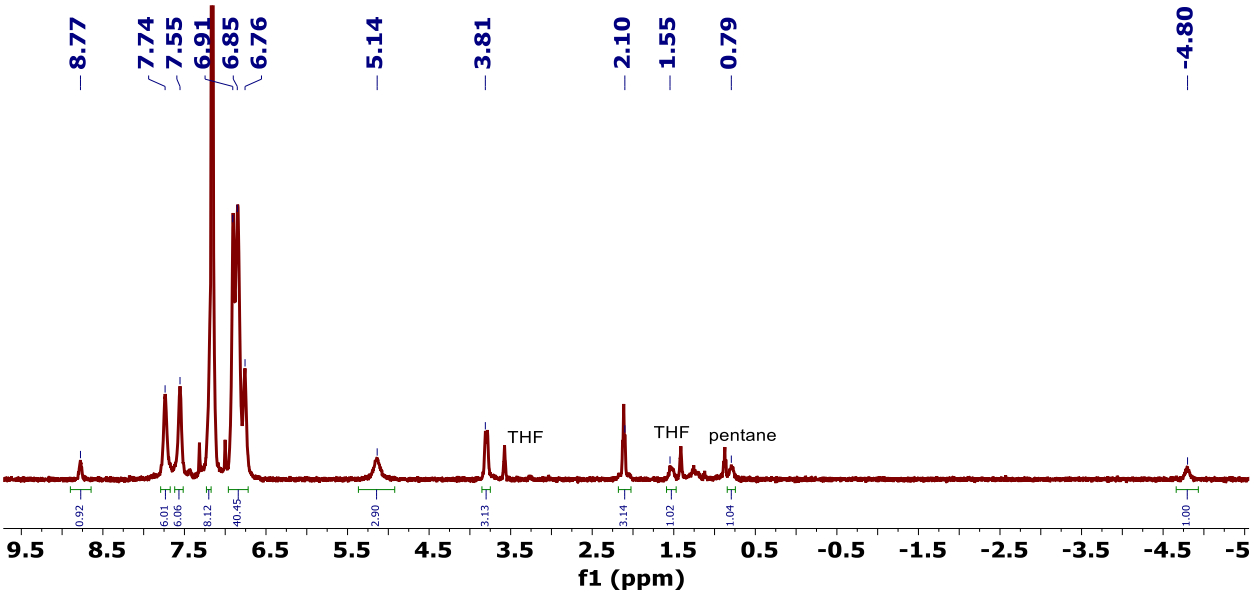

Figure 2.12. ^{1}H NMR spectrum of [Ni_3(dppm)$_3$(μ_3-H)(μ_3-Sn((Br)(H)(CH_2CH_3))], **3**, in C_6D_6. There is an overlap of the residual hydrogen peak in C_6D_6 with a phenyl peak in **3**.

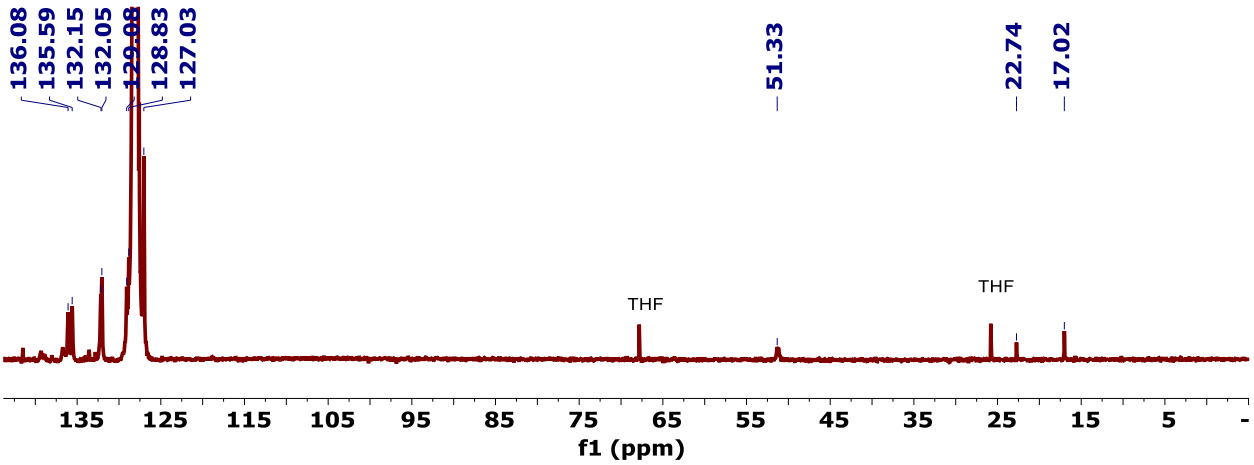

Figure 2.13. ^{13}C NMR spectrum of [Ni_3(dppm)$_3$(μ_3-H)(μ_3-Sn((Br)(H)(CH_2CH_3))], **3**, in C_6D_6. There is an overlap of the residual hydrogen peak in C_6D_6 with a phenyl peak in **3**.

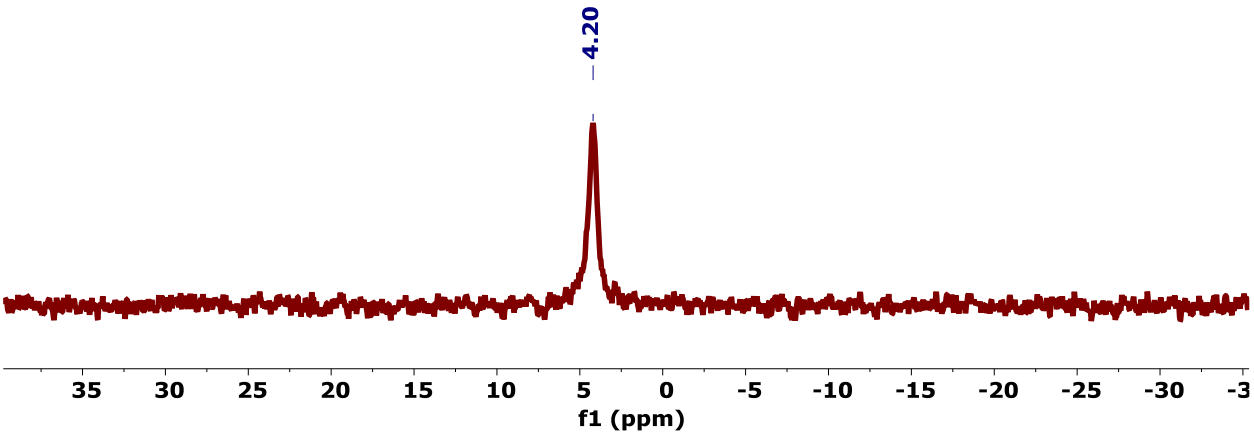

Figure 2.14. ^{31}P NMR spectrum of $[Ni_3(dppm)_3(\mu_3\text{-}H)(\mu_3\text{-}Sn((Br)(H)(CH_2CH_3))]$, **3**, in C_6D_6.

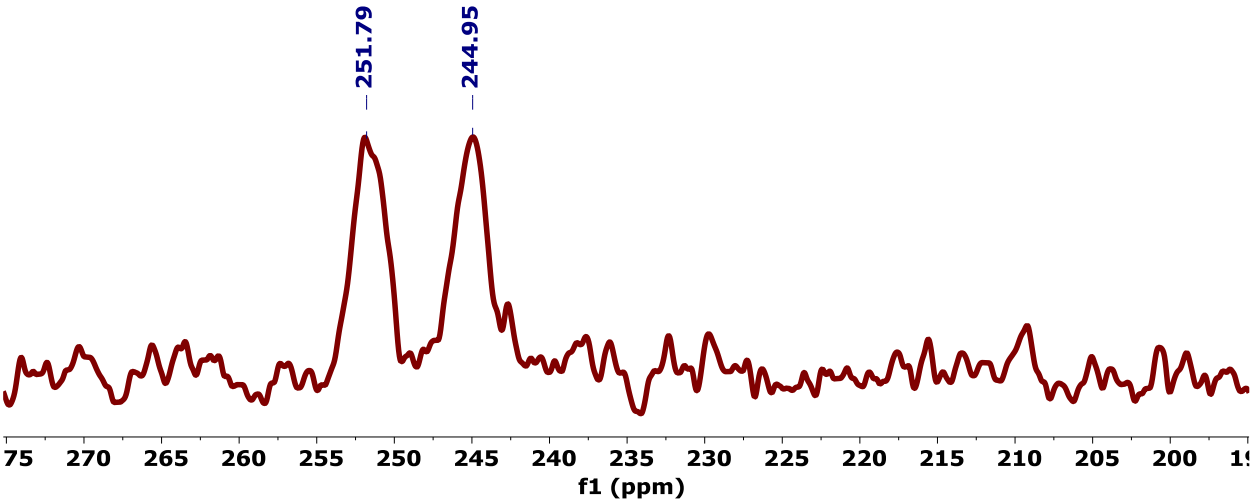

Figure 2.15. ^{119}Sn NMR spectrum of $[Ni_3(dppm)_3(\mu_3\text{-}H)(\mu_3\text{-}Sn((Br)(H)(CH_2CH_3))]$, **3**, in C_6D_6.

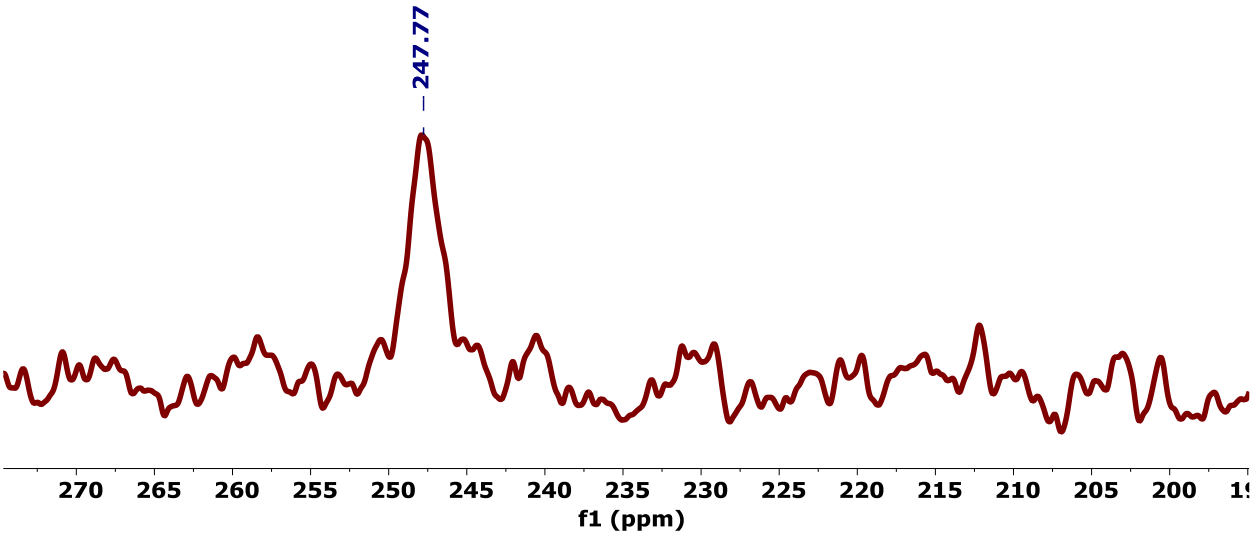

Figure 2.16. $^{119}Sn\{^{1}H\}$ NMR spectrum of $[Ni_3(dppm)_3(\mu_3\text{-}H)(\mu_3\text{-}Sn((Br)(H)(CH_2CH_3))]$, **3**, in C_6D_6.

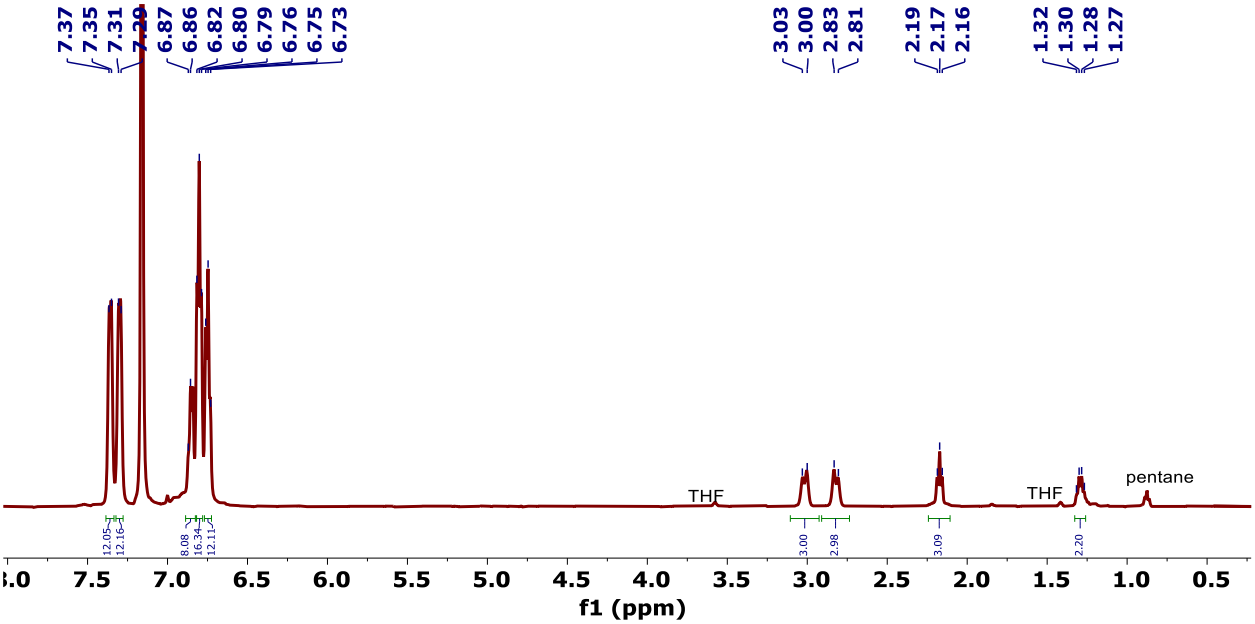

Figure 2.17. ^{1}H NMR spectrum of $[Ni_3(dppm)_3(\mu_3\text{-}I)(\mu_3\text{-}Sn(CH_2CH_3)]$, **4**, in C_6D_6.

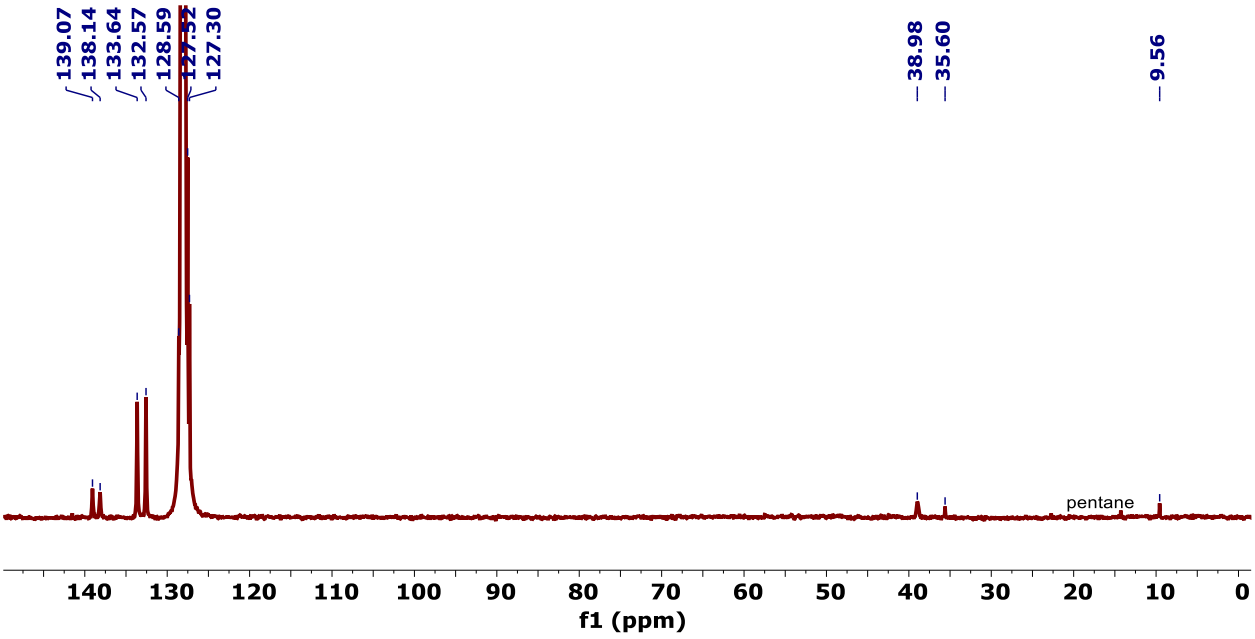

Figure 2.18. ^{13}C NMR spectrum of $[Ni_3(dppm)_3(\mu_3\text{-}I)(\mu_3\text{-}Sn(CH_2CH_3)]$, **4**, in C_6D_6. There is an overlap of the residual hydrogen peak in C_6D_6 with phenyl peaks in **4**.

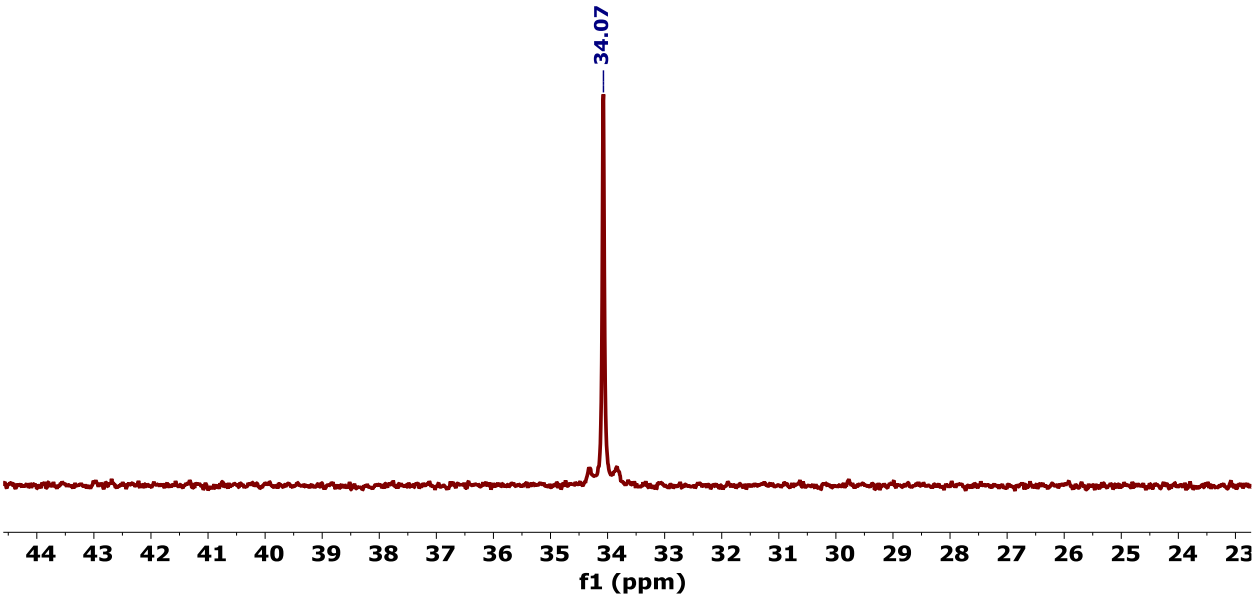

Figure 2.19. ^{31}P NMR spectrum of $[Ni_3(dppm)_3(\mu_3\text{-}I)(\mu_3\text{-}Sn(CH_2CH_3)]$, **4**, in C_6D_6.

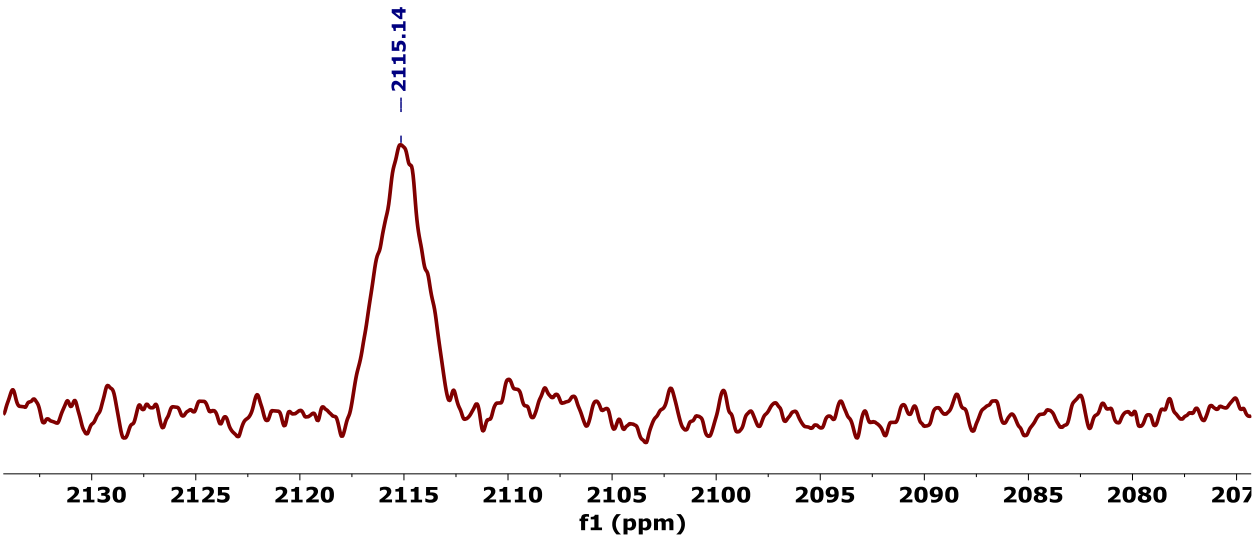

Figure 2.20. ^{119}Sn NMR spectrum of $[Ni_3(dppm)_3(\mu_3\text{-}I)(\mu_3\text{-}Sn(CH_2CH_3)]$, **4**, in C_6D_6.

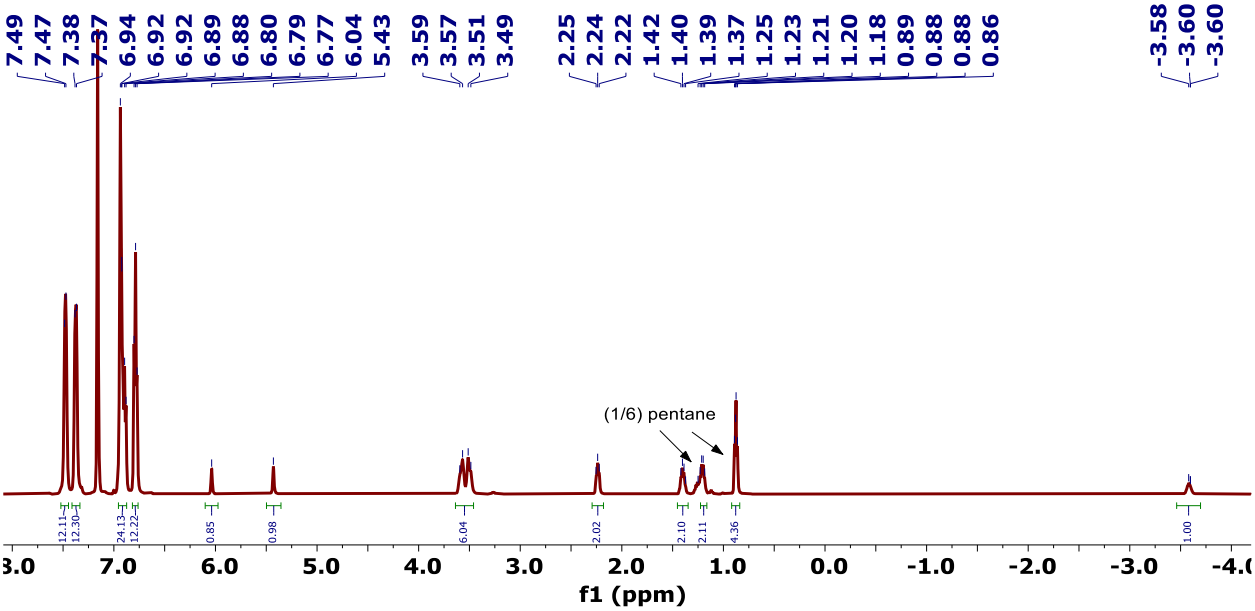

Figure 2.21. ^{1}H NMR spectrum of $[Ni_3(dppm)_3(\mu_3\text{-}H)(\mu_3\text{-}Sn(C_6H_{11})]$, **5**, in C_6D_6. There is an overlap of the residual hydrogen peak in C_6D_6 with a phenyl peak in **5**.

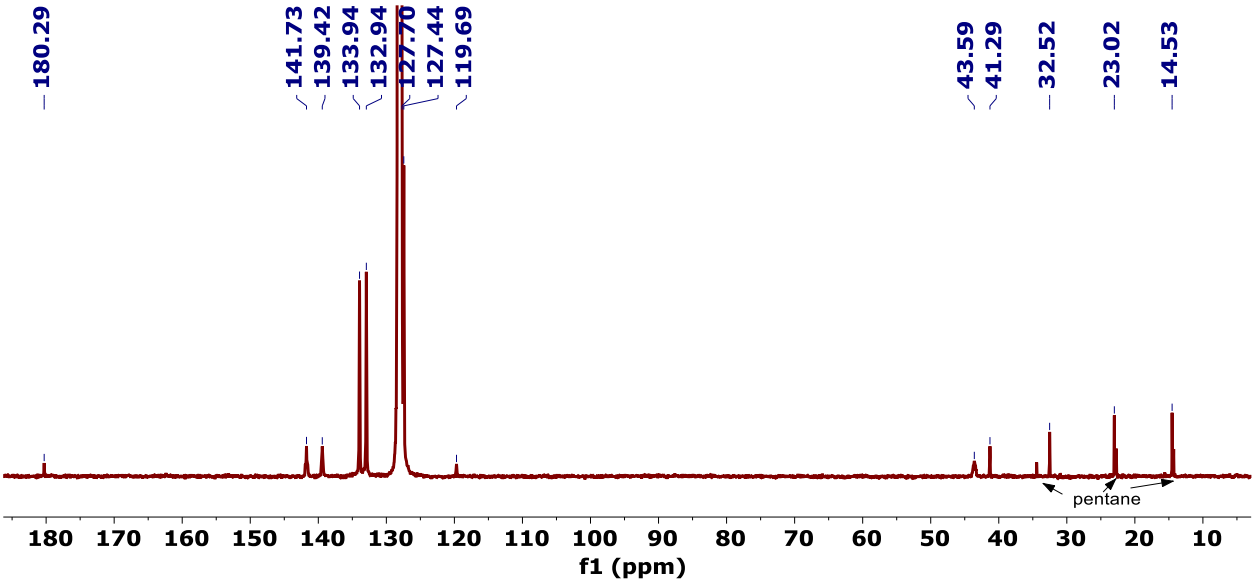

Figure 2.22. ^{13}C NMR spectrum of $[Ni_3(dppm)_3(\mu_3\text{-}H)(\mu_3\text{-}Sn(C_6H_{11})]$, **5**, in C_6D_6. There is an overlap of the residual hydrogen peak in C_6D_6 with phenyl peaks in **5**.

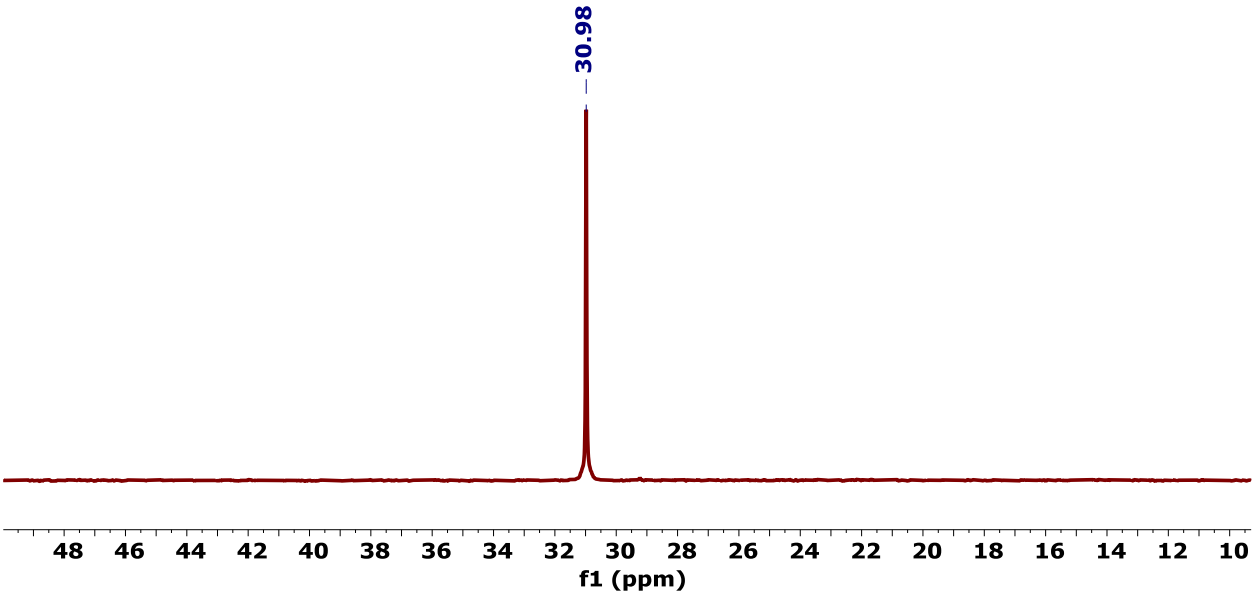

Figure 2.23. ^{31}P NMR spectrum of $[Ni_3(dppm)_3(\mu_3\text{-}H)(\mu_3\text{-}Sn(C_6H_{11})]$, **5**, in C_6D_6.

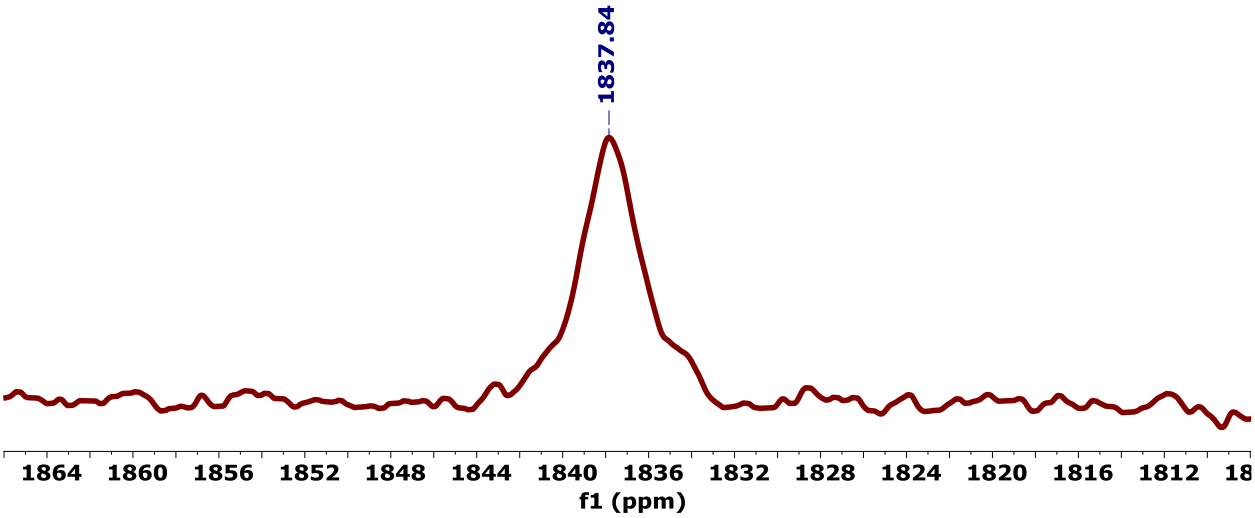

Figure 2.24. ^{119}Sn NMR spectrum of [Ni_3(dppm)$_3$(μ_3-H)(μ_3-Sn(C_6H_{11})], **5**, in C_6D_6.

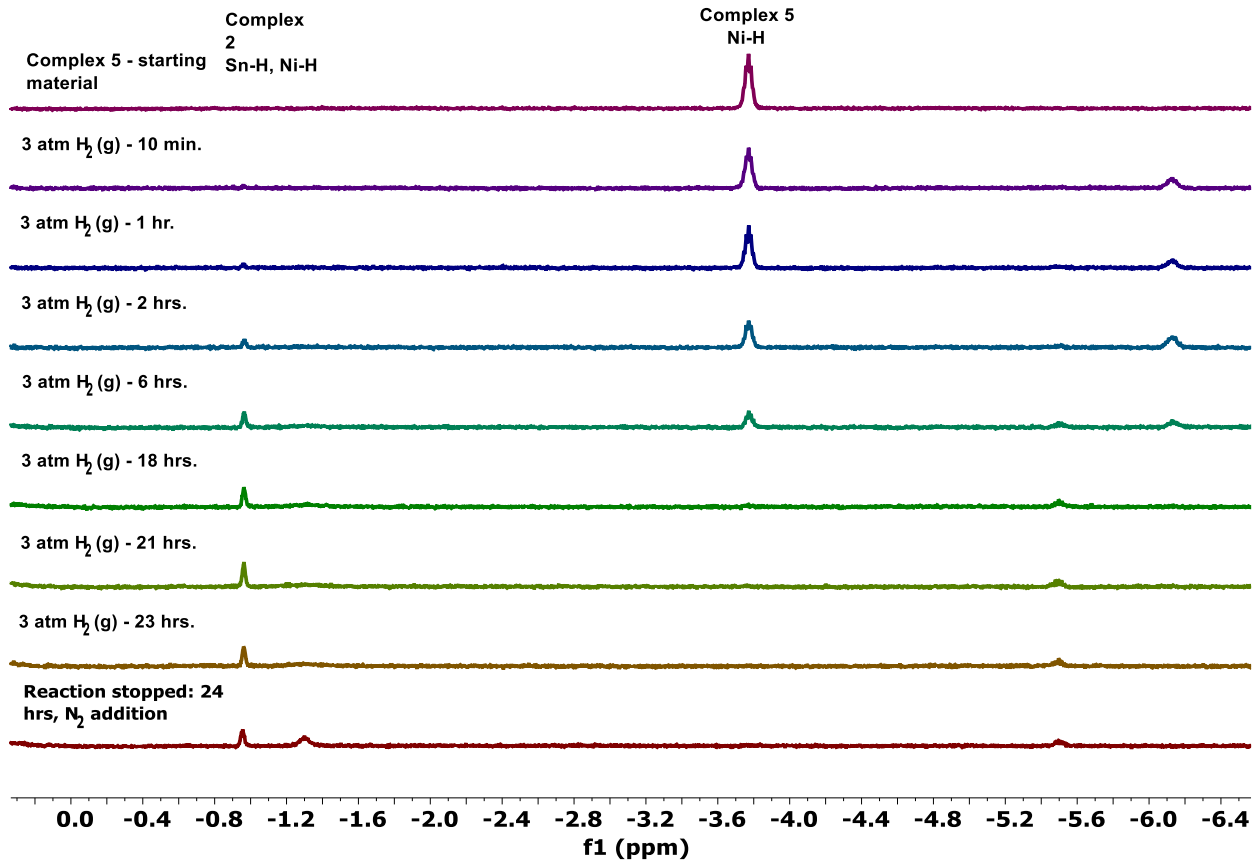

Figure 2.25. ^{1}H NMR spectrum of the hydride region over time of H_2 (g) addition to [Ni_3(dppm)$_3$(μ_3-H)(μ_3-Sn(C_6H_{11})], **5**, forming complex **2** in THF-d_8 at 22°C.

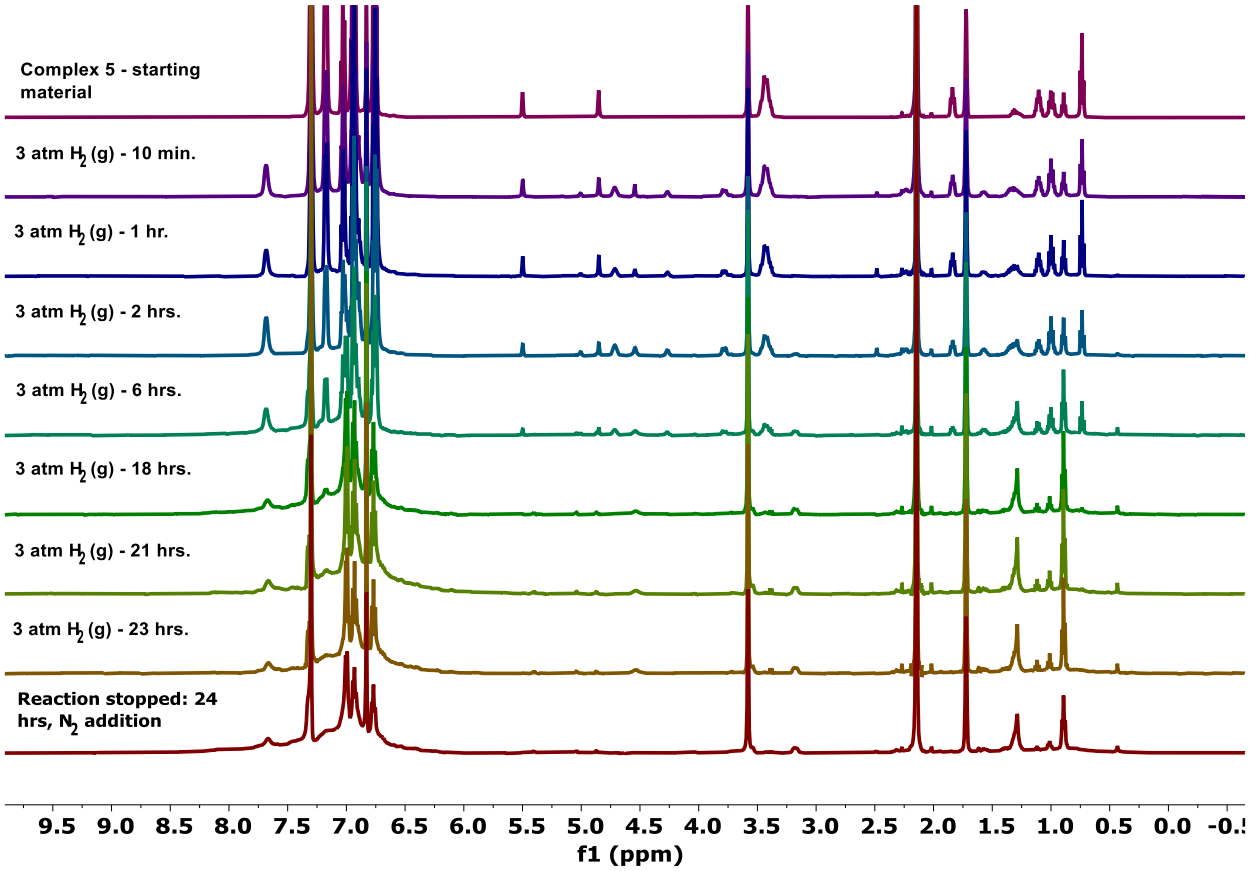

Figure 2.26. ^{1}H NMR spectrum over time of H_2 (g) addition to $[Ni_3(dppm)_3(\mu_3\text{-}H)(\mu_3\text{-}Sn(C_6H_{11})]$, **5**, forming complex **2** in THF-d_8 at 22°C.

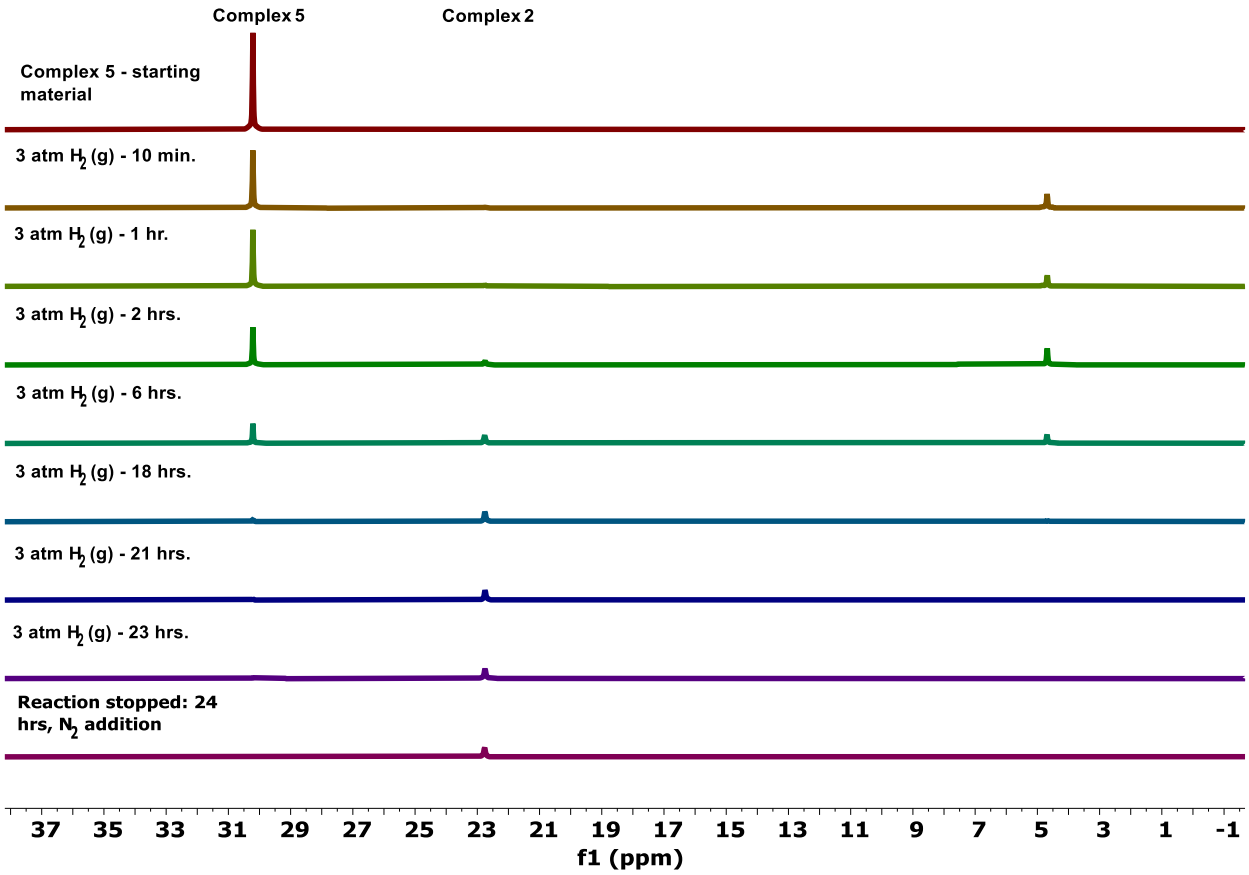

Figure 2.27. ^{31}P NMR spectrum over time of H_2 (g) addition to [Ni_3(dppm)$_3$(μ_3-H)(μ_3-Sn(C_6H_{11})], **5**, forming complex **2** in THF-d_8 at 22°C.

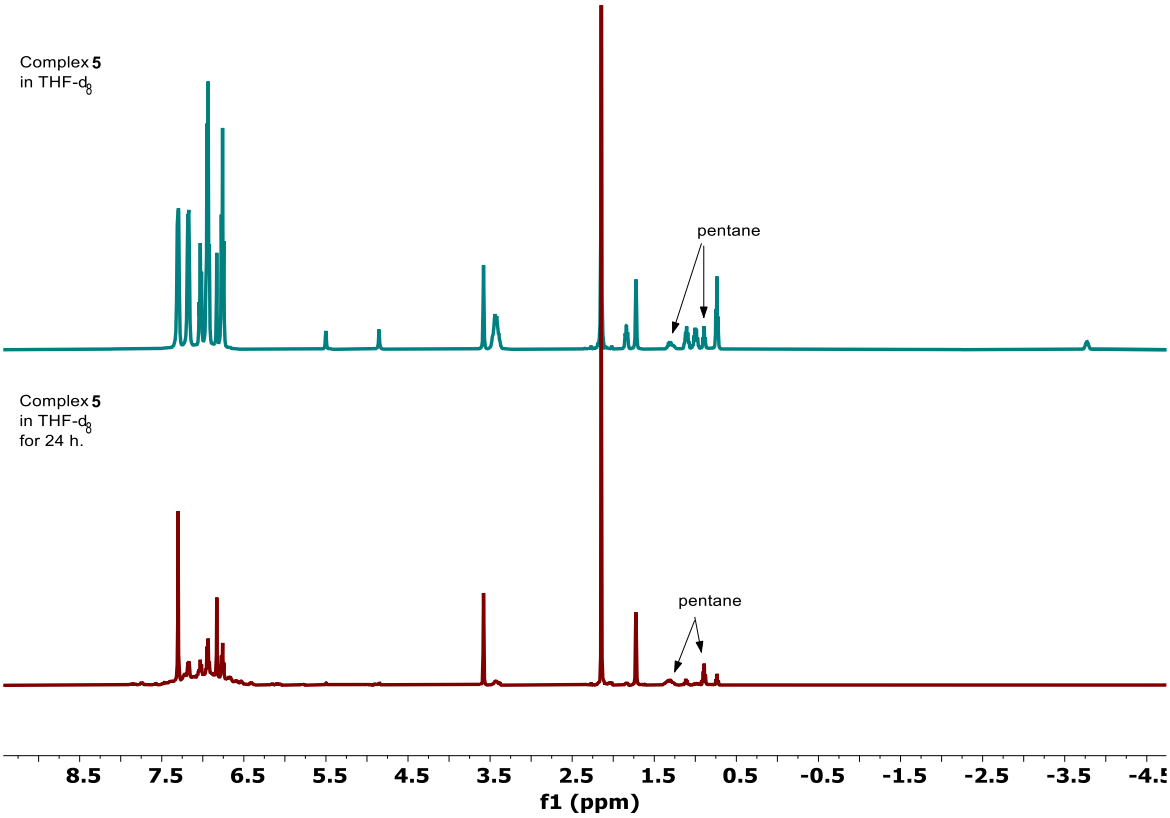

Figure 2.28. ^{1}H NMR spectrum over time of complex **5** in THF-d_8 at 22°C.

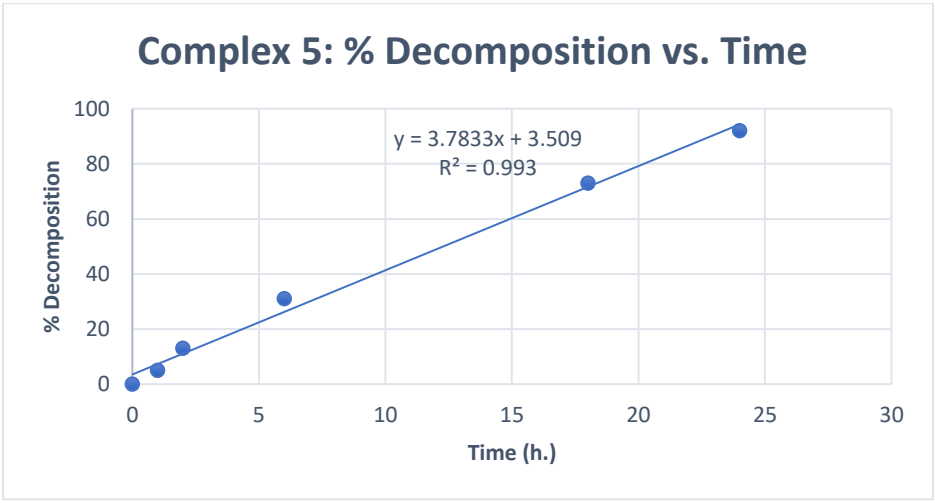

Figure 2.29. The decomposition of complex **5** in THF-d_8 at 22°C was tracked over the course of 24 hours via ^{1}H NMR spectroscopy. The graph depicts a linear trend where complex **5** degrades about 3.8% per hour, resulting in 92% decomposition over the course of 24 hours.

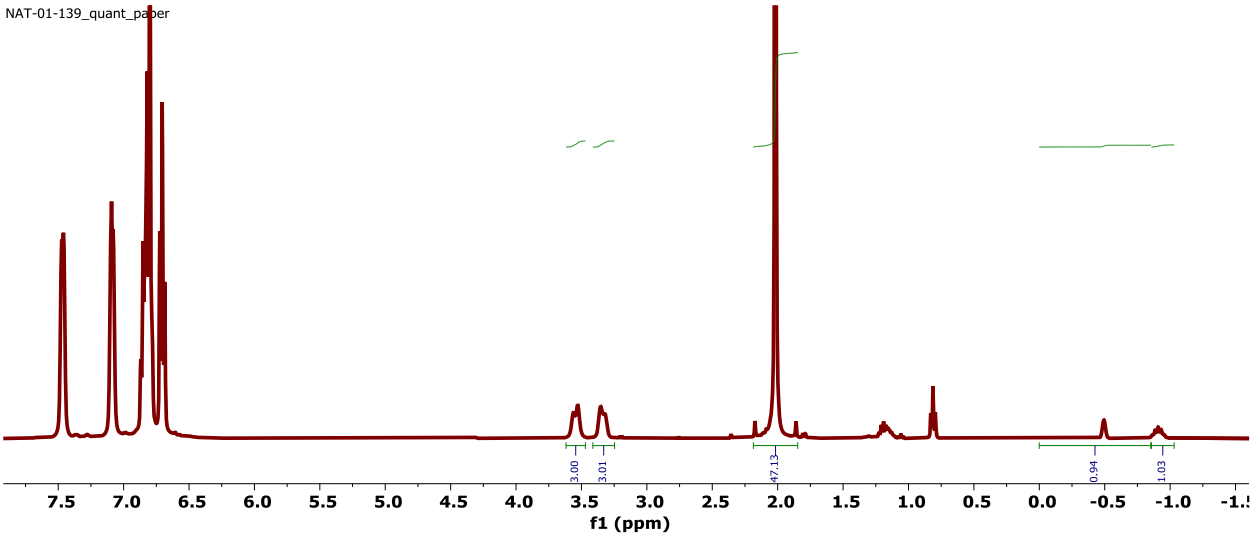

Figure 2.30. Quantitative ^{1}H NMR of **2** (13.5 mg, 0.00931 mmol) in reference to tetramethylbenzene (4.7 mg, 0.0350 mmol). The integration of the left dppm resonance on complex **2** against the methyl resonance on tetramethylbenzene depicts 96.9% purity.

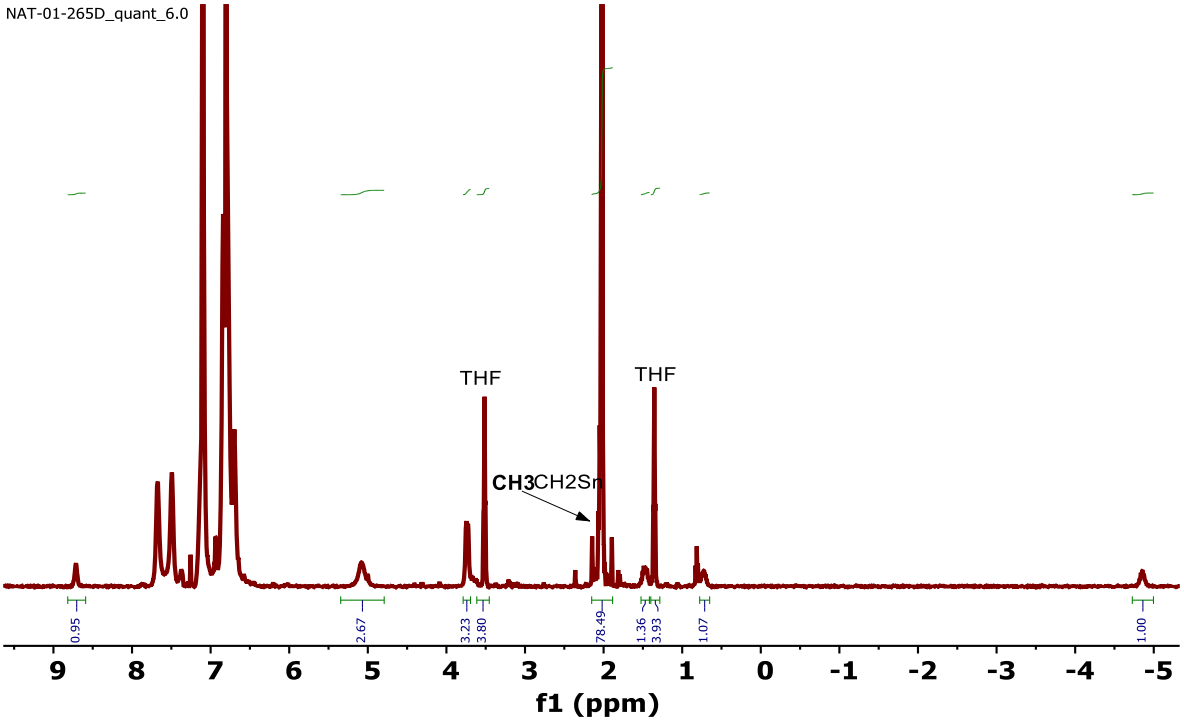

Figure 2.31. Quantitative ^{1}H NMR of **3** (8.0 mg, 0.0050 mmol) in reference to tetramethylbenzene (4.0 mg, 0.030 mmol). The integration of the Ni-H hydride resonance on complex **3** against the methyl resonance on tetramethylbenzene depicts 95.0% purity.

*The CH_3 peak on the CH_3CH_2 ligand on Sn is overlapped with the reference so 3 is subtracted from the integration of that peak in the calculations.

2.6.4 Electrochemistry Data

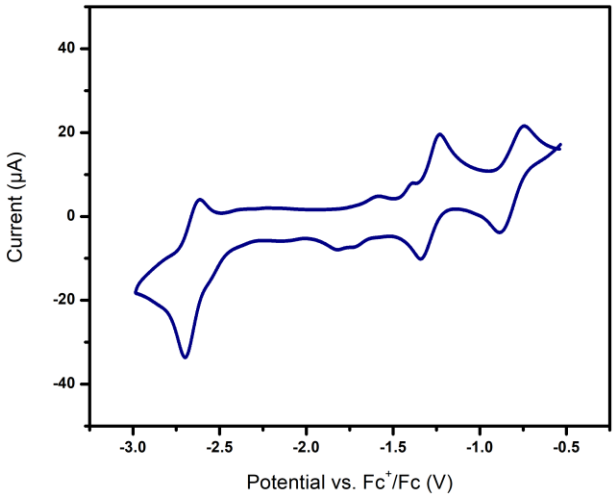

Figure 2.32. Cyclic voltammogram of 2 mM solution of **2** in THF with 0.3 M [$^{n}Bu_4N$][PF_6] supporting electrolyte. Scan rate: 100 mV/s.

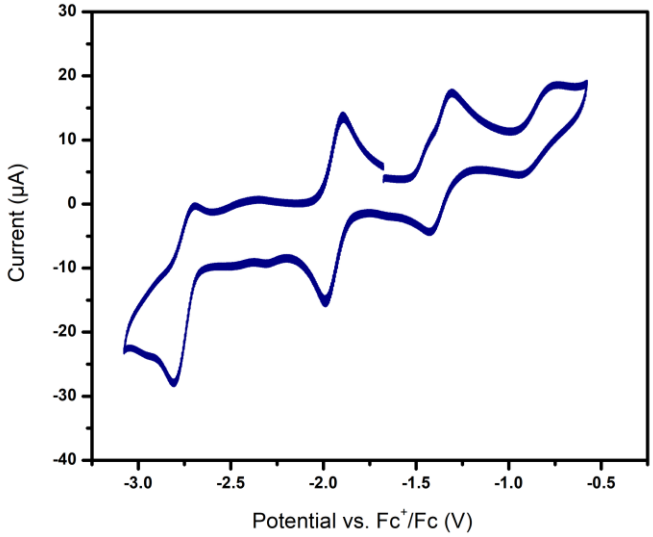

Figure 2.33. Cyclic voltammogram of 2 mM solution of **2** and 1 mM decamethylcobaltocene in tetrahydrofuran with 0.3 M [$^{n}Bu_4N$][PF_6] supporting electrolyte. Scan rate, 100 mV/s.

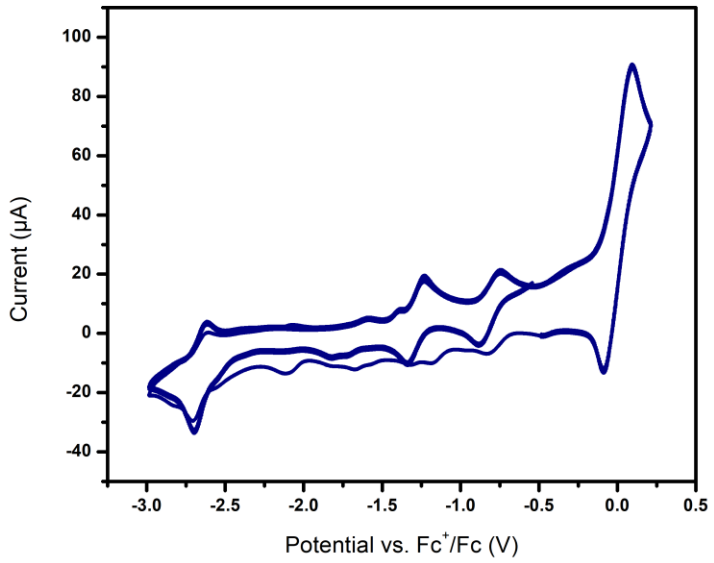

Figure 2.34. Cyclic voltammogram of 2 mM solution of **2** and 1 mM of ferrocene in tetrahydrofuran with 0.3 M [$^{n}Bu_4N$][PF_6] supporting electrolyte. Scan rate, 100 mV/s.

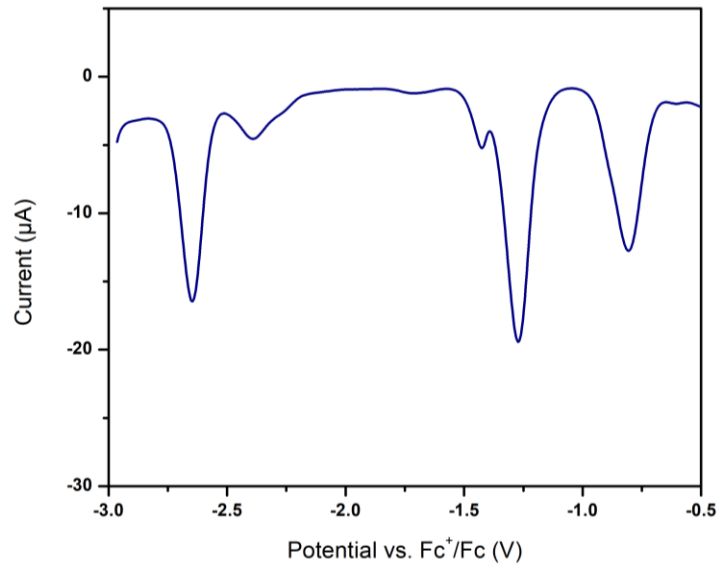

Figure 2.35. Differential pulse voltammogram (DPV) of 2 mM **2** in 0.3 M [$^{n}Bu_4N$][PF_6] THF solution. First reduction area = 82.72 μC, first oxidation area = 73.11 μC, second oxidation area = 91.86 μC. The area under the curve of the three peaks is a 1.1:1.3:1 ratio (left to right).

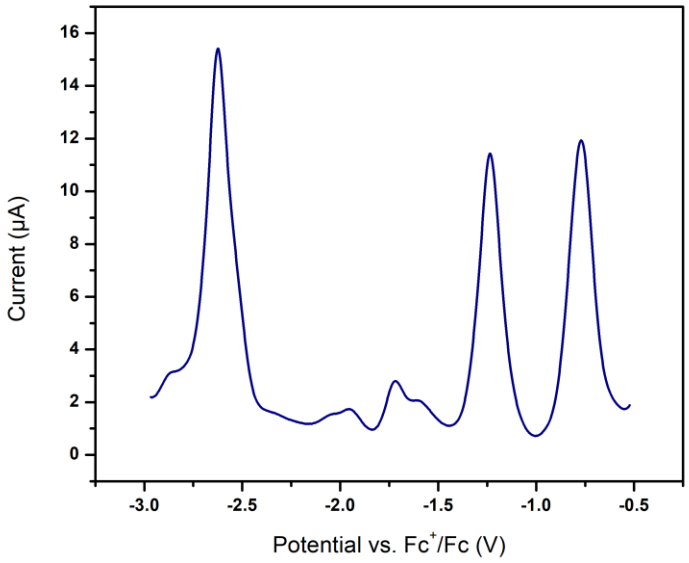

Figure 2.36. Differential pulse voltammogram (DPV) of 2 mM **2** in 0.3 M [$^{n}Bu_4N$][PF_6] THF solution. First reduction area = 93.72 μC, first oxidation area = 80.79 μC, second oxidation area = 76.04 μC. The area under the curve of the three peaks is a 1.2:1:1.1 ratio (left to right).

2.6.5. UV-Vis Spectroscopy

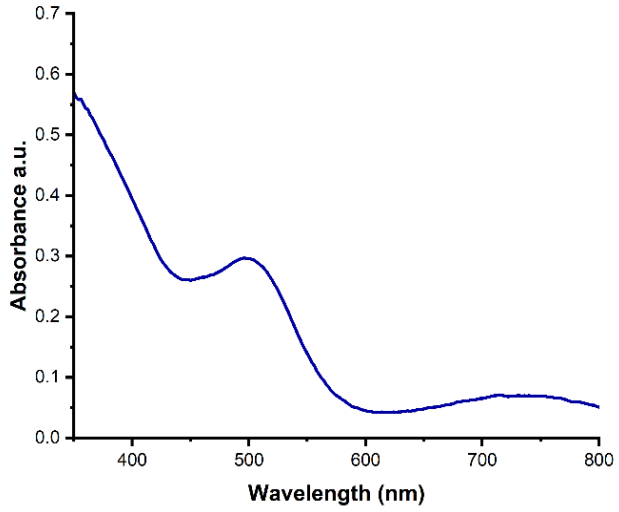

Figure 2.37. UV-Vis spectrum of **3** (0.040 mM) in benzene.

2.6.6 Computational Data

Basis set: B3LYP, Functional: LANL2DZ
Natural Population

Effective Core 136.00000
Core 173.88997 (99.9368% of 174)
Valence 430.52780 (99.6592% of 432)
Natural Minimal Basis 740.41777 (99.7868% of 742)
Natural Rydberg Basis 1.58223 (0.2132% of 742)
Sn 85 [core]5S(1.29)5p(1.89)6p(0.01)

NATURAL BOND ORBITAL ANALYSIS:

195. (1.66450) BD (1)Ni 84 -Sn 85
(20.57%) 0.4536*Ni 84 s(19.22%)p 4.17(80.24%)d 0.03(0.53%)
-0.0174 0.4379 0.0138 -0.0028 0.4638
0.0001 -0.0006 0.0121 -0.0033 0.0027
-0.7662 0.0001 -0.0090 0.0034 -0.0235
-0.0121 -0.0104 -0.0053 0.0340 0.0072
0.0560 0.0062
(79.43%) 0.8912*Sn 85 s(71.81%)p 0.39(28.19%)
0.8474 -0.0023 -0.4460 0.0165 -0.2874
0.0063 -0.0049 0.0074
196. (1.94573) BD (1)Sn 85 - H 153
(32.02%) 0.5658*Sn 85 s(20.54%)p 3.87(79.46%)
0.4532 0.0023 0.6066 0.0159 0.4042
0.0165 -0.5121 -0.0230
(67.98%) 0.8245* H 153 s(100.00%)
1.0 0.0022

<u>XYZ coordinates Complex 2</u>:
166
112_a_sq
P 13.757269 2.075515 5.715788
P 16.561115 4.178376 4.884267
P 15.048913 6.732107 3.940987
P 12.371210 5.972215 1.285301
P 12.504798 3.040610 0.395371
P 12.118075 1.131003 3.352606
C 12.987598 0.605959 4.902663
C 8.388369 4.345959 11.517733
C 6.408896 3.226724 8.693872
C 6.077957 4.001206 7.522629
C 7.446437 3.635065 10.669961
C 12.326885 2.814279 6.593607
C 11.436038 2.054110 7.363194
C 10.348379 2.663747 7.981009
C 10.153436 4.024274 7.855299

C 11.034804 4.786314 7.124039
C 12.110244 4.185932 6.477096
C 14.673012 1.244827 7.076515
C 14.520699 1.583562 8.416392
C 15.289427 0.962418 9.397537
C 16.209793 0.001028 9.048005
C 16.372192 -0.334454 7.720392
C 15.618394 0.296249 6.749977
C 16.787502 4.197208 6.713184
O 7.261178 3.953471 9.549309
C 15.717989 4.628026 7.493502
C 15.800669 4.687537 8.877837
C 16.974125 4.306964 9.509450
C 18.035397 3.868343 8.741397
C 17.951685 3.821537 7.366260
C 18.226019 3.640241 4.301712
C 19.392185 4.382603 4.511738
C 20.607513 3.939813 4.025764
C 20.685310 2.727962 3.349693
C 19.553013 1.979189 3.127402
C 16.661339 5.988587 4.470345
C 14.287450 7.425559 5.463756
C 12.950491 7.802498 5.391703
C 18.321777 2.440885 3.607244
C 12.289576 8.327319 6.486294
C 12.971378 8.489578 7.674400
C 14.313387 8.155448 7.767916
C 14.956345 7.619454 6.657995
C 15.727398 8.257780 3.164196
C 16.346367 9.253538 3.878592
C 16.896231 10.354328 3.245447
C 16.817421 10.497172 1.885640
C 16.202972 9.517209 1.171243
C 15.668042 8.397571 1.818186
C 12.535377 7.587611 0.406256
C 12.098852 8.736214 1.073128
C 12.256870 9.990573 0.487507
C 12.829162 10.129544 -0.758855
C 13.251511 9.023786 -1.399666
C 13.113504 7.748800 -0.826309
C 10.591598 6.049715 1.713939
C 9.606434 6.318946 0.772652
C 8.262283 6.321609 1.122186
C 7.908410 6.094785 2.446733
C 8.866068 5.844531 3.391085
C 10.211115 5.830777 3.036953
C 12.439321 4.806699 -0.150238
C 13.444917 2.241788 -0.964282
C 13.464540 2.675567 -2.282697
C 14.094413 1.947862 -3.263843
C 14.712329 0.754602 -2.951103
C 14.696320 0.303332 -1.648018
C 14.081317 1.046855 -0.663806
C 10.801416 2.466831 -0.035260
C 10.537978 1.616667 -1.126785
C 9.237719 1.196198 -1.378203

C 8.202112 1.625459 -0.594820
C 8.449965 2.450247 0.482908
C 9.749593 2.848850 0.766520
C 12.244023 -0.360036 2.290362
C 13.446985 -1.046195 2.201446
C 13.640193 -2.028004 1.244829
C 12.626210 -2.350599 0.364864
C 11.427355 -1.691373 0.443049
C 11.221429 -0.692190 1.399666
C 10.377662 1.100970 3.950645
C 9.700045 -0.079818 4.241923
C 8.426445 -0.047241 4.786152
C 7.816084 1.169271 5.037570
C 8.475622 2.350083 4.749359
C 9.758622 2.309667 4.212795
Ni 14.785987 3.254432 4.183974
Ni 13.655490 5.424281 2.940525
Ni 13.178777 2.789124 2.401048
Sn 15.378227 3.910252 1.825238
H 13.395756 3.944369 3.587315
H 11.575438 1.119211 7.461799
H 9.738935 2.141763 8.489963
H 9.408307 4.436924 8.276410
H 10.909950 5.726374 7.060096
H 12.699828 4.713320 5.951876
H 13.885242 2.244337 8.664714
H 15.178139 1.202643 10.310525
H 16.729156 -0.429990 9.717223
H 17.003035 -0.999661 7.472913
H 15.754026 0.070445 5.837189
H 14.909550 4.887029 7.067270
H 15.058260 4.988098 9.388677
H 17.047132 4.346848 10.455014
H 18.837978 3.592916 9.170173
H 18.701052 3.528944 6.860540
H 19.349218 5.200175 4.992821
H 21.389425 4.463649 4.153727
H 21.526352 2.414450 3.037812
H 19.606401 1.157436 2.653187
H 12.340901 0.182178 5.520432
H 12.481526 7.694747 4.572891
H 13.687318 -0.059319 4.683071
H 17.538717 1.924838 3.456715
H 11.374291 8.575665 6.421063
H 12.517197 8.832066 8.434958
H 14.787403 8.292475 8.579677
H 15.873723 7.380221 6.720987
H 16.398413 9.185690 4.824356
H 17.333601 11.021404 3.761054
H 17.183754 11.260680 1.452694
H 15.252678 7.717762 1.300110
H 11.694161 8.661992 1.928718
H 11.965377 10.763673 0.954854
H 12.923306 10.987022 -1.157476
H 13.650674 9.107976 -2.256942
H 13.426285 6.986627 -1.300095

H 9.855342 6.503577 -0.125817
H 7.594422 6.475955 0.465354
H 6.992000 6.115071 2.698258
H 8.610531 5.679368 4.290673
H 10.873267 5.670962 3.699533
H 13.034746 3.491245 -2.510292
H 14.104108 2.266396 -4.158449
H 15.145715 0.247549 -3.627128
H 15.111077 -0.522387 -1.428150
H 14.093780 0.736742 0.233237
H 11.247878 1.329839 -1.688521
H 9.066824 0.604826 -2.100863
H 7.313230 1.355198 -0.793977
H 7.731332 2.744657 1.030188
H 9.915009 3.395410 1.526172
H 14.150483 -0.837964 2.806231
H 14.471867 -2.483185 1.193058
H 12.759455 -3.024019 -0.290833
H 10.728455 -1.916278 -0.158961
H 10.387857 -0.238979 1.441518
H 10.115031 -0.916035 4.064535
H 7.974780 -0.857350 4.988069
H 6.941599 1.193212 5.408091
H 8.054224 3.185084 4.916399
H 10.213835 3.122039 4.023955
H 9.210310 4.524419 11.015815
H 8.597577 3.797922 12.303370
H 7.991570 5.193793 11.808060
H 5.578626 2.988699 9.178650
H 6.854603 2.386133 8.419151
H 5.505377 3.469957 6.929618
H 6.899704 4.246296 7.048843
H 5.601340 4.814622 7.792031
H 7.728677 2.686853 10.656838
H 6.568313 3.665121 11.125918
H 16.992882 6.478828 5.263694
H 17.322626 6.112468 3.743347
H 11.641530 4.943110 -0.718919
H 13.240929 5.008962 -0.695571

2.6.7 Crystallographic Data

Table 2.3. Crystallographic Experimental Details for [$Ni_3(dppm)_3(\mu_3\text{-}H)(\mu_3\text{-}SnH)$], **2**.

Empirical formula	$C_{79}H_{77}Ni_3OP_6Sn$
Formula weight	1523.04
Temperature/K	100
Crystal System	triclinic
Space group	P -1
a/Å	15.7957(16)
b/Å	15.8530(16)
c/Å	15.9408(16)
α/°	88.2340(10)
β/°	74.0990(10)
γ/°	85.0760(10)
Volume/$Å^3$	3824.7(7)
Z	2
$\rho_{calc}g/cm^3$	1.322
μ/mm^{-1}	1.217
F(000)	1566
Crystal size/mm^3	0.3 x 0.1 x 0.1
Radiation	MoKα (λ = 0.71073)
2Θ range for data collection/°	2.578 to 51.374
Index ranges	$-19 \leq h \leq 19, -19 \leq j \leq 19, -19 \leq l \leq 19$
Reflections collected	35268
Independent reflections	14525 [R_{int} = 0.0750, R_{sigma} = 0.0872]
Data/restraints/parameters	14525/211/913
Goodness-of-fit on F^2	1.035
Final R indexes [I≥2σ (I)]	R_1= 0.0434, wR_2= 0.1084
Final R indexes [all data]	R_1= 0.0536, wR_2= 0.1177
Largest diff. peak/hole / e $Å^{-3}$	0.86 and –0.49 e/$Å^3$

Table 2.4. Crystallographic Experimental Details for $[Ni_3(dppm)_3(\mu_3\text{-}H)(\mu_3\text{-}Sn((Br)(H)(CH_2CH_3))]$, **3**.

Empirical formula	$C_{81}H_{80}BrNi_3OP_6Sn$
Formula weight	1630.00
Temperature/K	100
Crystal System	triclinic
Space group	P -1
a/Å	12.6920(6)
b/Å	13.0930(8)
c/Å	24.4579(14)
α/°	90.583(2)
β/°	102.885(2)
γ/°	112.374(2)
Volume/Å^3	3643.3(4)
Z	2
ρ_{calc}g/cm^3	1.486
μ/mm^{-1}	1.828
F(000)	1666.0
Crystal size/mm^3	0.1 x 0.05 x 0.05
Radiation	MoKα (λ = 0.71073)
2Θ range for data collection/°	5.07 to 50.174
Index ranges	$-15 \leq h \leq 15$, $-15 \leq j \leq 15$, $-29 \leq l \leq 29$
Reflections collected	89348
Independent reflections	12914 [R_{int} = 0.1298, R_{sigma} = 0.0730]
Data/restraints/parameters	12914/3/842
Goodness-of-fit on F^2	1.017
Final R indexes [I≥2σ (I)]	R_1= 0.0464, wR_2= 0.0921
Final R indexes [all data]	R_1= 0.0852, wR_2= 0.1086
Largest diff. peak/hole / e Å^{-3}	0.98 and –0.89 e/Å^3

Table 2.5. Crystallographic Experimental Details for $[Ni_3(dppm)_3(\mu_3\text{-}I)(\mu_3\text{-}Sn(CH_2CH_3)]$, **4**.

Empirical formula	$C_{83}H_{77}INi_3P_6Sn$
Formula weight	1681.98
Temperature/K	100.0
Crystal System	monoclinic
Space group	$P2_1/c$
a/Å	16.0909(10)
b/Å	22.2524(12)
c/Å	20.2582(12)
α/°	90
β/°	103.455(2)
γ/°	90
Volume/Å^3	7159.2(7)
Z	4
ρ_{calc}g/cm^3	1.561
μ/mm^{-1}	1.733
F(000)	3408.0
Crystal size/mm^3	0.35 x 0.3 x 0.25
Radiation	MoKα (λ = 0.71073)
2Θ range for data collection/°	4.344 to 52.046
Index ranges	$-19 \leq h \leq 19$, $-27 \leq k \leq 27$, $-24 \leq l \leq 24$
Reflections collected	118231
Independent reflections	14079 [R_{int} = 0.0580, R_{sigma} = 0.0305]
Data/restraints/parameters	14079/0/855
Goodness-of-fit on F^2	1.052
Final R indexes [I≥2σ (I)]	R_1= 0.0274, wR_2= 0.0525
Final R indexes [all data]	R_1= 0.0404, wR_2= 0.0577
Largest diff. peak/hole / e Å^{-3}	1.23 and –0.61 e/Å^3

Table 2.6. Crystallographic Experimental Details for $[Ni_3(dppm)_3(\mu_3\text{-}H)(\mu_3\text{-}Sn(C_6H_{11})]$, **5**.

Empirical formula	$C_{81}H_{78}Ni_3P_6Sn$
Formula weight	1532.07
Temperature/K	100.0
Crystal System	triclinic
Space group	P -1
a/Å	11.9779(3)
b/Å	13.7494(4)
c/Å	23.0279(7)
α/°	91.234(2)
β/°	101.720(2)
γ/°	107.029(2)
Volume/Å^3	3537.25(18)
Z	2
ρ_{calc}g/cm^3	1.438
μ/mm^{-1}	5.286
F(000)	1576.0
Crystal size/mm^3	0.5 x 0.1 x 0.1
Radiation	CuKα (λ = 1.54178)
2Θ range for data collection/°	3.934 to 137.906
Index ranges	$-14 \leq h \leq 14$, $-16 \leq k \leq 15$, $-27 \leq l \leq 27$
Reflections collected	62692
Independent reflections	12796 [R_{int} = 0.0833, R_{sigma} = 0.0643]
Data/restraints/parameters	12796/27/844
Goodness-of-fit on F^2	1.031
Final R indexes [I≥2σ (I)]	R_1= 0.0494, wR_2= 0.1086
Final R indexes [all data]	R_1= 0.0690, wR_2= 0.1175
Largest diff. peak/hole / e Å^{-3}	0.72 and –1.26 e/Å^3

2.6.8 Appendix A References

[1] E. Simón-Manso, C. P. Kubiak, Agnew. Chem. Int. Ed. 2005, 44, 1125-1128.

[2] G. M. Sheldrick, Acta Crystallogr. A Found Adv. 2015, 71, 3-8.

[3] A. L. Spek, Acta Crystallogr. C Struct. Chem. 2015, 71, 9-18.

CHAPTER 3. H_2/D_2 Exchange by a μ_3-SnH, μ_3-H capped trinuclear Nickel Cluster

3.1 Introduction

Low-valent tin (II) hydrides have been of increasing interest in the past 20 years for their ability to activate small molecules, such as, H_2, CO_2, H_2O, alkenes, alkynes, and aldehydes.[1, 2] To further the structural and reactivity profile of these complexes, there have been reports of tin hydride functional groups coordinated to transition metals, featuring tin in the +2 oxidation state.[1, 3-8] These species have expanded the reactivity platform of low valent/tin (II) hydrides and provide insight on the interaction between the Sn-H moiety and transition metals. Although there are many examples of mononuclear transition metal coordinated Sn-H species[1, 3, 5-12], there are relatively few reports of Sn-H coordinated transition metal clusters.[4, 13-15] Metal cluster compounds have been an active area of inorganic chemistry due to their diverse structural and catalytic properties, their electrochemical behavior, and their ability to mimic catalyst metal surfaces.[16, 17] Therefore, in order to expand our understanding of the reactivity of tin hydrides in different chemical environments, we investigated different tin functional groups supported on trinuclear nickel clusters.[4, 18-20] Previous work from our group reported the synthesis, structural characterization and reactivity of a μ_3-SnH, μ_3-H capped trinuclear nickel cluster, $[Ni_3(dppm)_3(\mu_3\text{-}H)(\mu_3\text{-}SnH)]$, **1,** (dppm = bis(diphenylphosphino)methane).[4] In this study, it was found that **1** displays a wide range of reactivity, including oxidative addition of alkyl halides and and alkyne insertion to the μ_3-SnH. A particularly intriguing aspect of the reactivity profile of **1**, was the observation of reactivity of the Sn-H and Ni-H moieties on **1** with H_2 and D_2. Herein, we report the reversible exchange of **1** with H_2 and D_2 and provide mechanistic insight of this interaction through a variety of ^1H, ^2H, ^{31}P and ^{119}Sn nuclear magnetic resonance (NMR) spectroscopy studies.

3.2 Results and Discussion

The synthesis and structural determination of a μ_3-SnH, μ_3-H capped trinuclear nickel cluster, [Ni_3(dppm)$_3$(μ_3-H)(μ_3-SnH)], **1**, has been reported previously.[4] Treatment of **1** with 1 atm D_2 in benzene-d_6 at 22 °C resulted in conversion of **1** in 18 hours to the deuterated species, [Ni_3(dppm)$_3$(μ_3-D)(μ_3-SnD)], **1D**, with 76 ± 2 % conversion, and the partially deuterated species, [Ni_3(dppm)$_3$(μ_3-H)(μ_3-SnD)], **1HD**, and [Ni_3(dppm)$_3$(μ_3-D)(μ_3-SnH)], **1DH**, compromising the balance of the reaction products (Figure 3.1).

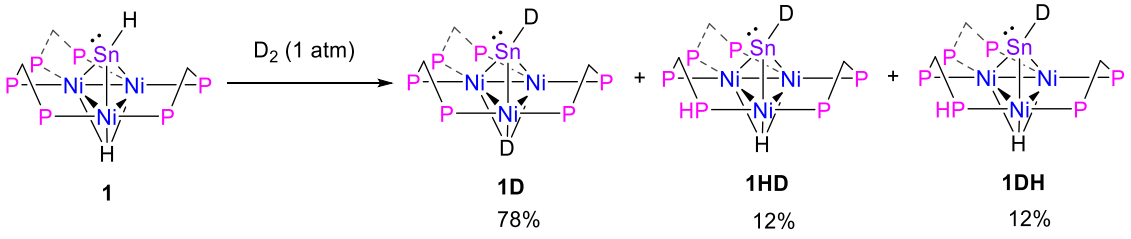

Figure 3.1 Addition of D_2 to **1** resulting in the formation of **1D**, **1HD** and **1DH**.

The progress of the deuteration reaction was studied by ^{1}H NMR spectroscopy in a medium walled J-Young tube at 22°C in benzene-d_6 solution with the goal of investigating the reaction dynamics of the μ_3-SnH and μ_3-H functionalities on **1** with 1 atm. D_2 (Figure 3.2). ^{31}P coupling of the μ_3-H resonance (normally a septet) was lost within 10 minutes, and the integrated intensity steadily decreased over six hours and completely vanished after 18 hours. Expansion of the Ni-H region suggests that the partially detuerated species, **1HD,** is also formed and is subsequently consumed (Figure 3.2, See Appendix B: Figure 3.7). Reaction at μ_3-SnH generates an intermediate state, presumed to be **1DH**, with a chemical shift at -0.36 ppm, which is locally maximized in concentration after one hour. This intermediate gradually converts over the subsequent 17 hours to form **1D**. Under these reaction conditions, integration of **1**, **1DH** and **1HD** ^{1}H NMR resonances indicates quantitative conversion of **1** to **1D** in 76 ± 2 % NMR yield and **1DH** and **1HD** species, both in 12 ± 2 % NMR yield (Figure 3.1). These structural assignments will be supported later in

this report. These results demonstrate conversion to the partially deuterated species, **1HD** and **1DH** on the path to complete deuteration to **1D**.

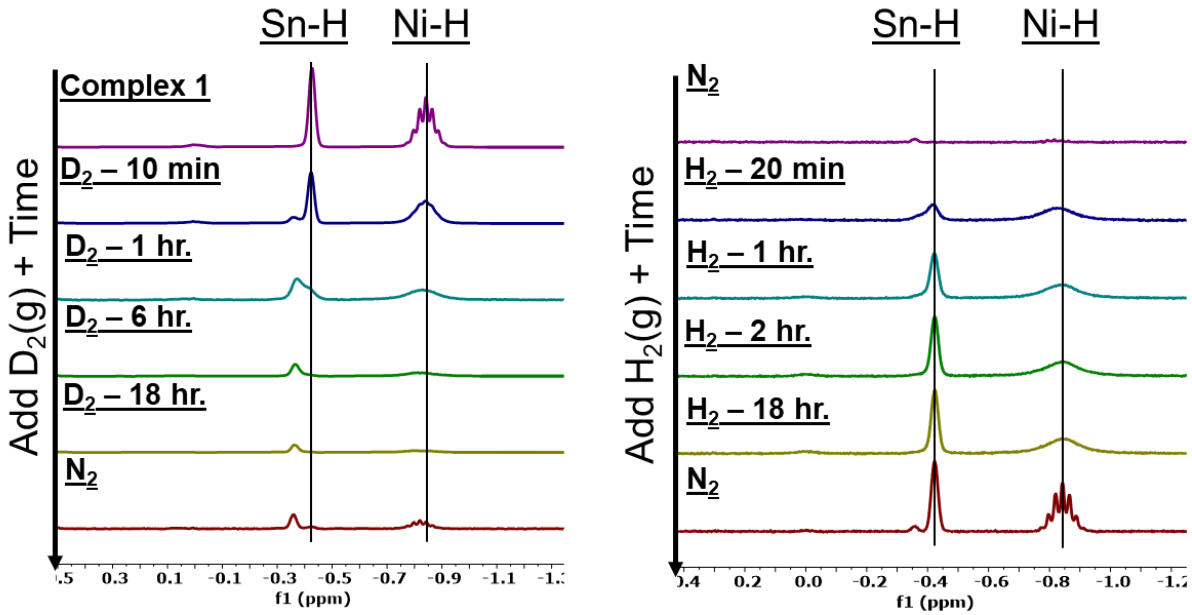

Figure 3.2. ^{1}H NMR spectra of **1** after addition of 1 atm D_2 in benzene-d_6 (left) and **1D** after addition of 1 atm H_2 in benzene-d_6 (right), focused in on the Sn-H and Ni-H resonance regions.

Increasing the D_2 pressure to 4 atm. resulted in a similar reaction progression to the results with 1 atm. D_2, but with an accelerated rate. After 4 hours, complete conversion of **1** and < 1 % of **1DH** and **1HD** was observed, suggesting > 98 % yield of **1D** by ^{1}H NMR (see Appendix B, Figure 3.8). The deuteration of **1** was also supported by ^{2}H NMR (Figure 3.3). A broad singlet was found at -0.49 ppm, presumed to belong to Sn-D group by analogy to the ^{1}H NMR spectrum of **1**. Upon replacement of residual D_2 atmosphere with N_2, the μ_3-D resonance appeared at -0.75 ppm and μ_3-SnD shifted slightly to -0.45 ppm. Complex **1D** is further characterized by ^{119}Sn{^{1}H} NMR, which revealed a broad singlet at 2929.0 ppm (see Appendix B, Figure 3.10).

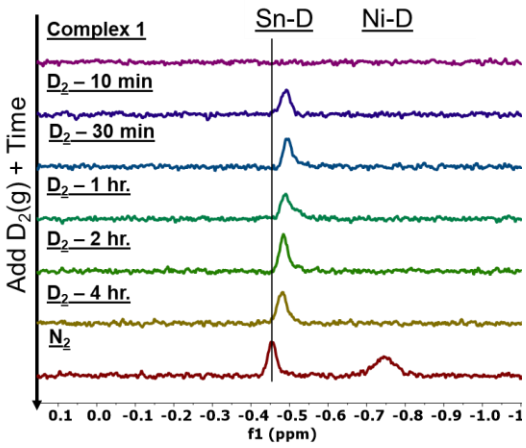

Figure 3.3. ^{2}H NMR spectra of **1** with 4 atm D_2 in benzene referenced to benzene-d_6, focused in on Sn-D and Ni-D resonance regions.

The reversibility of deuteration was probed by exposure of **1D** to 1 atm. H_2 in a similar ^{1}H NMR time course to that illustrated above (Figure 3.2). The μ_3-H signal rapidly increased in integrated intensity within the first 20 minutes, then tapered off over the next 18 hours. At the same time the μ_3-SnH functionality of **1** mostly returned in the first 2 hours, with **1DH** concentration reaching a maximum at 10 minutes. The broad, featureless μ_3-H resonance returned to its original appearance after replacement of residual H_2 atmosphere with N_2, indicating formation of **1** and the reversibility of H_2/D_2 exchange between **1** and **1D**. Finally, a control experiment featuring **1** exposed to 1 atm of H_2 revealed the same loss of coupling and broadening of μ_3-H signal, along with a 2.2 ppm shift in the ^{119}Sn{^{1}H} NMR spectrum, suggestive of a conformational change (see Appendix B, Figures 3.11, 3.12). The H_2 and D_2 induced conformational change at the Ni_3H core is presumed to be the result of a fluxional process where the μ_3-H shifts to μ_2-H or terminal position to provide space for H_2 addition to the other nickel centers. [21] The multitude of different binding enviornments then lead to the exhibited inhomogeneous line broadening.

To further probe the potential intermediates observed in the Sn-H region in the H_2 and D_2 exchange studies, 1.2 atm HD was added to a benzene-d_6 solution of **1** at 22 °C (Figure 3.4). Upon addition, the Sn-H resonance is shifted to -0.40 ppm and the Ni-H region lost coupling, broadened

and shifted to -0.82 ppm in the ^{1}H NMR spectra (Figure 3.5). After 22 hours, HD was removed and N_2 was added to the solution mixture, resulting in two Sn-H peaks at -0.36 and -0.42 ppm. In addition, the Ni-H heptet resonance was split resulting in two hepets slightly offset, and centered at -0.82 and -0.85 ppm, suggesting the formation of **1**, [Ni_3(dppm)$_3$(μ_3-H)(μ_3-SnD)] (**1HD**), [Ni_3(dppm)$_3$(μ_3-D)(μ_3-SnH)] (**1DH**), and **1D** in a 1:1:1:1 ratio (Figure 3.4, 3.5). ^{31}P NMR spectra also suggest multiple species (Figure 3.5). This product distribution was further supported by ^{2}H NMR which showed singlets at -0.39 and -0.45 ppm for the Sn-D species, and a broad singlet at -0.69 ppm presumably due to the two Ni-D resonances overlapped with one another (See Appendix B, Figure 3.13). In addition, ^{119}Sn NMR revealed a doublet at 2939.9 (**1**), a singlet at 2929.1 (**1D**), and overlapped signals at 2935.9 and 2933.7 (presumably **1DH** and **1HD**) further supporting the formation of 4 species (see Appendix B, Figure 3.14). The splitting of the Ni-H and Sn-H resonances after removal of the HD headspace is suggestive of a conformational change of cluster **1**. Furthermore, significant line broadening of the HD (g) resonance (normally a triplet) is observed, this is postulated to be strong evidence of an interaction between dissolved HD (g) and **1**. Therefore, it is proposed that the fluxional binding motifs of HD by the Ni_3H core under 1 atm HD resulted in the merging of the Sn-H and Ni-H ^{1}H NMR resonances of complexes **1**, **1DH**, and **1HD**. [21]

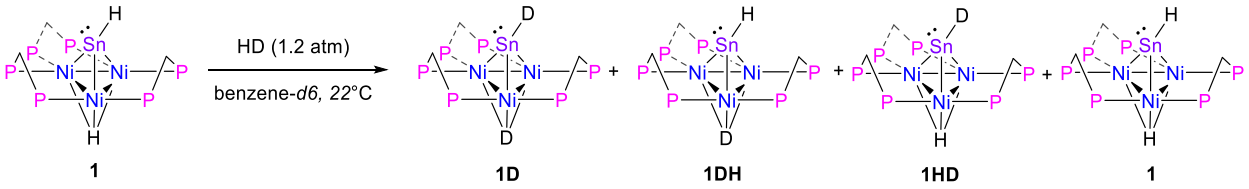

Figure 3.4. Addition of 1.2 atm HD to [Ni_3(dppm)$_3$(μ_3-H)(μ_3-SnH)], **1**, produces a 1:1:1:1 ratio of the four isotopomers, **1**, **1HD**, **1DH**, **and 1D.**

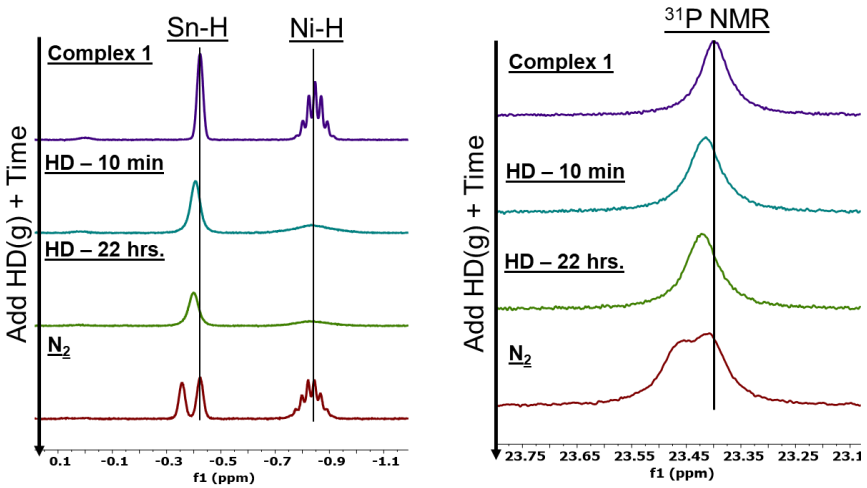

Figure 3.5. ^{1}H and ^{31}P NMR spectra of 1.2 atm HD addition to **1** in benzene-d_6.

To determine if this exchange proceeds *via* a biomolecular mechanism, addition of 1 equiv. of **1** to **1D** was performed. This resulted in equimolar formation of **1**, **1HD**, **1DH**, and **1D**, as determined by ^{1}H, ^{2}H, and ^{31}P NMR spectroscopy, supporting the facile scrambling of isotopologues. Given the vast literature precendence for Sn (II) hydride dimerization[1, 2, 22, 23], it is presumed that the ready stoichiometic scrambling procedes *via* intermolecular exchange at Sn resulting in a SnH dimeric complex. The considerable steric bulk around the Ni_3-H could make this group less accessible through dimerization with another Ni_3-H center, however, the less sterically impacted Sn-H species may be able to interact or it could proceed through an intramolecular process involving cooperation between the μ_3-H and μ_3-SnH.

To further study the dynamics of this reaction, variable-temperature (VT) NMR was used to investigate the properties of **1** under 1 atmosphere of N_2, H_2, and HD. First, ^{1}H NMR spectra of **1** under N_2 was measured between -50 and 60 °C in toluene-d_8. In these spectra, the aryl and methylene regions exhibited minor changes. However, the Sn-H and Ni-H exhibited a linear temperature dependence between 60 to -30 °C, demonstrated by a significant downfield shift of the Ni-H resonance in the ^{1}H NMR spectra from -1.14 to -0.62 ppm, and a slight upfield shift of

the Sn-H resonance from -0.45 to -0.54 ppm. (Figure 3.6A, also see Appendix B, Figures 3.15, 3.16, 3.21). At -50 °C the Sn-H and Ni-H resonances appear as one broad peak at -0.67 ppm (Figure 3.6A). The substantial chemical shift change of the Ni-H suggests an environmental change of the Ni-H functionality with temperature. The minor changes in the Sn-H chemical shift may be attributed to changes in the magnetic environment of the nearby Ni-H species.

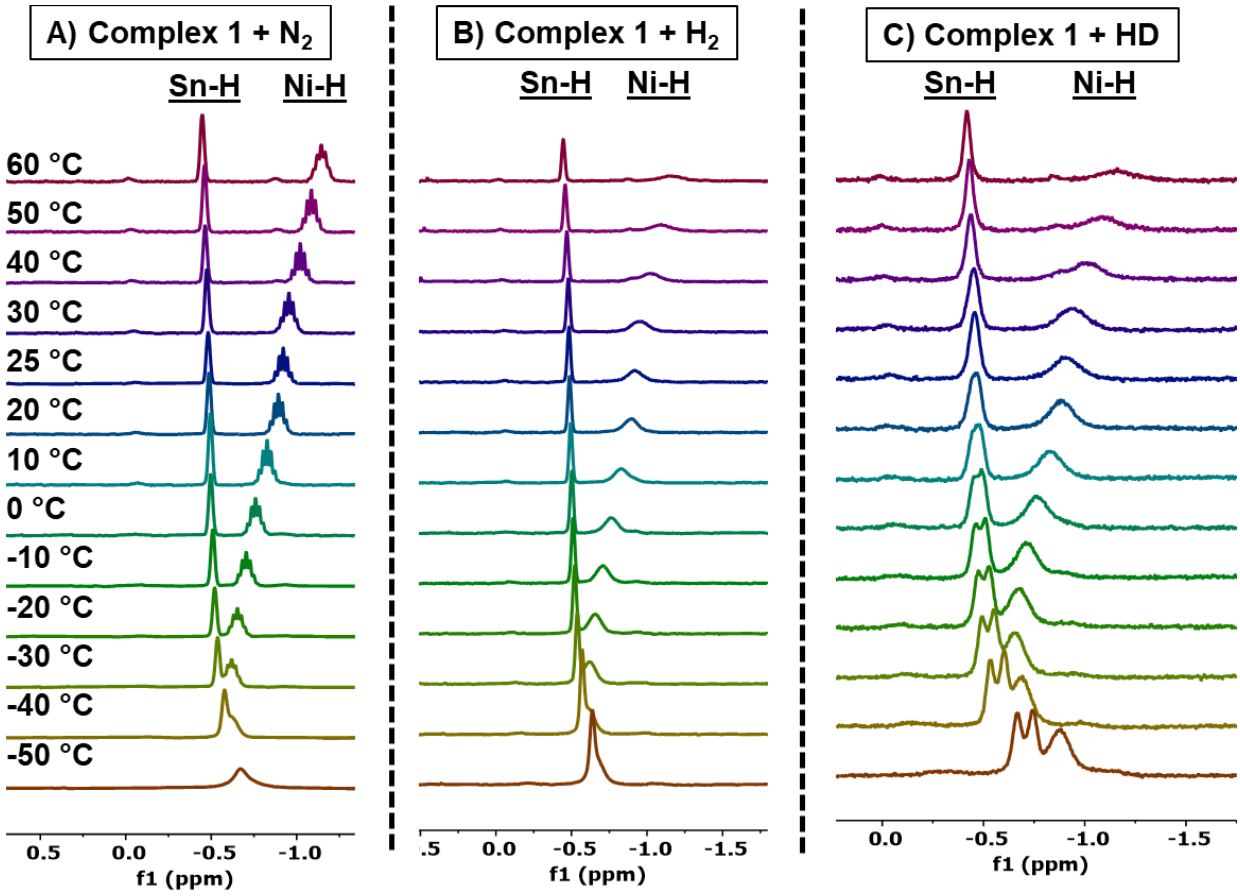

Figure 3.6. Variable temperature ^{1}H NMR spectra in toluene-d_8 of A) Complex **1** + 1 atm N_2, B) Complex **1** + 1 atm H_2, C) Complex **1** + 1 atm HD, all focused on the Sn-H and Ni-H region.

The addition of H_2 to **1**, probed by VT NMR, again revealed that the aryl and alkyl resonances remain relatively unchanged, while the Sn-H and Ni-H regions are the areas of largest chemical shift, with a similar linear chemical shift dependence to temperature as the VT ^{1}H NMR studies of **1** with N_2 (see Appendix B, Figure 3.21). The most notable difference in this VT ^{1}H NMR spectral series is the increase in intensity of the Ni-H resonance with cooling. At 60 °C the

Ni-H resonance is broadened with a full-width at half maximum (FWHM) of 67.3 Hz. With cooling, peak intensity is maximized around -30 °C, resulting in a FWHM of 37.8 Hz (Figure 3.6B, also see Appendix B, Figures 3.17, 3.18). The broadening of the Ni-H resonance as the temperature increases provides evidence of a potential conformational change of the Ni-H species while under an atmosphere of H_2.

Finally, VT ^{1}H NMR was obtained from -50 to 60 °C (Figure 3.6C, also see Appendix B, Figures 3.18 and 3.19) for addition of HD to **1**. Similar to the VT study of **1** with H_2, the Ni-H resonance increased in intensity with cooling. The prominent difference in this VT ^{1}H NMR group is that the Sn-H species starts as two signals, -0.67 and -0.74, at -50 °C and coalesces into one singlet resonance, -0.47 ppm, at 10 °C (Figure 3.6C). Furthermore, at lower temperatures, -50 and -40 °C, two new broad resonances near the HD (g) resonance peak appear, potentially suggesting a correlation to the two Sn-H resonances observed (See Appendix B, Figures 3.19, 3.20). The line broadening of the HD (g) resonance, along with the broadened Ni-H resonance throughout the spectra demonstrated interaction and binding of HD (g) with the Ni_3H core at temperatures as low as -50 °C. In the previous ^{1}H NMR study of **1** with HD, coalescence of the Sn-H resonances of **1** and **1DH** was observed, when under an atmosphere of HD. In this case, it appears that a similar process is taking place as cooling may slow down the HD activation and fluxional change of HD binding conformers at the Ni_3 core, allowing for the decoalescence of the Sn-H peaks of **1** and **1DH**. The coalescence of the Sn-H resonances correlates to the rate of HD activation and conformational change of the HD binding mode by the Ni_3 core. These spectra were modeled by WINDNMR, the simulated spectra predict the rate of exchange ($K_{exchange}$) with HD to be 84 ± 4 s^{-1} and Gibbs free energy $\Delta G^{\#}$ of this process at the coalescence temperature, 273 °C, is 13.53 ± 0.03kcal/mol (see Appendix, Figure 3.23 and Table 3.1).

Finally, to investigate dynamic exchange of the Sn-H resonance with the Ni-H resonance at 22 °C on an NMR timescale, a Nuclear Overhauser Effect Spectroscopy (NOESY) NMR spectrum of **1** in benzene-d_6 was obtained (see Appendix B, Figure 3.22). An opposite phase correlation is observed between the Sn-H and Ni-H resonances, demonstrating a NOE, but not active exchange.

3.3 Conclusion

In summary, we demonstrate the interaction of a μ_3-SnH, μ_3-H capped trinuclear nickel cluster, **1**, with H_2, D_2, and HD, through a variety of spectroscopic studies, including, ^{1}H, ^{2}H, ^{31}P, ^{119}Sn NMR and VT ^{1}H NMR. These experiments show reversible exchange of the μ_3-SnH and μ_3-H capping groups on the trinuclear nickel cluster with H_2 and D_2. Furthermore, ^{1}H and ^{2}H NMR experiments support conformational change of the Ni-H species under H_2, HD, and D_2 gases. Transition metal clusters are often cited as model systems for metal surfaces.[16, 17] Here, the presence of a Ni_3 core and an SnH group is found to lead to unusual activity for hydrogen exchange, but without apparent cooperativeity between the μ_3-SnH and μ_3-H groups. Future studies are focused on further understanding the reactivity profile of species of this class by probing additional reactivity with small molecule substrates.

3.4 Acknowledgements

Chapter 3, in full, is being prepared for submission for publication of the material entitled Torquato, N.A.; Palasz, J.M.; Mrse, A.A.; Kubiak, C.P. "H_2/D_2 Exchange by a μ_3-SnH, μ_3-H capped trinuclear Nickel Cluster," *Manuscript in Preparation*. The authors thank Dee-Hua Huang and Laura Pasternack at Scripps Research for VT NMR investigations. N.A.T. acknowledges Nick Myllenbeck for invaluable discussions. N.A.T acknowledges support from NSF for a Graduate Research Fellowship. Research support from NSF is also gratefully acknowledged (CHE-1853908). The dissertation author was the primary investigator and author of this paper.

3.5 References

1. Roy, M. M. D.; Omaña, A. A.; Wilson, A. S. S.; Hill, M. S.; Aldridge, S.; Rivard, E., Molecular Main Group Metal Hydrides. Chemical Reviews 2021, 121 (20), 12784-12965.

2. Mandal, S. K.; Roesky, H. W., Group 14 Hydrides with Low Valent Elements for Activation of Small Molecules. Accounts of Chemical Research 2012, 45 (2), 298-307.

3. Al-Rafia, S. M. I.; Malcolm, A. C.; Liew, S. K.; Ferguson, M. J.; Rivard, E., Stabilization of the Heavy Methylene Analogues, GeH2 and SnH2, within the Coordination Sphere of a Transition Metal. Journal of the American Chemical Society 2011, 133 (4), 777-779.

4. Torquato, N. A.; Palasz, J. M.; Bertrand, Q. C.; Brunner, F. M.; Chan, T.; Gembicky, M.; Mrse, A. A.; Kubiak, C. P., Synthesis, structure and reactivity of μ3-SnH capped trinuclear nickel cluster. Chemical Science 2022, 13 (38), 11382-11387.

5. Swarnakar, A. K.; McDonald, S. M.; Deutsch, K. C.; Choi, P.; Ferguson, M. J.; McDonald, R.; Rivard, E., Application of the Donor–Acceptor Concept to Intercept Low Oxidation State Group 14 Element Hydrides using a Wittig Reagent as a Lewis Base. Inorganic Chemistry 2014, 53 (16), 8662-8671.

6. Al-Rafia, S. M. I.; Shynkaruk, O.; McDonald, S. M.; Liew, S. K.; Ferguson, M. J.; McDonald, R.; Herber, R. H.; Rivard, E., Synthesis and Mössbauer Spectroscopy of Formal Tin(II) Dichloride and Dihydride Species Supported by Lewis Acids and Bases. Inorganic Chemistry 2013, 52 (9), 5581-5589.

7. Maudrich, J.-J.; Widemann, M.; Diab, F.; Kern, R. H.; Sirsch, P.; Sindlinger, C. P.; Schubert, H.; Wesemann, L., Hydridoorganostannylene Coordination: Group 4 Metallocene Dichloride Reduction in Reaction with Organodihydridostannate Anions. Chemistry – A European Journal 2019, 25 (70), 16081-16087.

8. Zhu, Q.; Fettinger, J. C.; Power, P. P., Hydrostannylation of carbon dioxide by a hydridostannylene molybdenum complex. Dalton Transactions 2021, 50 (36), 12555-12562.

9. Hayes, P. G.; Gribble, C. W.; Waterman, R.; Tilley, T. D., A Hydrogen-Substituted Osmium Stannylene Complex: Isomerization to a Metallostannylene Complex via an Unusual α-Hydrogen Migration from Tin to Osmium. Journal of the American Chemical Society 2009, 131 (13), 4606-4607.

10. Liu, H.-J.; Guihaumé, J.; Davin, T.; Raynaud, C.; Eisenstein, O.; Tilley, T. D., 1,2-Hydrogen Migration to a Saturated Ruthenium Complex via Reversal of Electronic Properties for Tin in a Stannylene-to-Metallostannylene Conversion. Journal of the American Chemical Society 2014, 136 (40), 13991-13994.

11. Widemann, M.; Eichele, K.; Schubert, H.; Sindlinger, C. P.; Klenner, S.; Pöttgen, R.; Wesemann, L., Synthesis and Hydrogenation of Heavy Homologues of Rhodium Carbynes: [(Me3P)2(Ph3P)Rh≡E-Ar*] (E=Sn, Pb). Angewandte Chemie International Edition 2021, 60 (11), 5882-5889.

12. Albertin, G.; Antoniutti, S.; Castro, J.; García-Fontán, S.; Zanardo, G., Preparation and Reactivity of Stannyl Complexes of Manganese and Rhenium. Organometallics 2007, 26 (11), 2918-2930.

13. Cardin, C. J.; Cardin, D. J.; Parge, H. E.; Power, J. M., Metal cluster expansion by addition of low-valent group 4B reagents: crystal and molecular structure of [Os3SnH2(CO)10{CH(SiMe3)2}2]; a compound with hydrogen bridging osmium and tin. Journal of the Chemical Society, Chemical Communications 1984, (9), 609-610.

14. Khan, M. M. M.; Ghosh, S.; Hogarth, G.; Tocher, D. A.; Richmond, M. G.; Kabir, S. E.; Roesky, H. W., Mixed main group transition metal clusters: Reactions of [Ru3(CO)10(μ-dppm)] with Ph3SnH. Journal of Organometallic Chemistry 2017, 840, 47-55.

15. Douglas, G.; Jennings, M. C.; Manojlović-Muir, L.; Muir, K. W.; Puddephatt, R. J., Synthesis and characterization of complexes with Pt3(μ3-SnX3) groups including the first SnF3– complex; possible models for heterogeneous Pt–Sn catalysts. Journal of the Chemical Society, Chemical Communications 1989, (3), 159-161.

16. Muetterties, E. L.; Rhodin, T. N.; Band, E.; Brucker, C. F.; Pretzer, W. R., Clusters and surfaces. Chemical Reviews 1979, 79 (2), 91-137.

17. Lemoine, P., Electrochemistry of transition metal clusters. Coordination Chemistry Reviews 1982, 47 (1), 55-88.

18. Breedlove, B. K.; Fanwick, P. E.; Kubiak, C. P., Tin-Capped Trinuclear Nickel Clusters: Redox Isomerism between μ3-Stannyl and μ3-Stannylene Clusters of the Class [Ni3(dppm)3(μ3-I)(μ3-SnClx)]n+ (x = 2, n = 1; x = 3, n = 0). Inorganic Chemistry 2002, 41 (17), 4306-4308.

19. Simón-Manso, E.; Kubiak, C. P., A Trihydroxy Tin Group That Resists Oligomerization in the Trinuclear Nickel Cluster [Ni3(μ-P,P′-PPh2CH2PPh2)3(μ3-L)- (μ3-Sn(OH)3)]. Angewandte Chemie International Edition 2005, 44 (7), 1125-1128.

20. Torquato, N. A.; Lara, J. K.; Bertrand, Q. C.; Mrse, A. A.; Gembicky, M.; Kubiak, C. P., Electronic structural studies of μ3-Sn(OR)3 capped trinuclear nickel clusters. Polyhedron 2022, 224, 116000.

21. Kan, Y.; Zhang, Q., Transition Metal Complexes for Hydrogen Activation. In Nanostructured Materials for Next-Generation Energy Storage and Conversion: Hydrogen Production, Storage, and Utilization, Chen, Y.-P.; Bashir, S.; Liu, J. L., Eds. Springer Berlin Heidelberg: Berlin, Heidelberg, 2017; pp 43-84.

22. Wang, S.; Sherbow, T. J.; Berben, L. A.; Power, P. P., Reversible Coordination of H2 by a Distannyne. *Journal of the American Chemical Society* **2018,** *140* (2), 590-593.

23. Rivard, E.; Fischer, R. C.; Wolf, R.; Peng, Y.; Merrill, W. A.; Schley, N. D.; Zhu, Z.; Pu, L.; Fettinger, J. C.; Teat, S. J.; Nowik, I.; Herber, R. H.; Takagi, N.; Nagase, S.; Power, P. P., Isomeric Forms of Heavier Main Group Hydrides: Experimental and Theoretical Studies

of the [Sn(Ar)H]2 (Ar = Terphenyl) System. *Journal of the American Chemical Society* **2007,** *129* (51), 16197-16208.

3.6 Appendix B

3.6.1 Experimental General Considerations

General considerations

All reactions and manipulations were carried out under an atmosphere of nitrogen using either Schlenk line techniques or VAC glovebox. Solvents were sparged with nitrogen, dried on a custom dry solvent system over alumina columns, and stored over molecular sieves before use. $SnCl_2$ (anhydrous), $Ni(COD)_2$, bis(diphenylphosphino)methane (dppm), $Ni(acac)_2$, $NaB(Et)_3H$ (1.0 M solution in THF), were obtained from commercial suppliers and used without further purification. Ultrahigh-purity H_2 was purchased from Airgas, D_2 (99.8% D) was purchased from Sigma Aldrich, and HD (96 mol% DH, 98% D) was purchased from Sigma Aldrich. Benzene-d_6 and toluene-d_8 was stored under nitrogen over 3Å molecular sieves. $HSnNi_3(dppm)_3H$, **1**, was prepared according to literature procedures.[1]

NMR Spectroscopy.

^1H and ^{31}P were recorded on a Jeol 400 and 500 MHz spectrometers. ^{119}Sn NMR spectra were recorded on a Jeol 400 MHz Spectrometers. Variable-temperature NMR spectroscopy was performed on a Bruker AV NEO 399 NMR Spectrometer. ^1H chemical shifts are reported relative to the residual hydrogen atoms in benzene-d_6 or toluene-d_8 solvents. ^{31}P chemical shifts are reported relative to 85% H_3PO_4.^{119}Sn NMR was referenced externally to $SnBu_4$ in benzene-d_6 {-11.7ppm}.

3.6.2 Experimental Procedures

Conversion of 1 to 1D.

A medium-walled j-young NMR tube was charged with complex **1** (15.0 mg, 0.010 mmol), an internal reference, tetramethylbenzene (0.6 mg, 0.004 mmol), and 0.5 ml benzene-d_6. The tube

was cycled onto a Schlenk line, freeze-pump thawed 3x, and cooled to liquid nitrogen temperature, -196 C. D_2 (g) was added to the NMR tube at -196 °C, resulting in the addition of 4 atm of D_2. This was allowed to warm up to 22°C and tracked via ^{1}H NMR spectroscopy over time. Over the course of 4 hours, complex **1** converted to complex **1D** in 99% conversion, as determined by ^{1}H NMR integration of the SnH and NiH resonances against P(CH_2)P and the internal standard, tetramethylbenzene. Formation of **1D** was supported by ^{2}H and ^{119}Sn NMR. (see Figure 2 in manuscript and S3)

Conversion of 1 to 1:1:1:1 mixture of 1, 1D, 1HD, and 1DH.

Route 1: A medium-walled j-young NMR tube was charged with complex **1** (10.0 mg, 0.000447 mmol), an internal reference, tetramethylbenzene (2.0 mg, 0.015 mmol), and 0.5 ml benzene-d_6. The tube was cycled onto a Schlenk line, freeze-pump thawed 3x, and warmed back up to room temperature, 22 °C. The NMR tube was charged with 1.2 atm HD and tracked via ^{1}H NMR spectroscopy over time. Over the course of 22 hours, complex **1** converted to a 1:1:1:1 mixture of **1**, **1D**, **1HD**, and **1DH**, as determined by ^{1}H NMR integration of the SnH and NiH resonances against P(CH_2)P and the internal standard, tetramethylbenzene. Formation of the mixture of species was supported by ^{2}H and ^{119}Sn NMR. (see S6 and S7)

Route 2: A j-young NMR tube was charged with **1** (10.2 mg, 0.00704), **1D** (10.2 mg, 0.00703), an internal reference, tetramethylbenzene (3.1 mg, 0.023 mmol) and 0.5 ml benzene-d_6. After 10 minutes, this resulted in the formation of a 1:1:1:1 mixture of **1**, **1D**, **1HD**, and **1DH**, as determined by ^{1}H NMR integration of the SnH and NiH resonances against P(CH_2)P and the internal standard, tetramethylbenzene.

Hydrogenation of 1.

A medium-walled j-young NMR tube was charged with **1** (17.4 mg, 0.0120 mmol) and benzene-d_6. The tube was cycled onto a Schlenk line, freeze-pump thawed 3x, and warmed back up to room temperature, 22 °C. The NMR tube was charged with 1 atm H_2 and tracked via ^{1}H NMR spectroscopy over time.

General Procedure for VT NMR experiments.

A medium-walled j-young NMR tube was charged with 1 (5.1 mg, 0.0035 mmol) and toluene-d_8. For the addition of H_2 and HD: The tube was cycled onto a Schlenk line, freeze-pump thawed 3x, and warmed back up to room temperature, 22 °C. The NMR tube was charged with 1 atm H_2 or HD. The H_2 reaction was allotted 2 hours to equilibrate before VT ^{1}H NMR spectra were obtained. Whereas the HD reaction was given 20 hours for equilibration before VT ^{1}H NMR spectra were obtained.

NMR procedure: VT ^{1}H NMR for 1 with N_2, H_2 and HD was obtained at temperatures from -50 to 60 °C.

3.6.3 NMR Spectroscopy

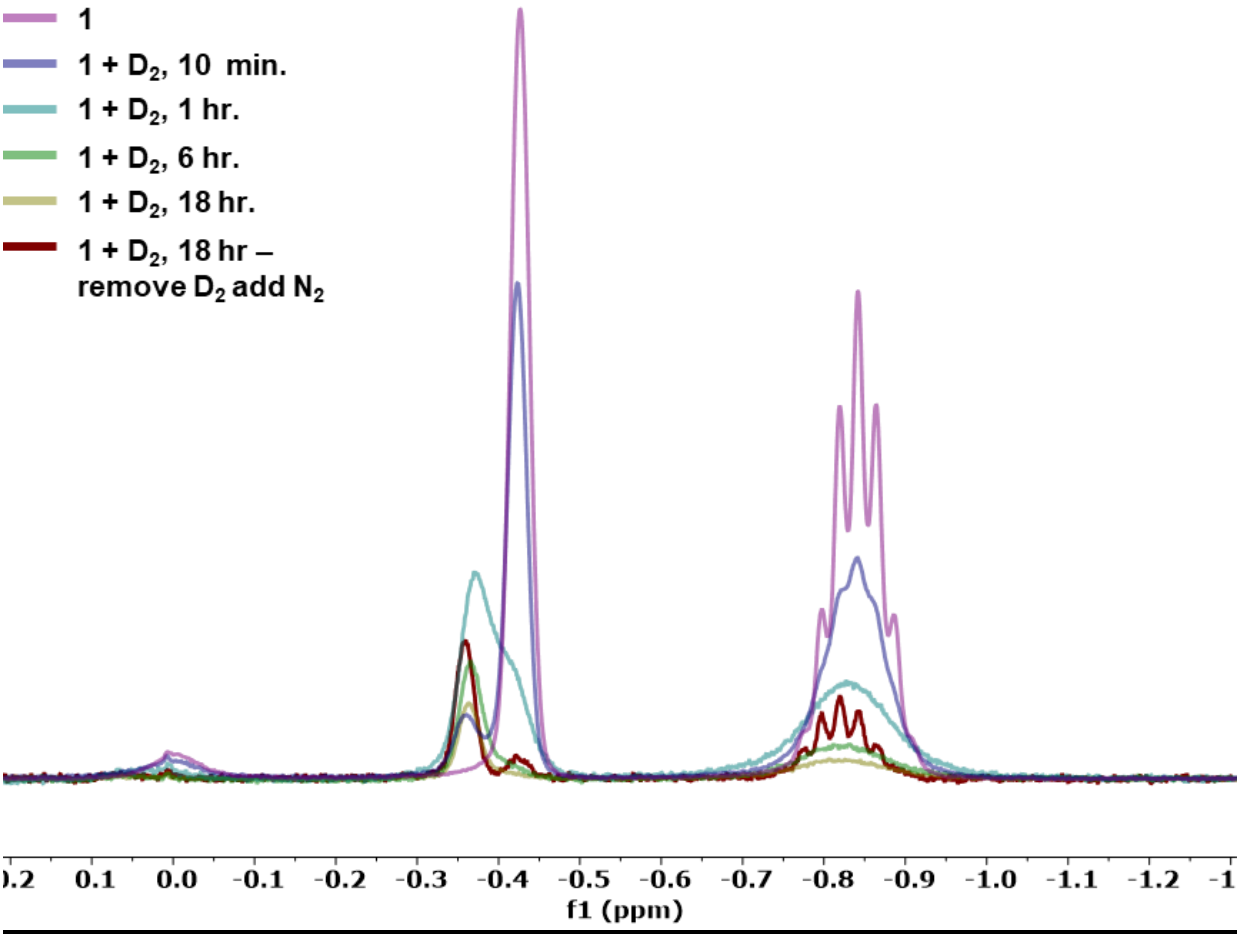

Figure 3.7. ^{1}H NMR spectra of **1** after addition of 1 atm D_2 in benzene-d_6, with various timepoints superimposed and focused in on the Sn-H and Ni-H resonance regions.

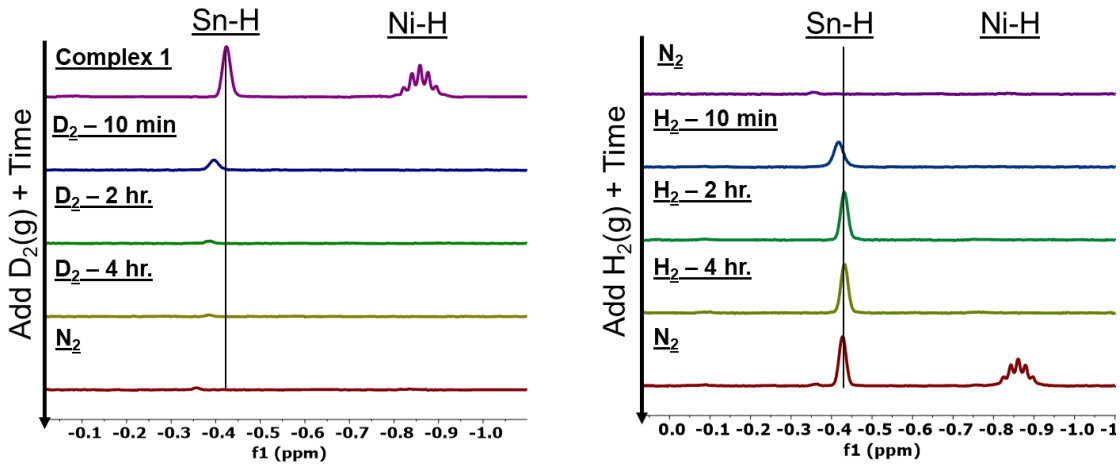

Figure 3.8. ^{1}H NMR spectra of **1** after addition of 4 atm D_2 in benzene-d_6 (left) and **1D** after addition of 4 atm H_2 in benzene-d_6 (right), focused in on the Sn-H and Ni-H resonance regions.

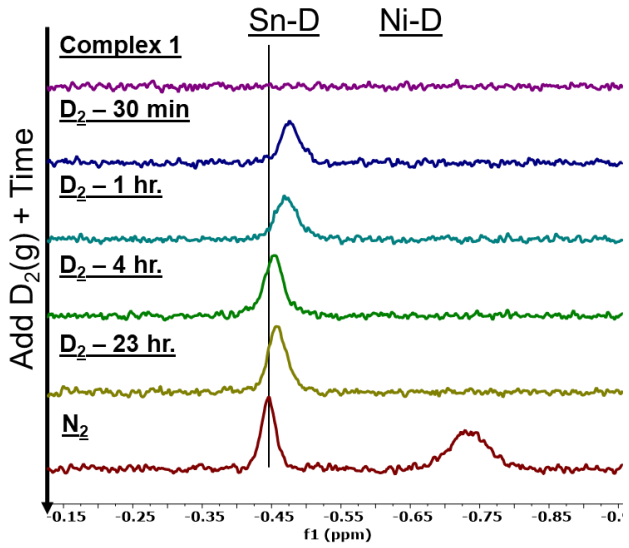

Figure 3.9. ^{2}H NMR spectra of **1** with 1 atm D_2 in benzene referenced to benzene-d_6, focused in on Sn-D and Ni-D resonance regions.

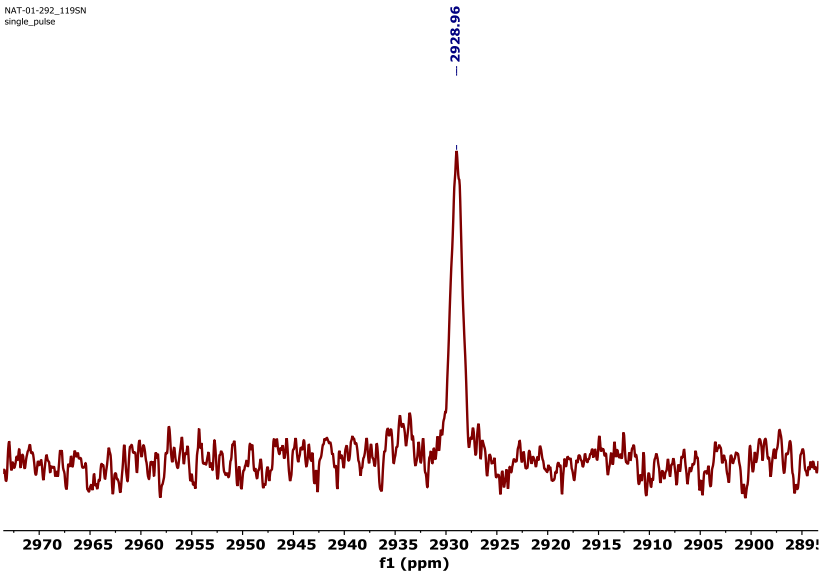

Figure 3.10. $^{119}Sn\{^{1}H\}$ NMR spectrum of **1D** in benzene-d_6.

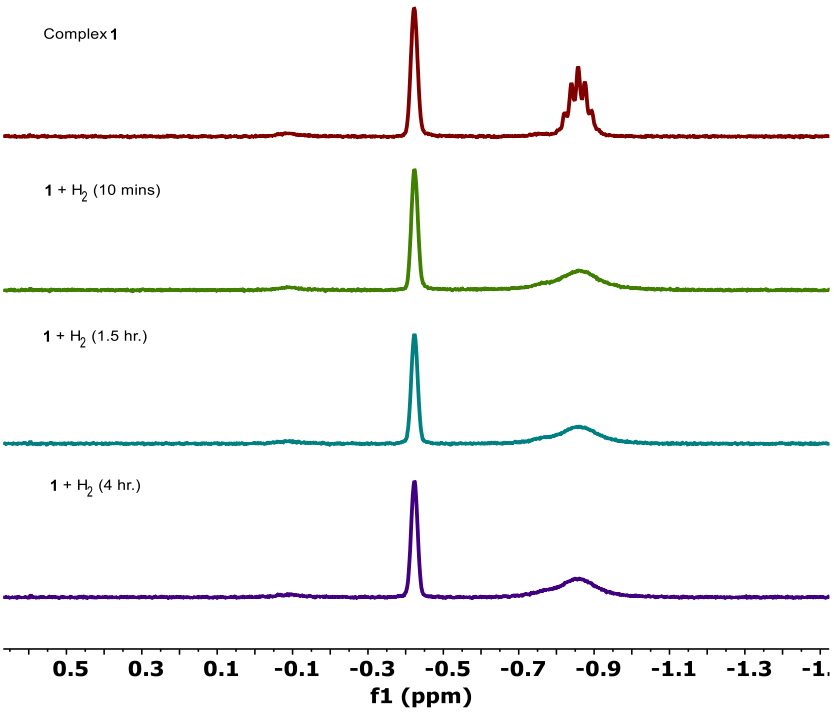

Figure 3.11. ^{1}H NMR spectra of **1** in benzene-d_6 under 1 atm H_2, focused in on Sn-H and Ni-H resonance regions. This reaction was monitored over the course of 4 hours. The integration of the Ni-H peak decreases in intensity upon addition of H_2, the integration of the Ni-H becomes constant after the 1.5-hour timepoint.

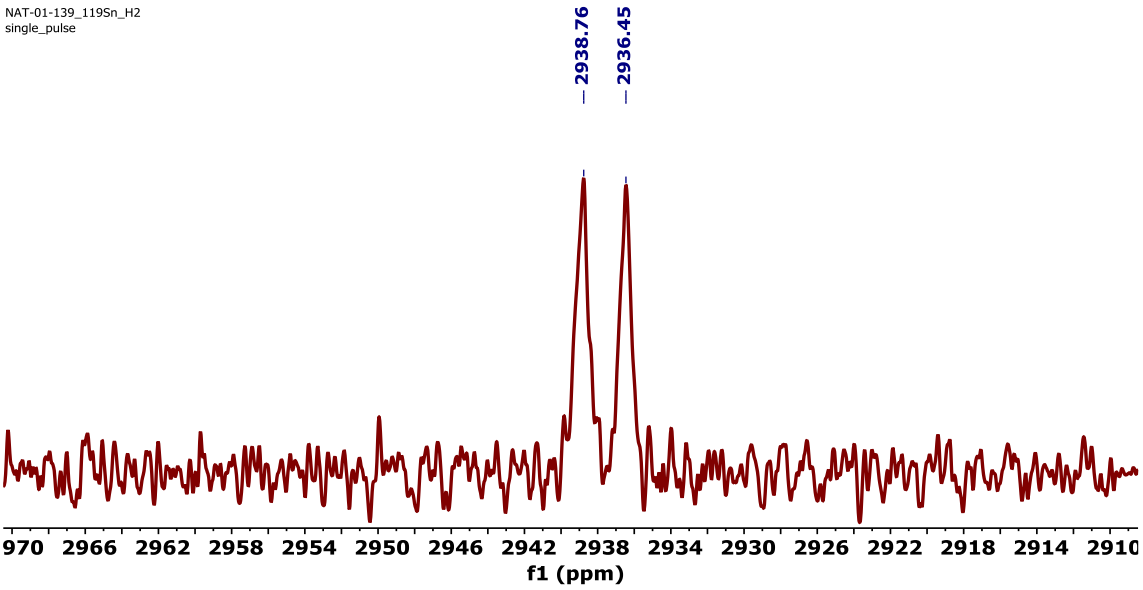

Figure 3.12. $^{119}Sn\{^{1}H\}$ NMR spectrum of **1** under 1 atm H_2 in benzene-d_6.

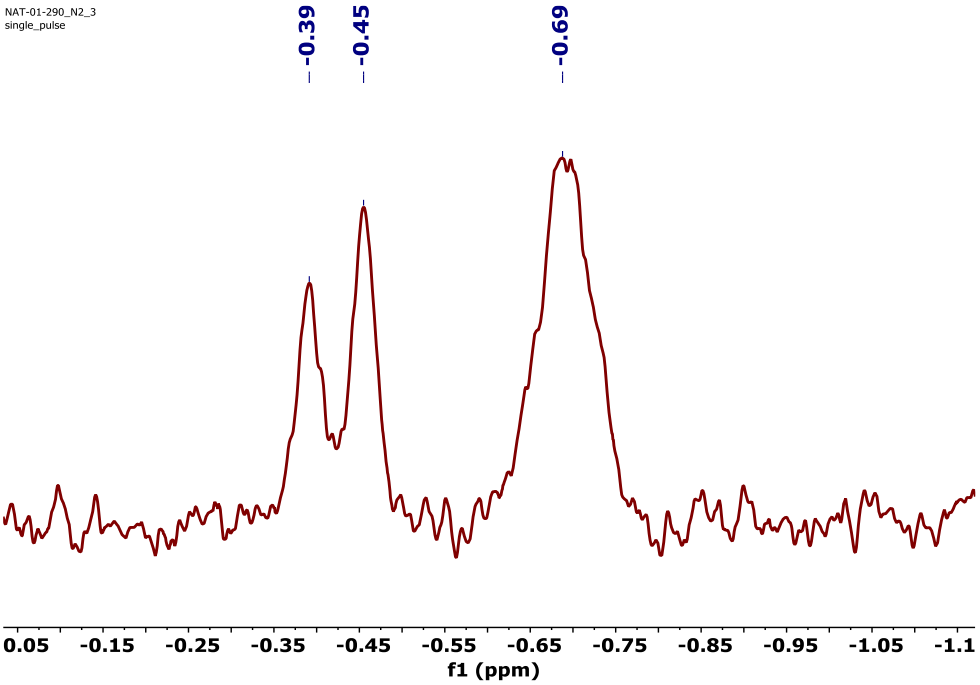

Figure 3.13. ^{2}H NMR spectrum of a 1:1:1:1 ratio of **1**, **1D**, **1HD** and **1DH**, focused in on Sn-D and Ni-D resonance regions.

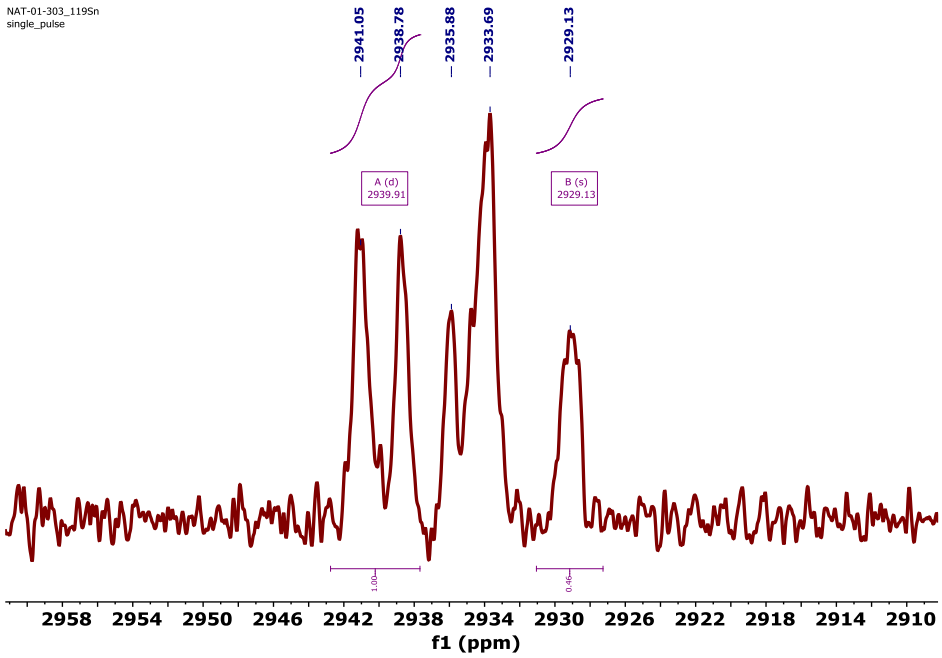

Figure 3.14. $^{119}Sn\{^{1}H\}$ NMR spectrum of a 1:1:1:1 ratio of **1**, **1D**, **1HD** and **1DH 1**.

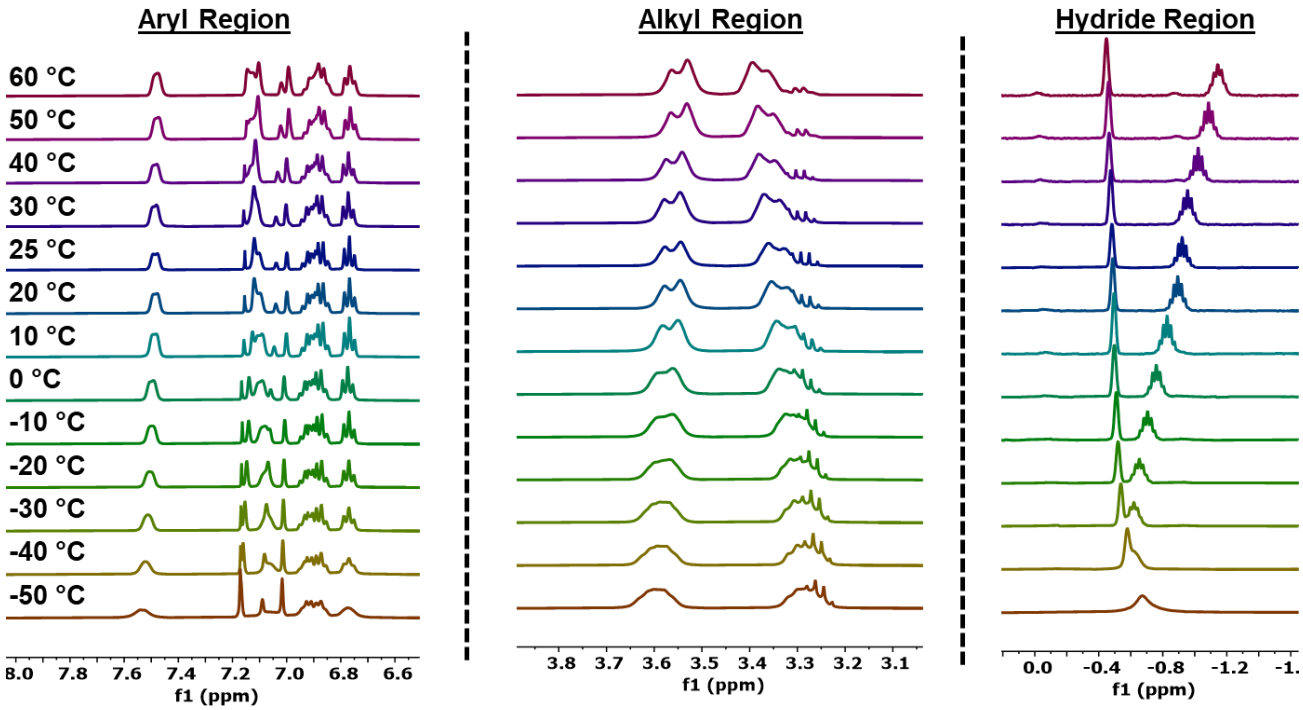

Figure 3.15. Variable Temperature ^{1}H NMR spectra of complex **1** under 1 atm N_2 in toluene-d_8, zoomed in on aryl, alkyl and hydride regions for better visualization – intensities are not to scale (see Figure 3.16).

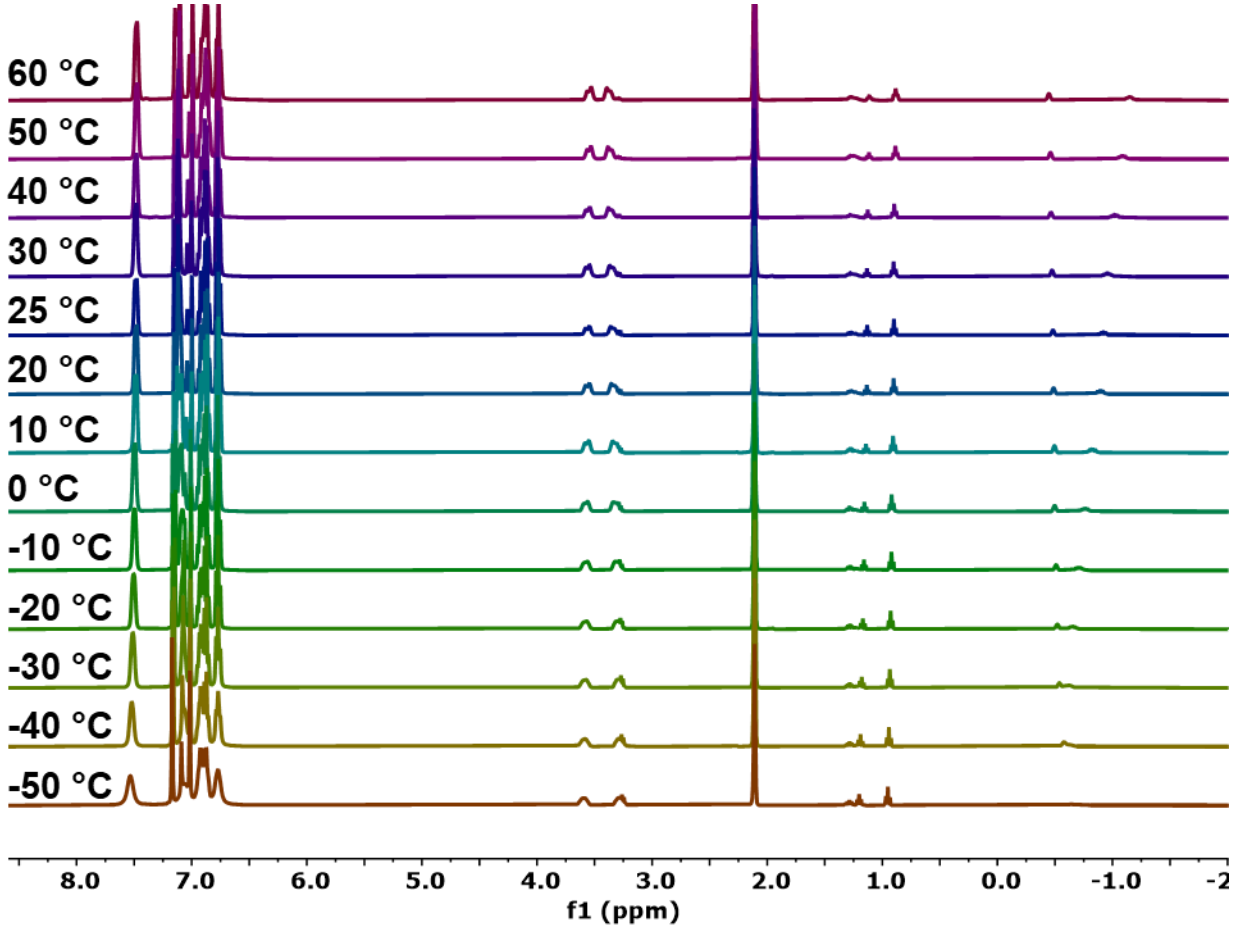

Figure 3.16. Variable Temperature ^{1}H NMR spectra of **1** with N_2 full spectrum from 60 °C to -50 °C.

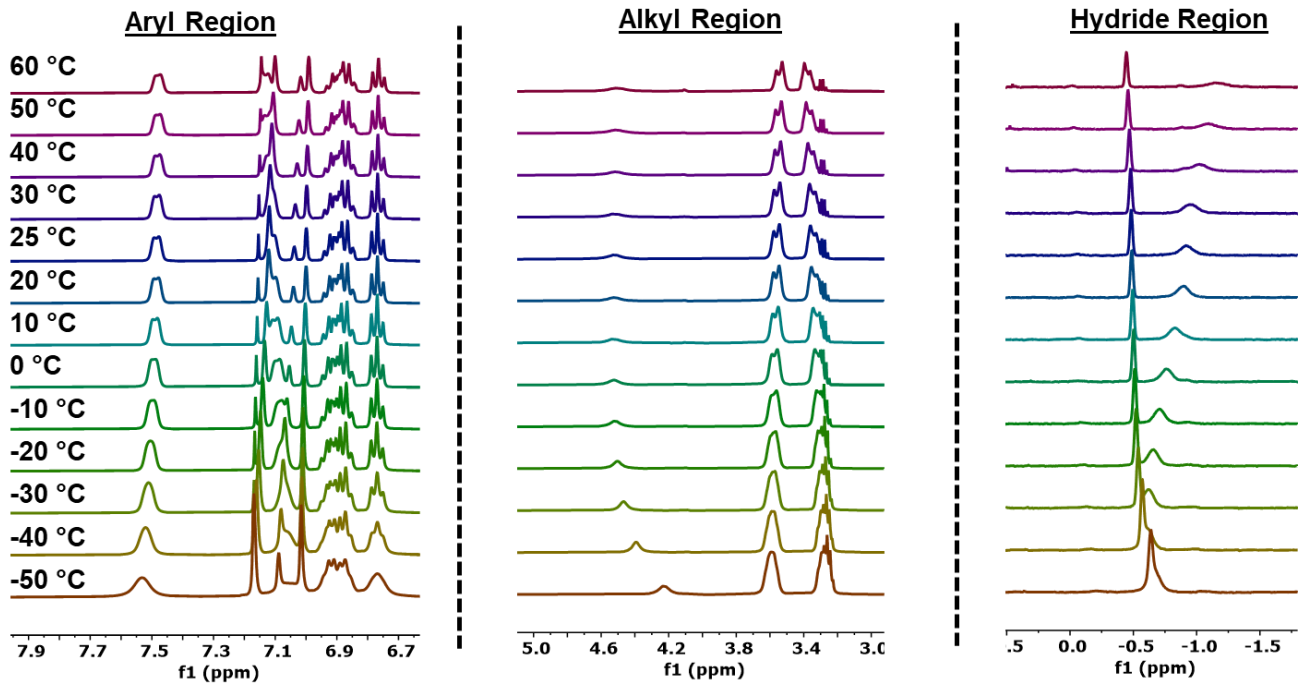

Figure 3.17. Variable Temperature ^{1}H NMR Spectra of complex **1** under 1 atm H_2 in toluene-d_8, zoomed in on aryl, alkyl and hydride regions for better visualization – intensities are not to scale (see Figure 3.18).

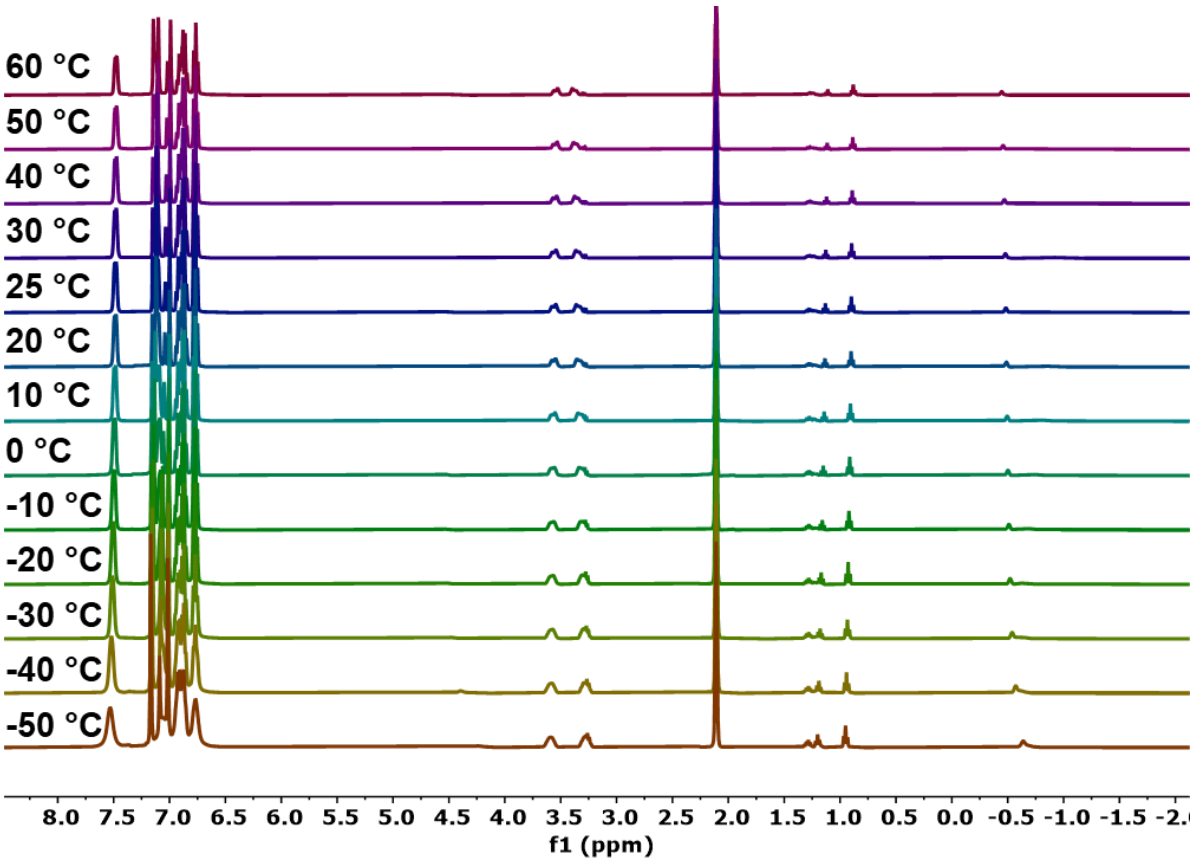

Figure 3.18 Variable Temperature ^{1}H NMR of **1** with H_2 in toluene-d_8 full spectrum from 60 °C to -50 °C.

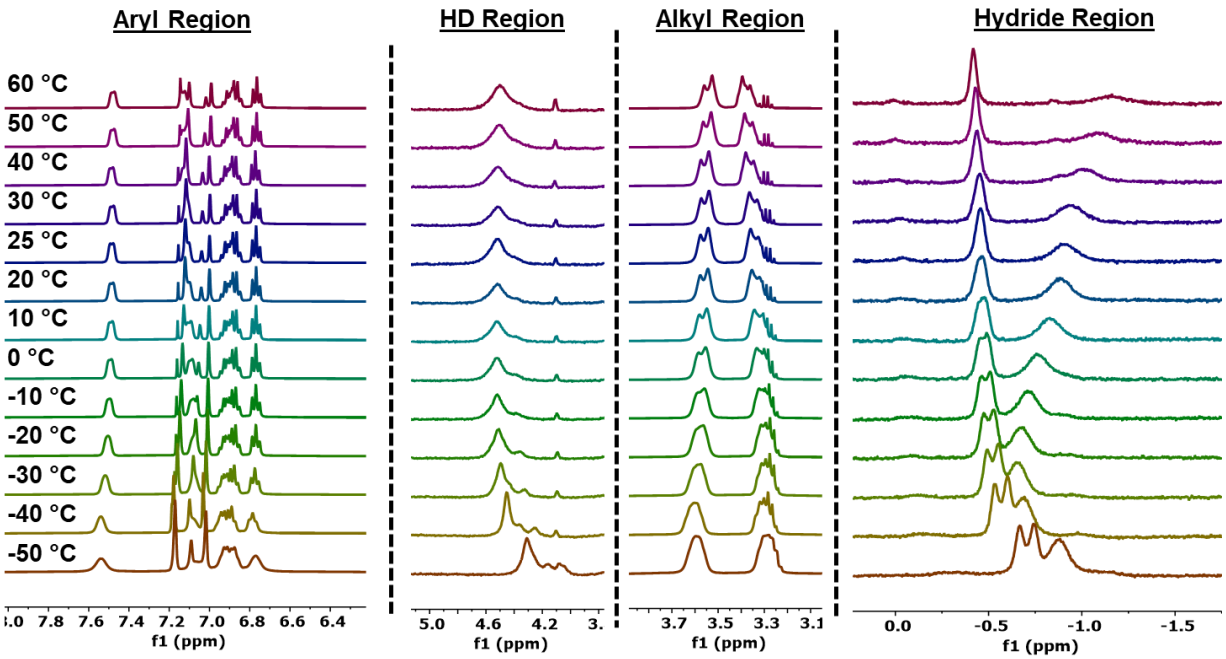

Figure 3.19. Variable Temperature 1H NMR spectra of complex **1** under 1 atm HD in toluene-d_8, zoomed in on aryl, alkyl and hydride regions for better visualization – intensities are not to scale (see Figure 3.20).

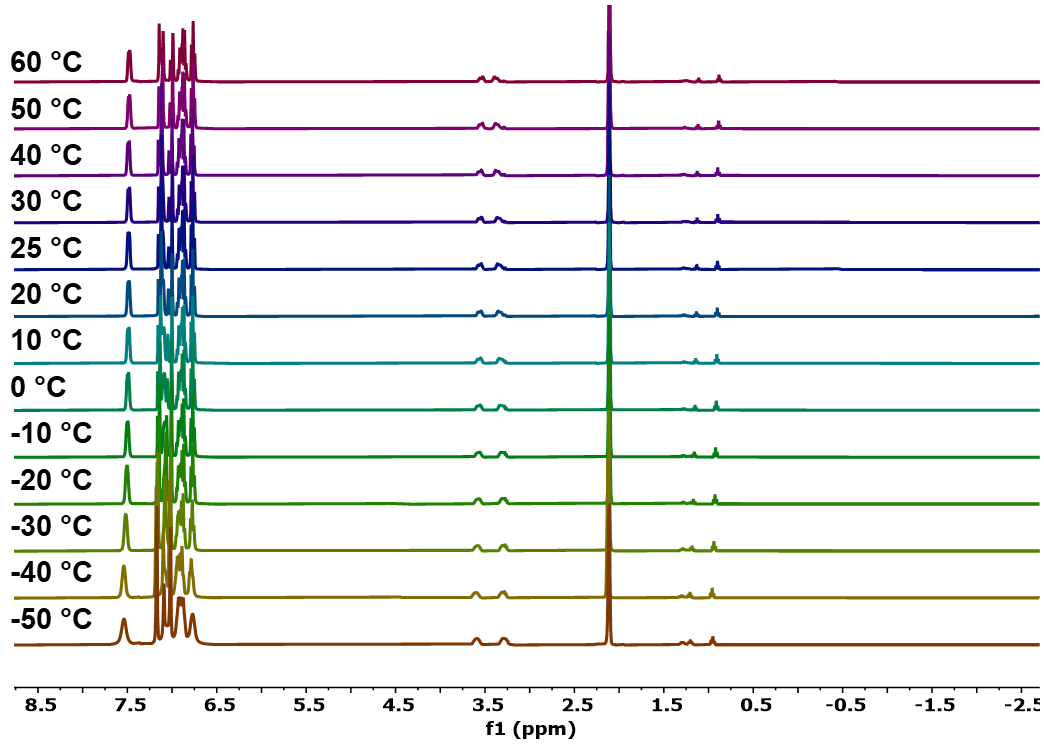

Figure 3.20. Variable Temperature ^{1}H NMR of **1** with HD in toluene-d_8 full spectrum from 60 °C to -50 °C.

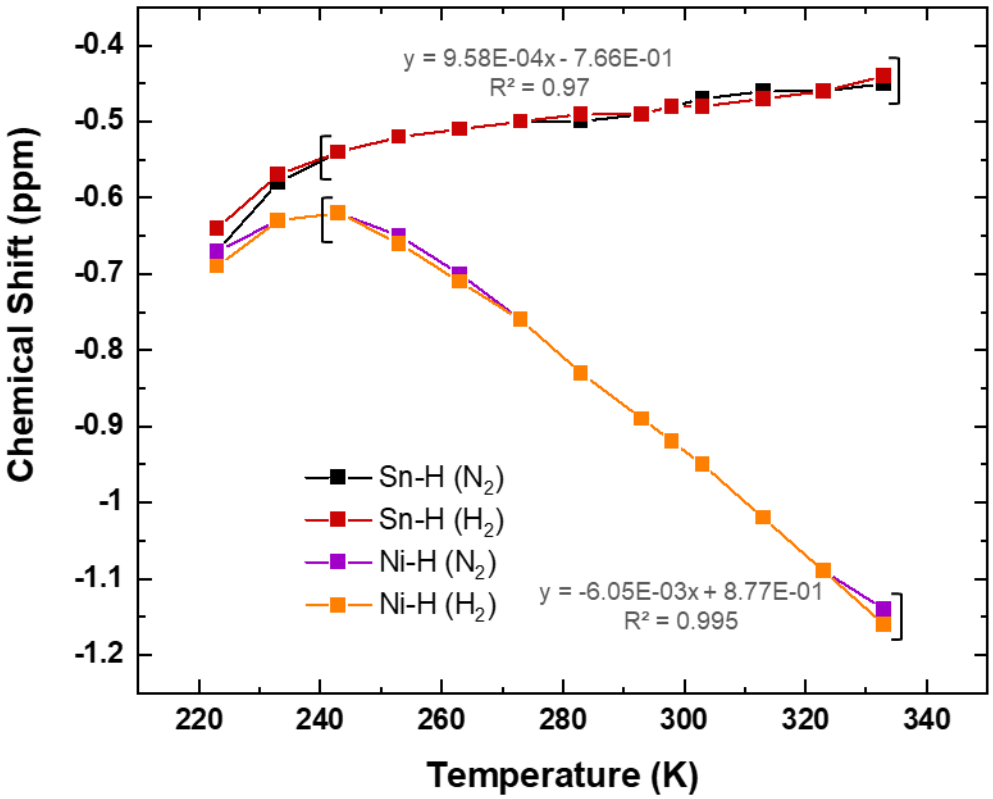

Figure 3.21. Chemical Shift (ppm) vs. Temperature (K) graph of VT ^{1}H NMR studies of 1 with N_2 and H_2.

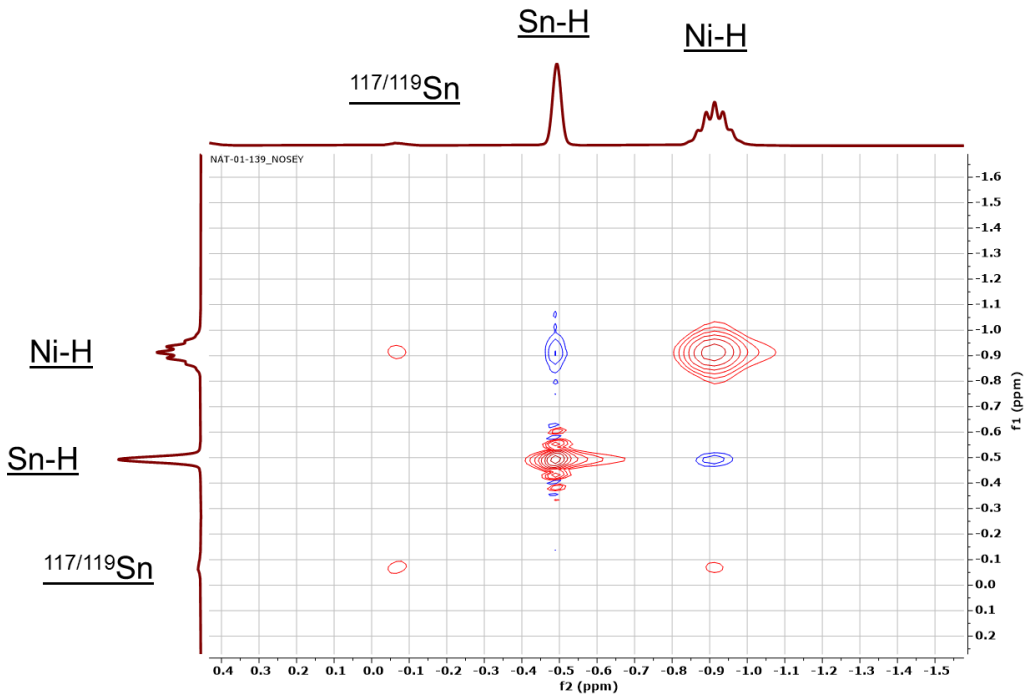

Figure 3.22. ^{1}H Nuclear Overhauser Effect Spectroscopy (NOESY) NMR of **1** in benzene-d_6, focused in on the Sn-H and Ni-H resonance region.

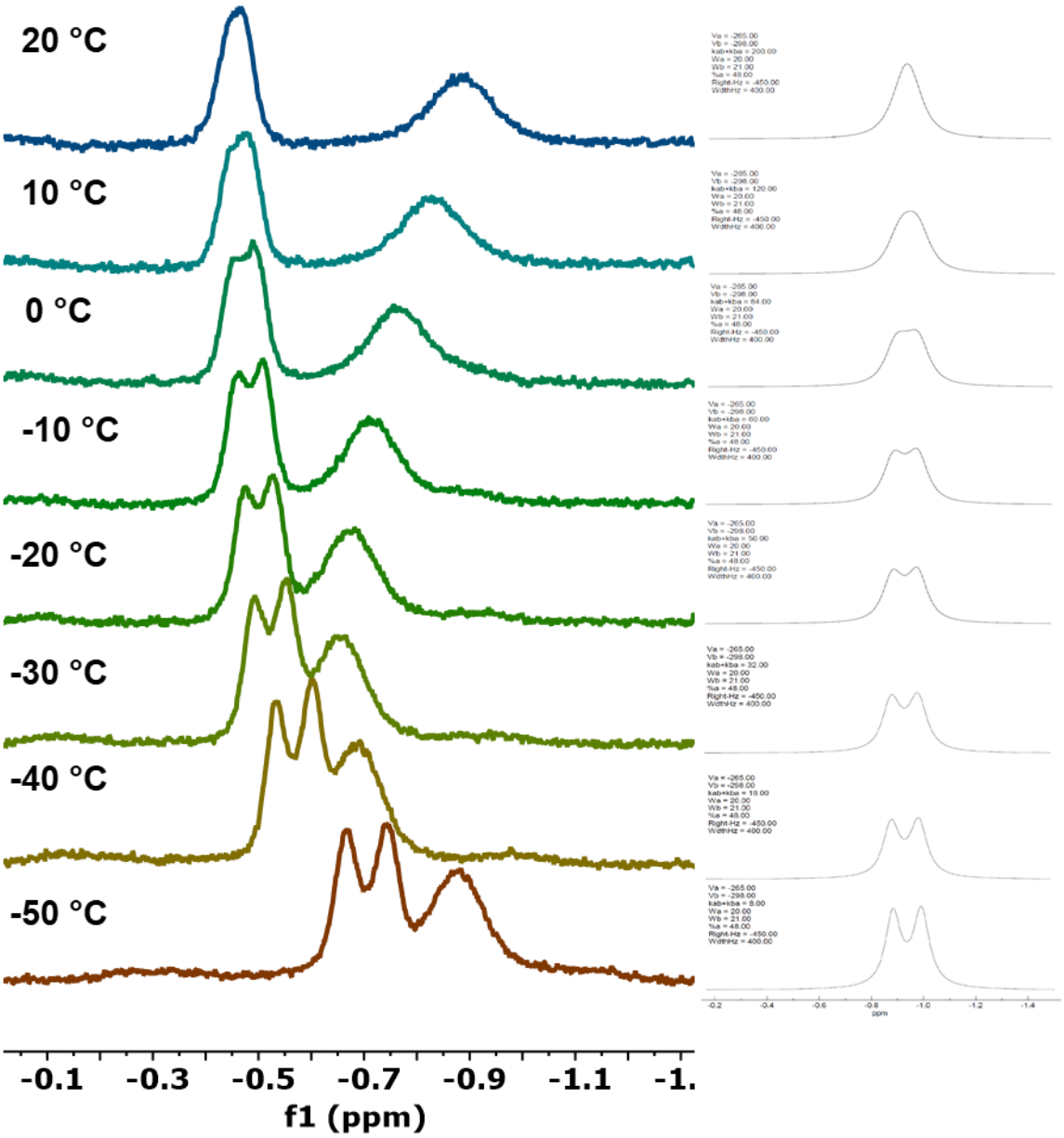

Figure 3.23. Variable Temperature ^{1}H NMR spectra of complex **1** under 1 atm HD in toluene-d_8, zoomed in on hydride regions for better visualization (left). Coalescence of Sn-H peaks modeled by WINDNMR (right). Simulated data output shown below (Table S1).

Table 3.1. WindD NMR simulation Data output.

TEMP K:	223.16	233.16	243.16	253.16	263.16	273.16	283.16	293.16
TEMP C:	-50.00	-40.00	-30.00	-20.00	-10.00	0.00	10.00	20.00
KAB+KBA	8.000	18.00	32.00	50.00	60.00	84.00	120.00	200.00
%A	48.00	48.00	48.00	48.00	48.00	48.00	48.00	48.00
KAB	4.160	9.360	16.640	26.000	31.200	43.680	62.400	104.000
ΔG#(AB)	12.30	12.45	12.78	13.10	13.54	13.89	14.22	14.44
KBA	3.840	8.640	15.360	24.000	28.800	40.320	57.600	96.000
ΔG#(BA)	12.34	12.53	12.81	13.14	13.58	13.93	14.26	14.49

3.6.4 Appendix B References

1. Torquato, N.A.; Palasz, J.M.; Bertrand, Q.C.; Brunner, F.M.; Chan, T; Gembicky, M.; Mrse, A.A.; Kubiak, C.P. Synthesis, structure and reactivity of μ_3-SnH capped trinuclear nickel cluster, *Chem. Sci.*, **2022**, 13, 11382-11387.

CHAPTER 4. Electronic structural studies of μ_3-Sn(OR)$_3$ capped trinuclear nickel clusters

4.1 Introduction

Over the past 20 years, there have been multiple advancements in the tin chemistry platform as the production of low valent and highly reduced tin species have led to the observation of transition-metal like reactivity, including activation of small and unsaturated molecules.[1] Further developments have come from coupling stannyl ligands to transition metal complexes resulting in new electronic features and reactivity modes.[2-5] Previous work by our group has focused on the synthesis of trinuclear nickel clusters capped by X and/or L type substituents that exhibit a wide range of reactivities and electronic structures associated with the trinuclear nickel core. [6-10] In the early 1990s, our group reported that $[Ni_3(\mu_3\text{-}CNCH_3)(\mu_3\text{-}I)(\mu_2\text{-}dppm)_3]^+$ is a competent catalyst in the 2-electron disproportionation of CO_2 to CO and CO_3^{2-}.[9] In addition, $Ni_3(\mu_3\text{-}I)_2(\mu_2\text{-}dppm)_3$ has been used in the photochemical generation of the radical anion of carbon dioxide, $CO_2^{\bullet-}$.[11] Further studies in our group have demonstrated that the electronics of the cluster is dependent on the capping substituent on the trinuclear nickel core. This is evidenced by cyclic voltammetry as the μ_3-I and μ_3-isocyanide capped clusters undergo a single redox event, whereas, a telluride-capped cluster, $[Ni_3(dppm)_3(\mu_3\text{-}Te)_2]$, features three reversible single electron redox couples.[6, 7] More recently, our group investigated the synthesis of μ_3-stannyl capped trinuclear nickel clusters and began studying the effects of stannyl capping groups on the reactivity and electronics of the clusters. These studies led to the development of $(Cl)_3Sn$ and $(OH)_3Sn$ capped trinuclear nickel clusters, $[Ni_3(dppm)_3(\mu_3\text{-}I)(\mu_3\text{-}SnCl_3]$ and $[Ni_3(dppm)_3(\mu_3\text{-}Cl)(\mu_3\text{-}Sn(OH)_3]$.[3, 12] These complexes showed labilization of the substituents attached to tin upon electrochemical reduction. They also participated in condensation of CO_2 and epoxides.[3, 12] To further advance our knowledge of this series, we investigated the relationship between ligand substitution on tin and

the structure and redox properties of the clusters. Herein, we report the synthesis, reactivity, and electronic properties of $(OPh)_3Sn$, $(OEt)_3Sn$ and $(C_3H_5O_3)Sn$ capped trinuclear nickel clusters, $[Ni_3(dppm)_3(\mu_3\text{-}Cl)(\mu_3\text{-}Sn(OEt)_3)]$ (**1**), $[Ni_3(dppm)_3(\mu_3\text{-}Cl)(\mu_3\text{-}Sn(OPh)_3)]$ (**2**) and $[Ni_3(dppm)_3(\mu_3\text{-}Cl)(\mu_3\text{-}Sn(C_3H_5O_3))]$ (**3**).

4.2 Experimental

All reactions and manipulations were carried out under an atmosphere of nitrogen using either Schlenk line techniques or VAC Atmospheres glovebox. Solvents were sparged with nitrogen, dried on a custom dry solvent system over alumina columns, and stored over 3Å molecular sieves before use. $SnCl_2$ (anhydrous), $Ni(COD)_2$, bis-diphenylphosphinomethane (dppm), $Ni(acac)_2$, KOEt,, NaOPh, and glycerol were obtained from commercial suppliers and used without further purification unless otherwise noted. Benzene-d_6 was sparged with nitrogen and stored in the dark, under nitrogen, over a 50:50 mixture of 3Å and 4Å molecular sieves. $[Ni_3(dppm)_3(\mu_3\text{-}Cl)(\mu_3\text{-}SnCl_3]$ was prepared according to literature procedures.[12] ^1H and ^{31}P NMR spectra were obtained in benzene-d_6 using a Jeol 500 MHz spectrometer. ^{13}C NMR spectra were obtained using a Jeol 500 MHz for complex **2** and a Joel 400 MHz for complex **1** and **3**. ^1H and ^{13}C spectra are referenced to internal solvent peaks; ^{31}P NMR signals are reported with respect to external 85% H_3PO_4. ^{119}Sn NMR was obtained in benzene-d_6 using a Jeol 400 MHz spectrometer and referenced externally to $SnBu_4$ in benzene-d_6 {-11.7ppm}. Carbon, hydrogen, and nitrogen elemental analyses were performed by Midwest Microlab. Electrochemical measurements were performed on a BASi Epislon potentiostat. A single-compartment cell was used for cyclic voltammetry experiments with a glassy carbon working electron (3 mm in diameter, Bioanalytical Systems, Inc.), glassy carbon counter electrode, and Ag/AgCl pseudo-reference electrode. All potentials are referenced to the $Fc^{+/0}$ couple using Cp_2Co and Cp^*_2Fe as internal references.

4.2.1. $Ni_3(dppm)_3(\mu_3\text{-}Cl)(\mu_3\text{-}Sn(OEt)_3)$ (1)

A 22 mL scintillation vial was charged with $[Ni_3(dppm)_3(\mu_3\text{-}Cl)(\mu_3\text{-}SnCl_3]$ (200.1 mg, 0.126 mmol), KOEt (63.5 mg, 0.755 mmol), 10 ml THF, and a stir bar. The solution was heated to 40 °C and after 1 h. complete conversion of the starting material was observed by $^{31}P\{^1H\}$ NMR spectroscopy. Volatile compounds were removed *in vacuo* to afford a purple residue, which was then dissolved in benzene and filtered over a celite plug to remove undissolved solids (presumably including KCl). The solution was then concentrated to 2 mL and layered with pentane (approx. 18 mL). After 2 days at 22 °C, a dark purple solid formed, and a light purple supernatant was carefully decanted. The solid was washed with -20 °C diethyl ether (5 x 2 ml) and then additional pentane (2 x 4 ml). After the solid was allowed to settle, the supernatant was carefully decanted; residual volatile compounds were removed *in vacuo* to yield **1** as a purple powder (86% yield). Layering of pentane (18 mL) over a THF solution of **1** (2 mL) at -20 °C afforded X-ray quality crystals. ^1H NMR (500.16 MHz, C_6D_6, 298 K) δ 7.81 (d, J = 7.2 Hz, 12H, ArH), 7.43 (d, J = 7.5 Hz, 12H, ArH), 6.87 (t, J = 7.3 Hz, 6H, ArH), 6.78 (dt, J = 12.2, 7.3 Hz, 18H, ArH), 6.67 (t, J = 7.5 Hz, 12H, ArH), 6.05 (d, J = 12.7 Hz, 3H, $P(CH_2)P$), 5.13 (q, J = 6.9 Hz, 6H, OCH_2CH_3), 3.50 (d, J = 12.5 Hz, 3H, $P(CH_2)P$), 1.88 (t, J = 6.9 Hz, 9H, OCH_2CH_3). ^{13}C NMR (125.77 MHz, C_6D_6) δ 136.69, 135.70, 135.06, 132.82, 129.09, 127.46, 127.35, 61.35, 53.98, 21.54. ^{31}P NMR (202.47 MHz, C_6D_6, 298 K) δ -0.54. ^{119}Sn NMR (148.99 MHz, C_6D_6, 298 K) δ -36.41 (p, $^2J_{(119Sn/117Sn\text{-}31P)}$ = 110.5 Hz). Elemental analysis (%) calcd for $C_{81}H_{81}ClNi_3O_3P_6Sn$: C 60.11, H 5.04; found: C 59.88, H 5.38.

4.2.2. $Ni_3(dppm)_3(\mu_3\text{-}Cl)(\mu_3\text{-}Sn(OPh)_3)$ (2)

A 22 mL scintillation vial was charged with $[Ni_3(dppm)_3(\mu_3\text{-}Cl)(\mu_3\text{-}SnCl_3]$ (100 mg, 0.063 mmol), NaOPh (43.8 mg, 0.377 mmol), 10 ml THF, and a stir bar. The solution was maintained at 22 °C and after 3 hrs. complete conversion of the starting material was observed by $^{31}P\{^1H\}$ NMR

spectroscopy. Volatile compounds were removed *in vacuo* to afford a purple residue, which was then dissolved in benzene and filtered over a celite plug to remove undissolved solids (presumably including NaCl and excess NaOPh). The solution was then concentrated to 2 mL and layered with pentane (approx. 18 mL). After 2 days at 22 °C, a dark purple solid formed, and a light purple supernatant was carefully decanted. The solid was washed with diethyl ether (5 x 2 ml) and then additional pentane (2 x 4 ml). After the solid was allowed to settle, the supernatant was carefully decanted; residual volatile compounds were removed *in vacuo* to yield **2** as a purple powder (93% yield). Vapor diffusion of diethyl ether into a THF solution of **2** at -20 °C afforded X-ray quality crystals. ^{1}H NMR (500.16 MHz, C_6D_6, 298 K) δ 7.76 (d, *J* = 7.4 Hz, 12H, ArH), 7.53 – 7.47 (m, 6H, ArH), 7.30 (dd, *J* = 8.5, 7.1 Hz, 6H, ArH), 7.21 (d, *J* = 7.3 Hz, 12H, ArH), 6.88 (q, *J* = 7.0 Hz, 9H, ArH), 6.77 (t, *J* = 7.5 Hz, 12H, ArH), 6.66 (t, *J* = 7.3 Hz, 6H, ArH), 6.50 (t, *J* = 7.6 Hz, 12H, ArH), 5.80 (d, *J* = 12.8 Hz, 3H, P(CH_2)P), 3.51 (d, *J* = 13.2 Hz, 3H, P(CH_2)P). ^{13}C NMR (100.56 MHz, C_6D_6) δ 164.00 (Ar), 141.51 (Ar), 135.47 (Ar), 134.47 (Ar), 132.74 (Ar), 129.63 (Ar), 129.30 (Ar), 127.47 (Ar), 121.45 (Ar), 117.40 (Ar), 52.58 (P(CH_2)P). ^{31}P NMR (202.47 MHz, C_6D_6, 298 K) δ -0.31. ^{119}Sn NMR (148.99 MHz, C_6D_6, 298 K) δ -136.00 (p, $^{2}J_{(119Sn/117Sn-31P)}$= 121.4 Hz). Elemental analysis (%) calcd for $C_{93}H_{81}ClNi_3O_3P_6Sn$: C 63.37, H 4.63; found: C 62.91, H 4.91.

4.2.3 $Ni_3(dppm)_3(\mu_3\text{-}Cl)(\mu_3\text{-}Sn(C_3H_5O_3))$ (3)

A 22 mL scintillation vial was charged with **1** (100 mg, 0.062 mmol), glycerol (57.3 mg, 0.622 mmol), 10 ml of THF, and a stir bar. The solution was heated to 40 °C and after 1 h. complete conversion of starting material was observed by ^{31}P{^{1}H} NMR spectroscopy. Volatile compounds were removed *in vacuo* to afford a purple residue. The solid was redissolved in 2 mL of THF and layered with Et_2O at 22°C to afford purple crystalline material. The supernatant was carefully

removed and the solid was washed Et_2O (3 x 5 mL) to help remove any excess glycerol. After the solid was allowed to settle, the supernatant was carefully decanted; residual volatile compounds were removed *in vacuo* to yield **4** as a purple powder (41% yield). Vapor diffusion of diethyl ether into a THF solution of **4** at -20°C afforded X-ray quality crystals. ^{1}H NMR (500.16 MHz, C_6D_6, 298 K) δ 7.65 – 7.45 (m, 24H, ArH), 6.88 – 6.67 (m, 36H, ArH), 5.53 (s, 3H, P(CH_2)P), 5.37 (t, *J* = 7.3 Hz, 1H, OCH), 5.26 (d, *J* = 7.2 Hz, 2H, OCH_2), 5.02 (h, *J* = 0.7 Hz, 2H, OCH_2), 3.73 (d, *J* = 13.1 Hz, 3H, P(CH_2)P). ^{13}C NMR (100.56 MHz, C_6D_6) δ 141.52 (Ar), 135.01 (Ar), 133.52 (Ar) 73.48 (OCH_2), 53.24 (P(CH_2)P). ^{31}P NMR (202.47 MHz, C_6D_6, 298 K) δ 1.78. (Low solubility of **4** after crystallization led to low resolution in ^{13}C NMR and made it so we were not able to obtain ^{119}Sn NMR). Elemental analysis (%) calcd for $C_{78}H_{71}ClNi_3O_3P_6Sn$: C 59.58, H 4.55; found: C 57.36, H 4.04.

4.2.4 X-ray data collection

Single crystal X-ray diffraction studies of **1** was carried out on a Bruker/Nonius Microstar 592 equipped with Cu Kα radiation (λ= 1.54178 Å), while **2** and **3** were carried out on a Bruker 3 circle diffractometer equipped with APEX II CCD detector and Cu Kα radiation. The crystals were mounted on a Cryo-loop with paratone oil and data were collected under a nitrogen gas stream at 100(2) K using f and v scans. The data were integrated using the Bruker SAINT software program and scaled using the SADABS software program. Solution by direct methods (SHELXT[13]) produced a complete phasing model consistent with the proposed structure. All nonhydrogen atoms were refined anisotropically by full-matrix least-squares (SHELXL-2014).[13] For highly disordered diethyl ether and pentane molecules, a solvent mask was used to account for the corresponding electrons as a diffuse contribution to the overall scattering without specific atom positions. To model disordered structures SADI and RIGU commands have been used.

4.3 Results and Discussion

In a previous study, we described the synthesis and reactivity of $[Ni_3(dppm)_3(\mu_3\text{-}Cl)(\mu_3\text{-}SnCl_3]$ [12], which we used as a starting material and treated with varying alkoxide salts to afford the corresponding $(OR)_3Sn$ capped nickel clusters. Treatment of $[Ni_3(dppm)_3(\mu_3\text{-}Cl)(\mu_3\text{-}SnCl_3]$ with 6 eq. KOEt at 40 °C for one hour in THF afforded the $(OEt)_3Sn$-capped cluster (**1**) (Figure 4.1). This reaction was quantitative based on ^{31}P NMR spectroscopy with an isolated yield of 86%. To gauge the reactivity of complex **1** with alcohols, 10 eq. of glycerol was added to complex **1** in THF at 40 °C, which hydrolyzed the ethoxide ligands and liberates ethanol and yields the $(C_3H_8O_3)Sn$-capped cluster (**3**) in 41% yield. In an effort to change the electronic profile of the ligand on tin, 6 eq. NaOPh was added to $[Ni_3(dppm)_3(\mu_3\text{-}Cl)(\mu_3\text{-}SnCl_3]$ in THF generating the $(OPh)_3Sn$-capped cluster (**2**) in 93% yield (Figure 4.1). To elucidate the structural impact of changing the ligands on the tin, complexes **1**, **2**, and **3** were characterized spectroscopically, structurally, and electrochemically.

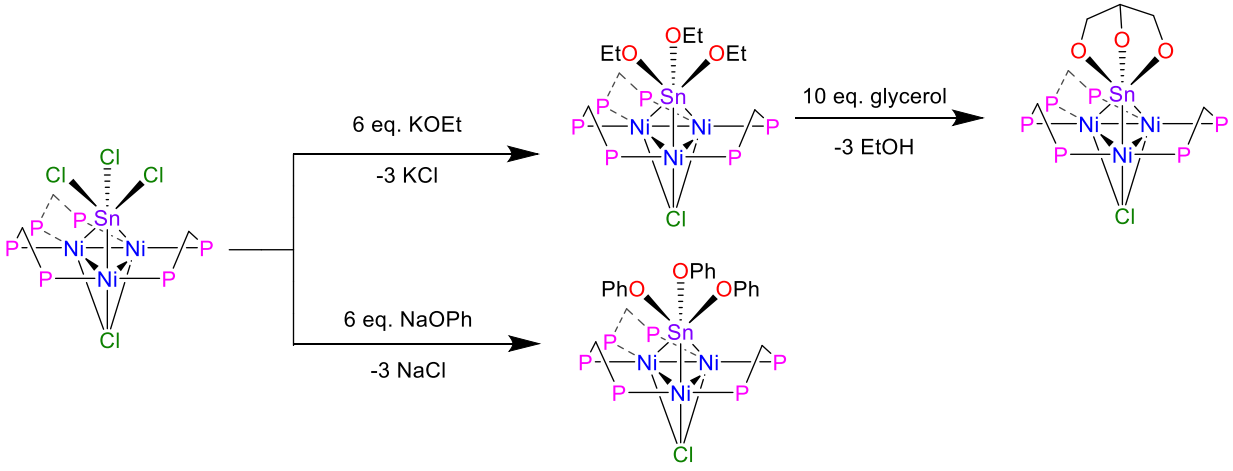

Figure 4.1. Synthesis of complex **1**, **2**, and **3**, where P = PPh_2.

4.3.1 Nuclear Magnetic Resonance (NMR) Spectroscopy

Further details of the molecular and electronic structure were elucidated by ^{31}P, ^{1}H, and ^{119}Sn NMR spectroscopy. The ^{31}P NMR spectroscopy of **1**, **2**, and **3** in benzene-d_6 revealed symmetrical binding of the μ_3-Sn(OR)$_3$ and μ_3-Cl capping groups on the NMR timescale as demonstrated by an isolated sharp singlet resonance centered at -0.54, -0.31 and 1.78 ppm, respectively, flanked by satellites arising from the two-bond coupling of the ^{31}P resonance to $^{119/117}Sn$ (See Appendix C, Figures S3, S6, S9). ^{119}Sn NMR spectroscopy was obtained for complex **1** and **2**. Complex **1** presents a partially resolved septet at -36.41 ppm featuring significant two-bond coupling to the six phosphorus atoms ($^2J_{(119Sn/117Sn-31P)}$ = 110.5 Hz) (Figure 4.2). Complex **2** features a significant downfield ^{119}Sn NMR shift at -136.00 ppm and features a change in the $^2J_{Sn-P}$ ($^2J_{(119Sn/117Sn-31P)}$= 121.4 Hz) (Figure 4.3). Overall, the modest shifts in the ^{31}P spectra and similar $^2J_{Sn-P}$ reveal the modest impact of ligand substitution by alkyl and aryl oxides at the Sn.

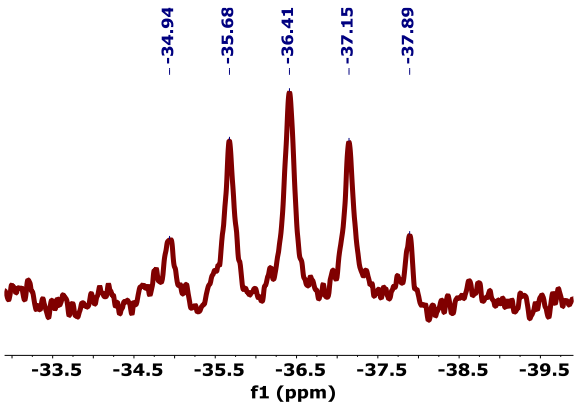

Figure 4.2. ^{119}Sn NMR spectrum of **1** in C_6D_6.

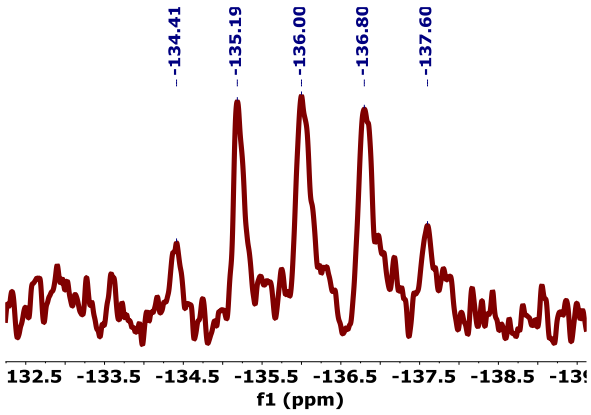

Figure 4.3. ^{119}Sn NMR spectrum of **2** in C_6D_6.

4.3.2. Molecular structure

Layering of pentane over a THF solution of **1** at -20 °C gave dark purple crystals suitable for single crystal X-ray crystallography, crystallizing in trigonal R-3 space group. Vapor diffusion of diethyl ether into a THF solution of **2** and **3** at -20 °C gave dark purple crystals that crystallize in the triclinic space group P-1. **1**, **2**, and **3** revealed a μ_3-Sn atom and a μ_3-Cl atom capping a triangular face consisting of three nickel atoms supported by three bridging diphenylphosphinomethane (dppm) ligands. Single-crystal X-ray diffraction and selected bond distances for complexes **1**, **2**, and **3** are shown in Figs. 4.4, 4.5, and 4.6. In complex **1**, the average Ni-Ni, Sn-Ni, and Cl-Ni, P-Ni bond distance is 2.4444, 2.6305, 2.4093, 2.1935 [Å], respectively. These values shift upon introduction of phenoxide ligands, complex **2**, where the average Ni-Ni and P-Ni bond distance slightly increase (2.4527 and 2.2022 Å). In addition, there is a slight reduction in the average Sn-Ni and Cl-Ni bond distances (2.6126 and 2.3983 Å). In comparison to **1**, the average Ni-Ni, Sn-Ni, P-Ni bond distances slightly decrease in complex **3** (2.4296, 2.5939, 2.1895 Å). Whereas there is a slight increase in the Ni-Cl bond distance in complex **3** (2.4141 Å). The slight bond distance changes between complex **1**, **2** and **3** depict minimal structural differences upon changing the ligands on the tin.

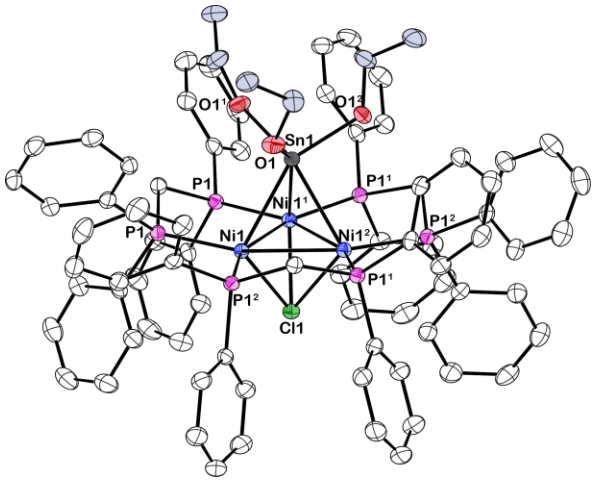

Figure 4.4. Solid-state structure of **1** as determined by single-crystal X-ray diffraction. Thermal ellipsoids were set at the 50% probability level. Carbon bound hydrogens were omitted for clarity.*

*Selected bond lengths [Å] and angles [°]: Sn1-Ni(average) 2.6305, Sn(1)-O(average) 2.0372, Ni(1)-Ni(average) – 2.4444, Cl(1)-Ni(average) 2.4093, Ni-P(average) 2.1935; Ni-Sn-Ni (average) 55.374, Ni-Ni-Ni (average) 60.0, Ni-Cl-Ni (average) 60.97.

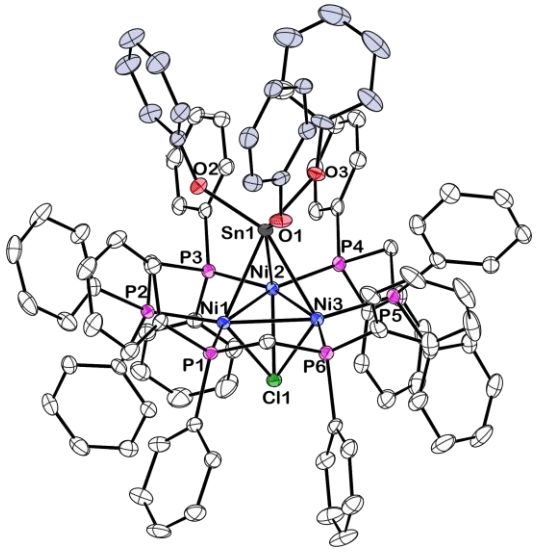

Figure 4.5. Solid-state structure of **2** as determined by single-crystal X-ray diffraction. Thermal ellipsoids were set at the 50% probability level. Carbon bound hydrogens were omitted for clarity.*

* Selected bond lengths [Å] and angles [°]: Sn(1)-Ni(1) 2.5908(3), Sn(1)-Ni(2) 2.6201(3), Sn(1)-Ni(3) 2.6273(3), Sn(1)-O(1) 2.0637(13), Sn(1)-O(2) 2.0649(13), Sn(1)-O(3) 2.0441(13), Ni(1)-Ni(2) 2.4584(4), Ni(1)-Ni(3) 2.4513(4), Ni(2)-Ni(3) 2.4485(4), Cl(1)-Ni(1) 2.3882(5), Cl(1)-Ni(2) 2.4069(5), Cl(1)-Ni(3) 2.3998(5), Ni-P(average) 2.2022; Ni-Sn-Ni (average) 55.987, Ni(3)-Ni(1)-Ni(2) 59.827(12), Ni(3)-Ni(2)-Ni(1) 59.941(12), Ni(1)-Ni(3)-Ni(2) 60.232(12), Ni(1)-Cl(1)-Ni(2) 61.686(14), Ni(1)-Cl(1)-Ni(3) 61.588(14), Ni(3)-Cl(1)-Ni(2) 61.245(14)

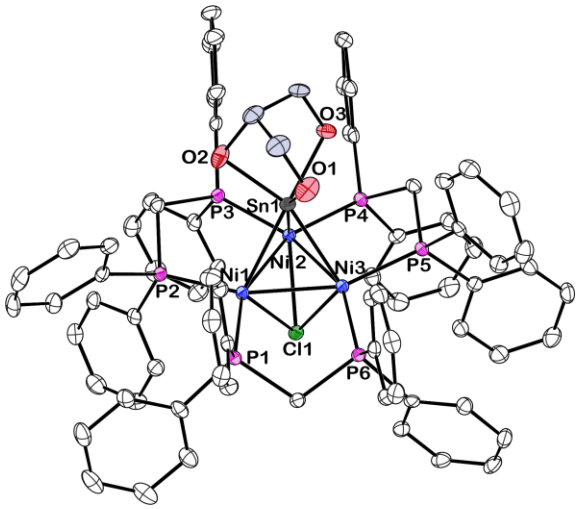

Figure 4.6. Solid-state structure of **3** as determined by single-crystal X-ray diffraction. Thermal ellipsoids were set at the 50% probability level. Carbon bound hydrogens were omitted for clarity.

* Selected bond lengths [Å] and angles [°]: Sn(1)-Ni(1) 2.6065(4), Sn(1)-Ni(2) 2.6032(4), Sn(1)-Ni(3) 2.5720(3), Sn(1)-O(1) 2.0416(16), Sn(1)-O(2) 2.0580(15), Sn(1)-O(3) 2.0645(14), Ni(1)-Ni(2) 2.4312(5), Ni(1)-Ni(3) 2.4304(5), Ni(2)-Ni(3) 2.4273(5), Cl(1)-Ni(1) 2.4029(6), Cl(1)-Ni(2) 2.4504(6), Cl(1)-Ni(3) 2.3891(6), Ni-P(average) 2.1895; Ni-Sn-Ni (average) 55.851, Ni(3)-Ni(1)-Ni(2) 59.905(13), Ni(3)-Ni(2)-Ni(1) 60.032(14), Ni(1)-Ni(3)-Ni(2) 60.063(13), Ni(1)-Cl(1)-Ni(2) 60.114(15), Ni(1)-Cl(1)-Ni(3) 60.953(16), Ni(3)-Cl(1)-Ni(2) 60.191(16).

4.3.3 Electrochemical Studies

A previous study by our group investigated the electronics of the Cl_3Sn capped nickel cluster, $[Ni_3(dppm)_3(\mu_3\text{-}I)(\mu_3\text{-}SnCl_3]$, which presents an unexpected redox feature associated with loss of chloride from tin upon electrochemical reduction, resulting in an irreversible reduction wave. This feature becomes reversible upon addition of excess tetrabutylammonium chloride to the electrochemical cell.[3] To determine whether ligand substitution on the tin changes the electrochemical behavior of these clusters, cyclic voltammograms of complex **1**, **2**, and **3** (Figure 4.7) were obtained. Complex **1** exhibits one reversible oxidation wave at -0.51 V *vs.* $[Cp_2Fe]^{0/+}$ and one reversible reduction wave at -2.21 V *vs.* $[Cp_2Fe]^{0/+}$. A positive shift is seen in complex **3** in both the oxidative and reductive event, which is demonstrated by a reversible oxidation at -0.33 V *vs.* $[Cp_2Fe]^{0/+}$ and reduction at -2.11 V *vs.* $[Cp_2Fe]^{0/+}$. Finally, complex **2**, depicts one reversible oxidation at -0.38 V *vs.* $[Cp_2Fe]^{0/+}$ and a breaking in the reversibility of the reduction event,

demonstrated by one pseudo-reversible reduction event at -2.14, -1.351 V *vs.* $[Cp_2Fe]^{0/+}$. To determine if the pseudo-reversible reduction becomes reversible with excess NaOPh, the electrochemical solution of **2** was charged with 0.5 mmol of NaOPh (100 mM) and this was scanned at varying rates from 50-1000 mV/s, however, this did not increase the reversibility of the pseudo-reversible reduction event, indicating that the dissociation of the phenoxide on tin is quite rapid. Overall, complex **1** and **3** exhibit stable and reversible redox events close to one another, while slight electronic changes occur with complex **2** leading to a pseudo-reversible reduction event, presumably related to phenoxide dissociation. The difference between the reduction and oxidation potentials may be reflective of the change in the donor capability of the ligand on the tin, as phenoxide is a less electronically donating ligand than the alkoxide derivatives thereby potentially leading to changes in the electronics of these structures and a more readily dissociable phenoxide group. This is surprising as there were only slight spectroscopic changes in the ^{1}H, ^{31}P, and ^{119}Sn NMR and minor structural changes in the single crystal XRD of these molecules (Fig 4.2, 4.3, 4.4, 4.5). This study provides evidence that substituting the ligands on tin provides minor electronic impact to clusters of this class.

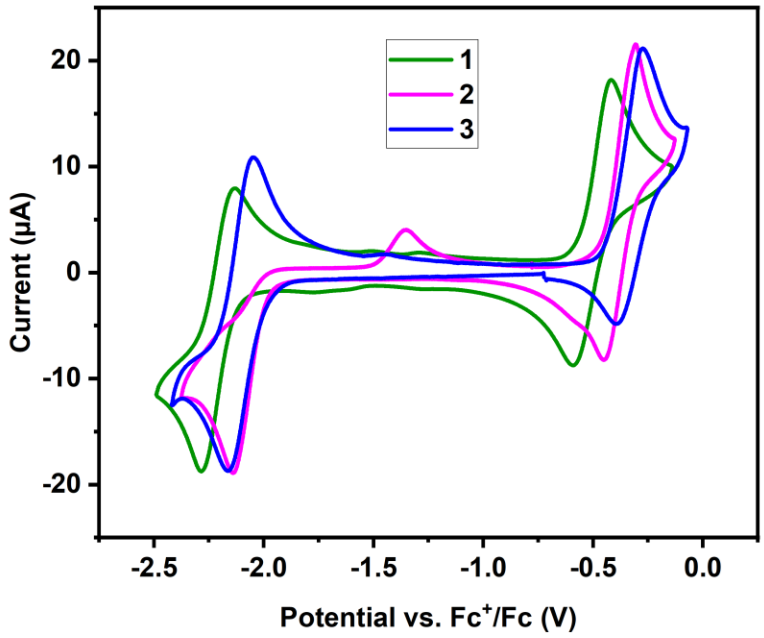

Figure 4.7. Cyclic voltammogram of 2 mM solution of **1**, **2**, and **3** in THF with 0.3 M [$^{n}Bu_4N$][PF_6] supporting electrolyte. Scan rate: 100 mV/s.

4.4 Conclusions

In summary, we have structurally and electronically characterized a new class of $(OR)_3Sn$ capped nickel clusters. Complex **1** and **3** exhibit reversible oxidation and reduction peaks, while complex **2**, shows a slightly different electrochemical response in a pseudo-reversible reduction. Overall, these complexes present similar structural and spectroscopic features as evidenced by NMR and single-crystal XRD studies. Future studies are focused on understanding how the electronics of the trinuclear nickel platform play a role in the reactivity of the ligands on tin at an electrochemical bias.

4.5 Acknowledgements

Chapter 4, in full, is a reprint of the material as it appears in Torquato, N.A.; Lara, J.K.; Bertrand, Q.C.; Mrse, A.A.; Gembicky, M.; Kubiak, C.P. "Electronic structural studies of μ_3-$Sn(OR)_3$ capped trinuclear nickel clusters," *Polyhedron*, 2022, 224, 116000. N.A.T acknowledges

support from NSF for a Graduate Research Fellowship. Research support from the National Science Foundation (CHE-1853908) is gratefully acknowledged. The dissertation author was the primary investigator and author of this paper.

4.6 References

1. Power, P. P., Main-group elements as transition metals. Nature 2010, 463 (7278), 171-177.

2. Somerville, R. J.; Campos, J., Cooperativity in Transition Metal Tetrylene Complexes. Eur. J. Inorg. Chem. 2021, 2021 (34), 3488-3498.

3. Breedlove, B. K.; Fanwick, P. E.; Kubiak, C. P., Tin-Capped Trinuclear Nickel Clusters: Redox Isomerism between μ3-Stannyl and μ3-Stannylene Clusters of the Class [Ni3(dppm)3(μ3-I)(μ3-SnClx)]n+ (x = 2, n = 1; x = 3, n = 0). Inorg. Chem. 2002, 41 (17), 4306-4308.

4. Kuwabara, T.; Guo, J.-D.; Nagase, S.; Sasamori, T.; Tokitoh, N.; Saito, M., Synthesis, Structures, and Electronic Properties of Triple- and Double-Decker Ruthenocenes Incorporated by a Group 14 Metallole Dianion Ligand. J. Am. Chem. Soc. 2014, 136 (37), 13059-13064.

5. Less, R. J.; Wright, D. S., Group 14 Metal–Metal Bonds. In Molecular Metal-Metal Bonds, 2015; pp 485-517.

6. Ferrence, G. M.; Fanwick, P. E.; Kubiak, C. P., A telluride capped trinuclear nickel cluster [Ni3(μ3-Te)2(μ-PPh2CH2PPh2)3]+ with four accessible redox states (n=–1, 0, 1, 2). Chem. Comm. 1996, (13), 1575-1576.

7. Morgenstern, D. A.; Ferrence, G. M.; Washington, J.; Henderson, J. I.; Rosenhein, L.; Heise, J. D.; Fanwick, P. E.; Kubiak, C. P., A Class of Halide-Supported Trinuclear Nickel Clusters [Ni3(μ3-L)(μ3-X)(μ2-dppm)3]n+ (L = I-, Br-, CO, CNR; X = I-, Br-; n = 0, 1; dppm = Ph2PCH2PPh2): Novel Physical Properties and the Fermi Resonance of Symmetric μ3-η1 Bound Isocyanide Ligands. J. Am. Chem. Soc. 1996, 118 (9), 2198-2207.

8. Wittrig, R. E.; Ferrence, G. M.; Washington, J.; Kubiak, C. P., Infrared spectroelectrochemical and electrochemical kinetics studies of the reaction of nickel cluster radicals [Ni3(μ2-dppm)3(μ3-L) (μ3I)]•(L = CNR, R = CH3, i-C3H7, C6H11, CH2C6H5, t-C4H9, 2,6-Me2C6H3; L = CO) with carbon dioxide. Inorganica Chim. Acta 1998, 270 (1), 111-117.

9. Ratliff, K. S.; Lentz, R. E.; Kubiak, C. P., Carbon dioxide chemistry of the trinuclear complex [Ni3(.mu.3-CNMe)(.mu.3-I)(dppm)3][PF6]. Electrocatalytic reduction of carbon dioxide. Organometallics 1992, 11 (6), 1986-1988.

10. Simón-Manso, E.; Gantzel, P.; Kubiak, C. P., Synthesis, molecular structure and electrochemical studies of the bis(diphenylphosphino)amine bridge triangular nickel clusters. Polyhedron 2003, 22 (13), 1641-1644.

11. Morgenstern, D. A.; Wittrig, R. E.; Fanwick, P. E.; Kubiak, C. P., Photoreduction of carbon dioxide to its radical anion by nickel cluster [Ni3(.mu.3-I)2(dppm)3]: formation of two carbon-carbon bonds via addition of carbon dioxide radical anion to cyclohexene. J. Am. Chem. Soc. 1993, 115 (14), 6470-6471.

12. Simón-Manso, E.; Kubiak, C. P., A Trihydroxy Tin Group That Resists Oligomerization in the Trinuclear Nickel Cluster [Ni3(μ-P,P′-PPh2CH2PPh2)3(μ3-L)- (μ3-Sn(OH)3)]. Angew. Chem. Int. Ed. 2005, 44 (7), 1125-1128.

13. Sheldrick, G. M., SHELXT - integrated space-group and crystal-structure determination. Acta Crystallogr. A: Found. Adv. 2015, 71 (Pt 1), 3-8.

4.7 Appendix C

4.7.1 NMR Spectrum

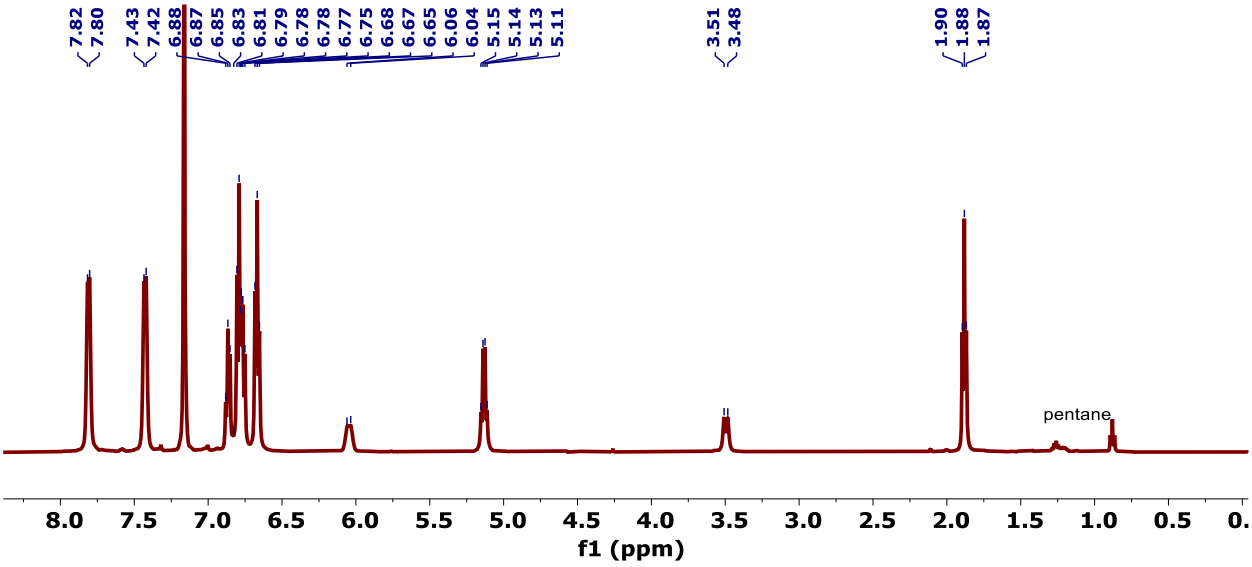

Figure 4.8. ^{1}H NMR spectrum of [$Ni_3(dppm)_3(\mu_3\text{-}Cl)(\mu_3\text{-}Sn(OEt)_3)$] (**1**) in C_6D_6.

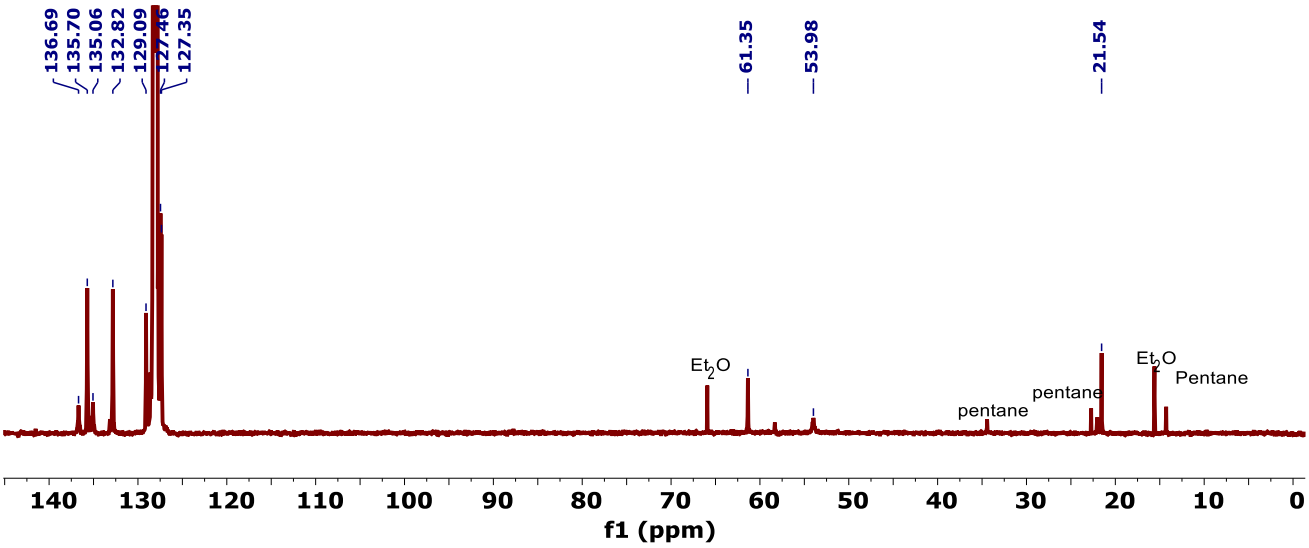

Figure 4.9. ^{13}C NMR spectrum of $[Ni_3(dppm)_3(\mu_3\text{-}Cl)(\mu_3\text{-}Sn(OEt)_3)]$ (**1**) in C_6D_6.

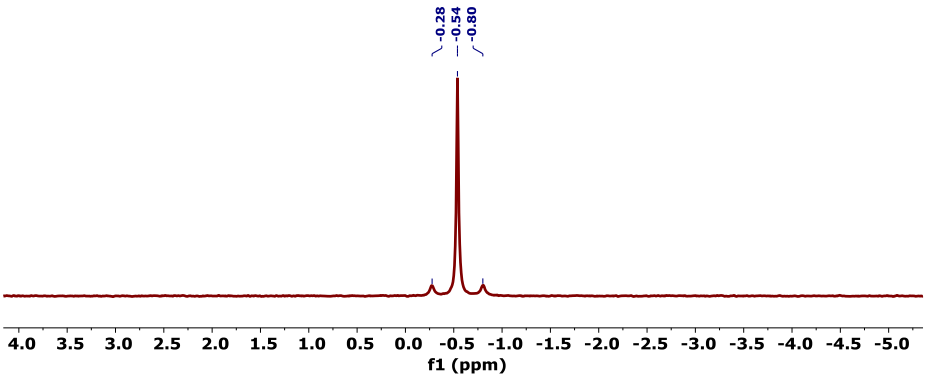

Figure 4.10. ^{31}P NMR Spectrum of $[Ni_3(dppm)_3(\mu_3\text{-}Cl)(\mu_3\text{-}Sn(OEt)_3)]$ (**1**) in C_6D_6.

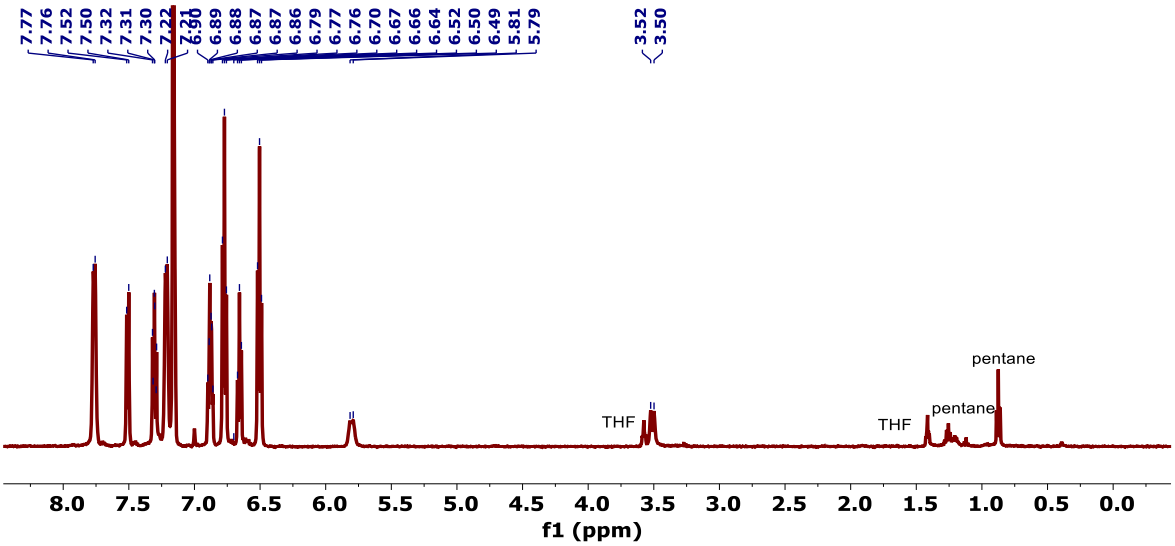

Figure 4.11. ^{1}H NMR spectrum of $[Ni_3(dppm)_3(\mu_3\text{-}Cl)(\mu_3\text{-}Sn(OPh)_3)]$ (**2**) in C_6D_6.

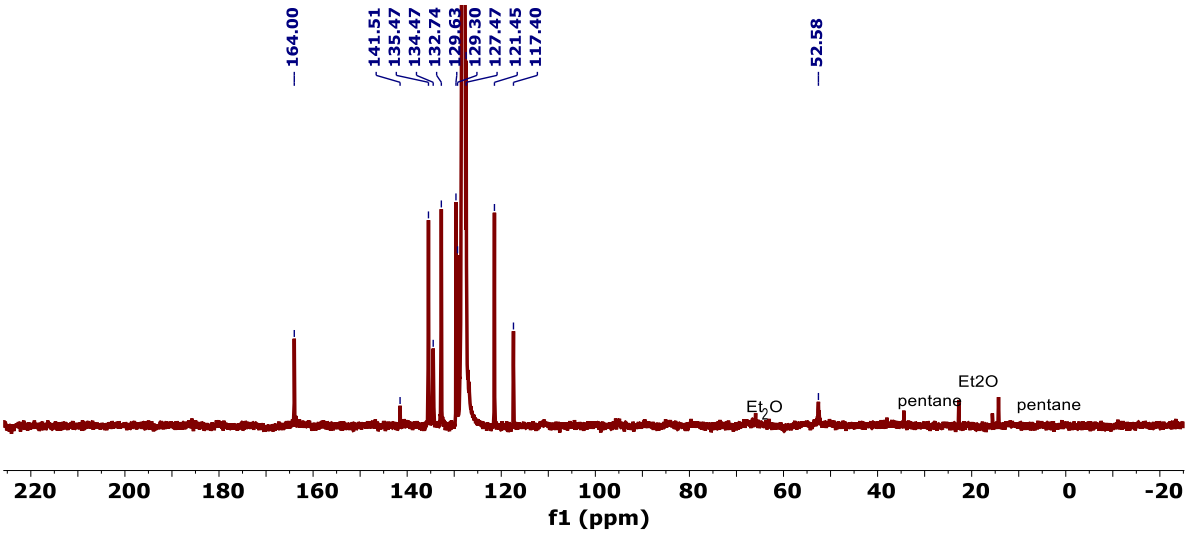

Figure 4.12. ^{13}C NMR spectrum of $[Ni_3(dppm)_3(\mu_3\text{-}Cl)(\mu_3\text{-}Sn(OPh)_3)]$ (**2**) in C_6D_6.

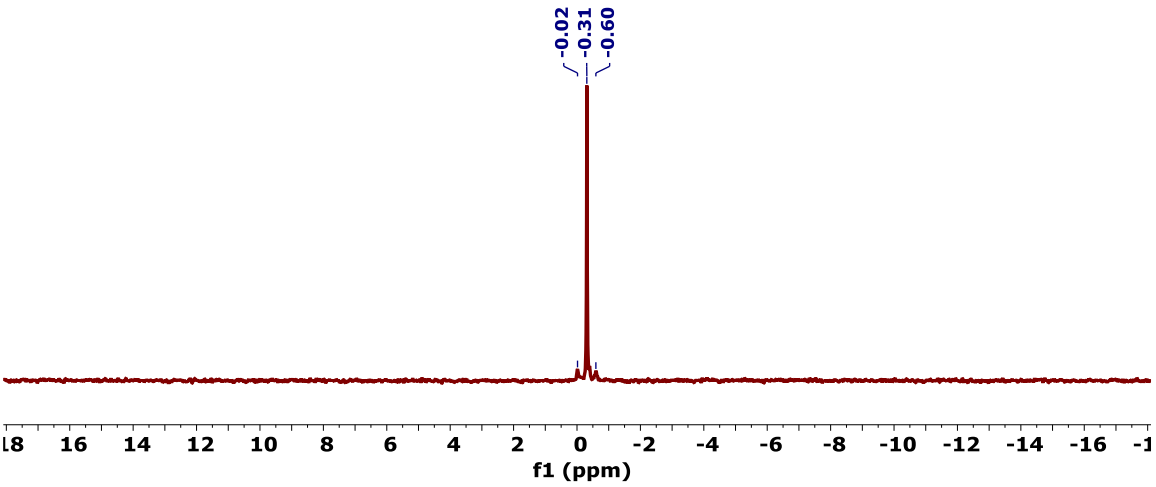

Figure 4.13. ^{31}P NMR spectrum of $[Ni_3(dppm)_3(\mu_3\text{-}Cl)(\mu_3\text{-}Sn(OPh)_3)]$ (**2**) in C_6D_6.

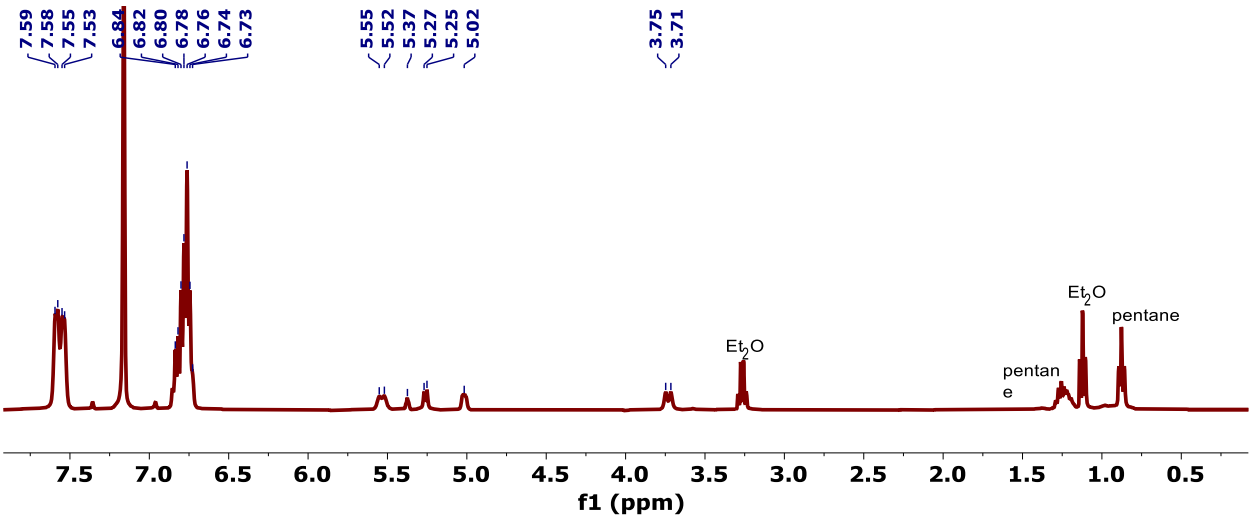

Figure 4.14. ^{1}H NMR spectrum of $[Ni_3(dppm)_3(\mu_3\text{-}Cl)(\mu_3\text{-}Sn(C_3H_5O_3))]$ (**3**) in C_6D_6.

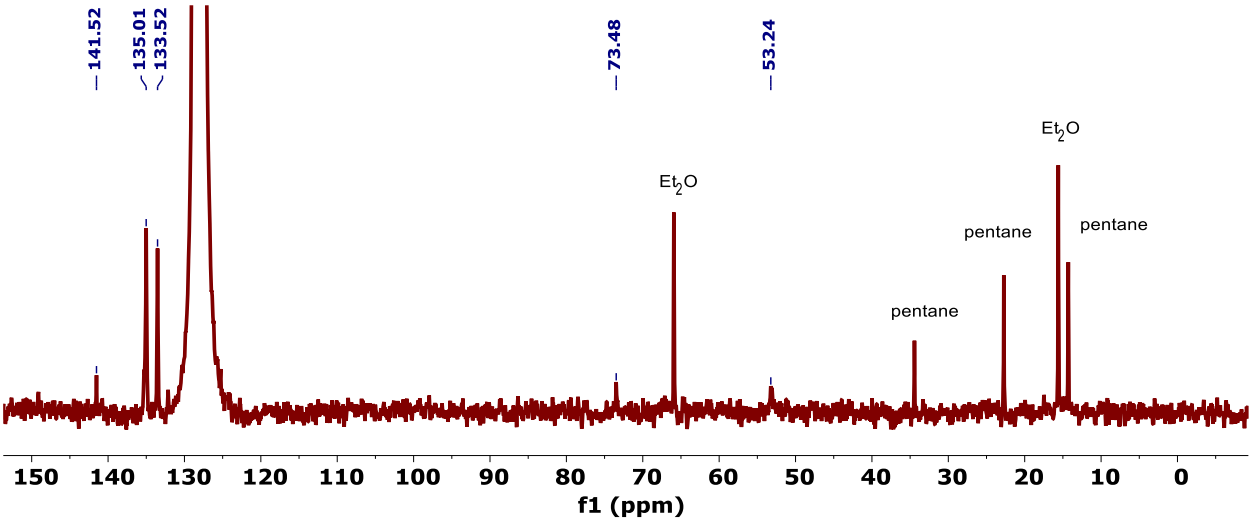

Figure 4.15. ^{13}C NMR spectrum of $[Ni_3(dppm)_3(\mu_3\text{-}Cl)(\mu_3\text{-}Sn(C_3H_5O_3))]$ (**3**) in C_6D_6.

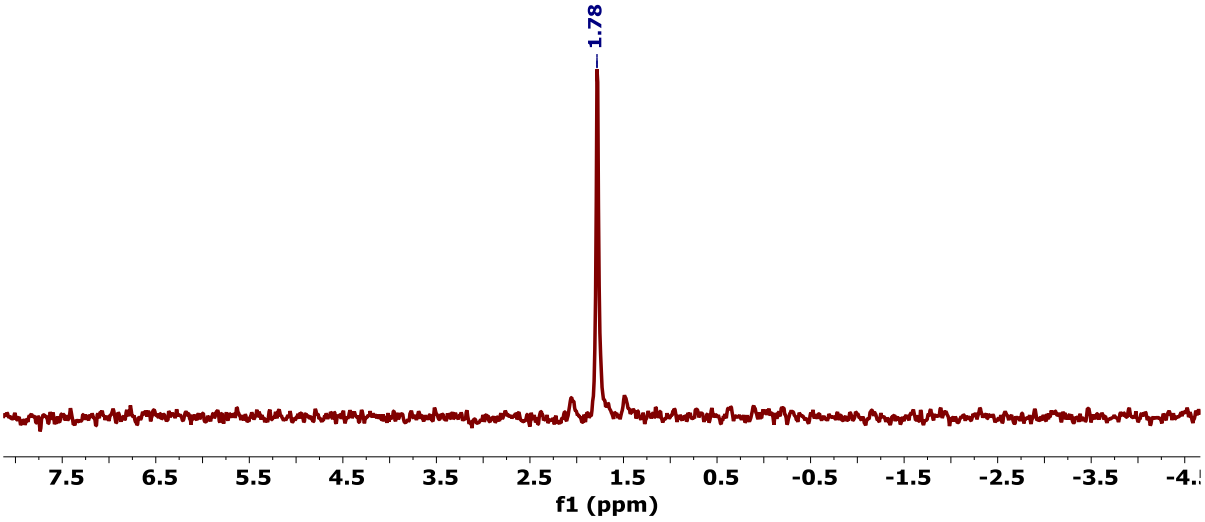

Figure 4.16. ^{31}P NMR spectrum of $[Ni_3(dppm)_3(\mu_3\text{-}Cl)(\mu_3\text{-}Sn(C_3H_5O_3))]$ (**3**) in C_6D_6.

4.7.2 Electrochemical Data

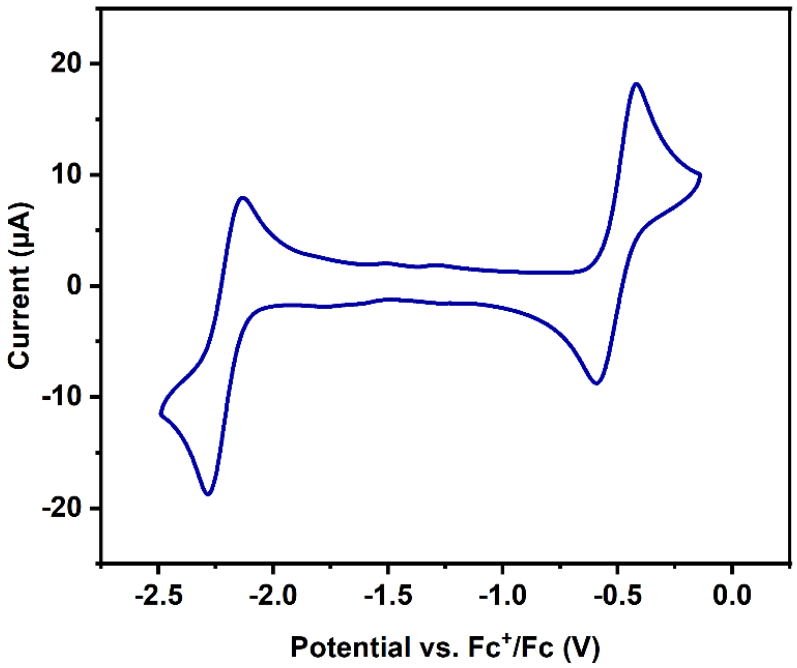

Figure 4.17. Cyclic voltammogram of 2 mM solution of **1** in THF with 0.3 M [$^{n}Bu_4N$][PF_6] supporting electrolyte. Scan rate: 100 mV/s.

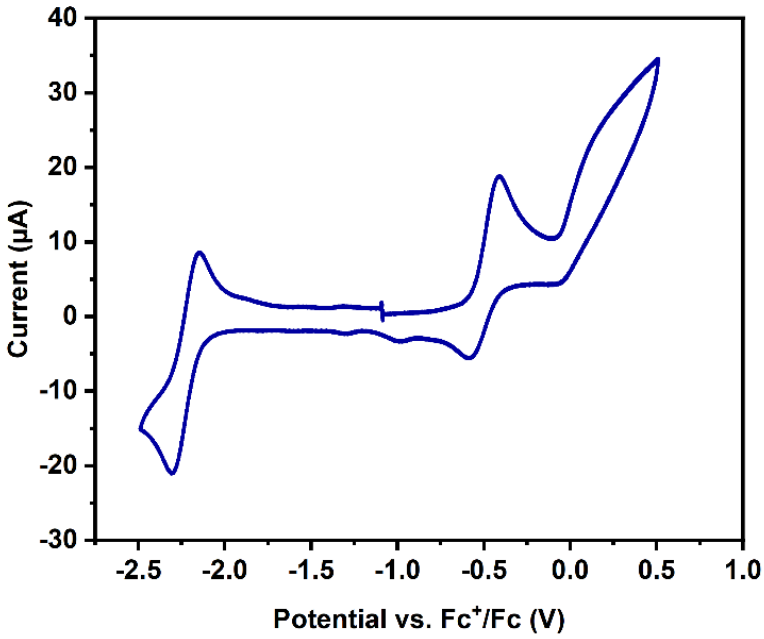

Figure 4.18. Cyclic voltammogram of 2 mM solution of **1** in THF with 0.3 M [$^{n}Bu_4N$][PF_6] supporting electrolyte. Scan rate: 100 mV/s.

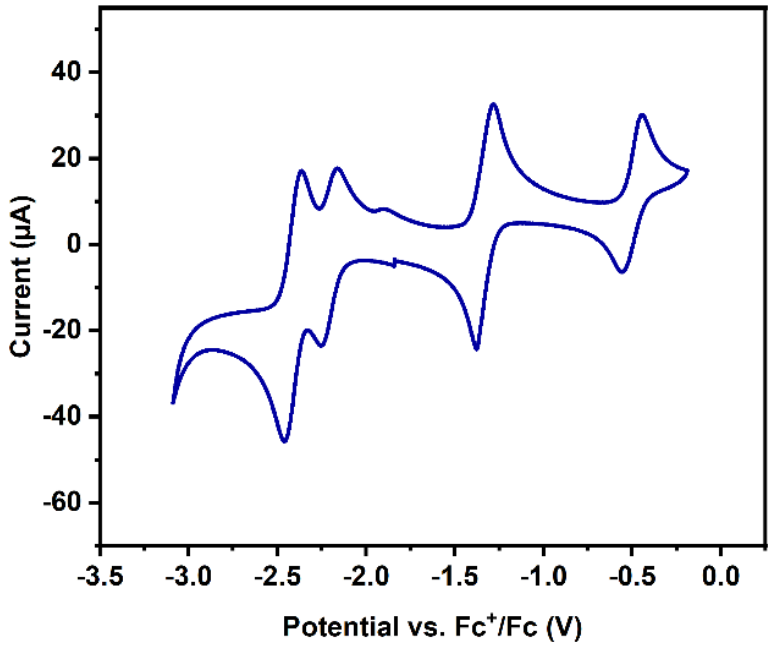

Figure 4.19. Cyclic voltammogram of 2 mM solution of **1** and 1 mM of cobaltocene in tetrahydrofuran with 0.3 M [$^{n}Bu_4N$][PF_6] supporting electrolyte. Scan rate, 100 mV/s.

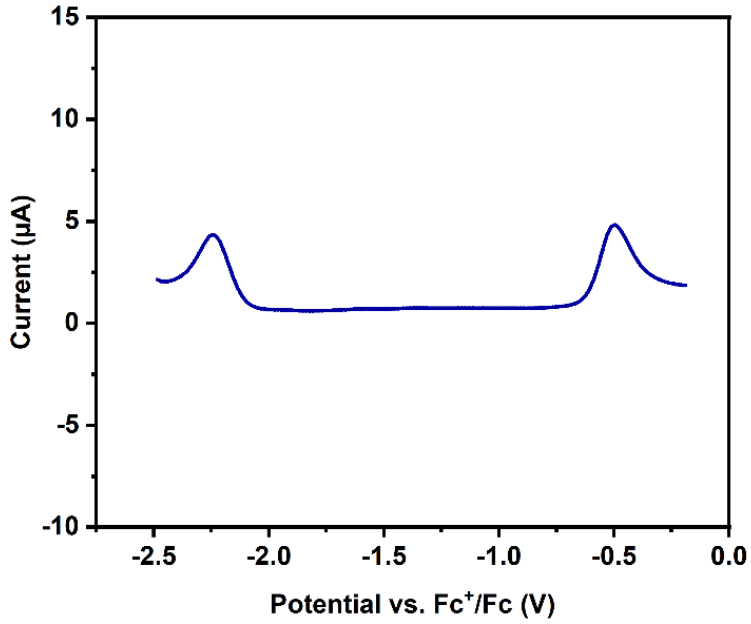

Figure 4.20. Differential pulse voltammogram (DPV) of 2 mM **1** in 0.3 M [^{n}Bu$_4$N][PF$_6$] THF solution. Scan rate: 50 mV/s. Reduction event = 23.6 µC, Oxidation event = 30.98 µC. The area under the curve of the two peaks is a 1:1.3 ratio (left to right).

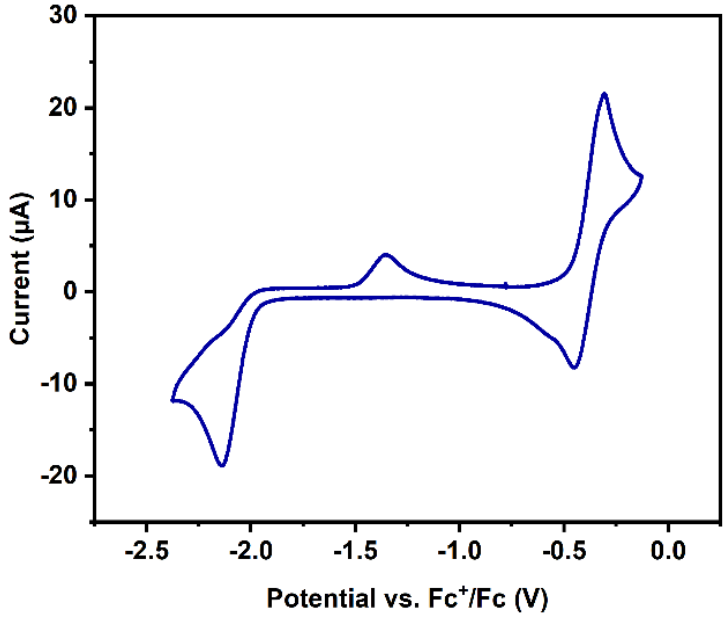

Figure 4.21. Cyclic voltammogram of 2 mM solution of **2** in THF with 0.3 M [^{n}Bu$_4$N][PF$_6$] supporting electrolyte. Scan rate: 100 mV/s.

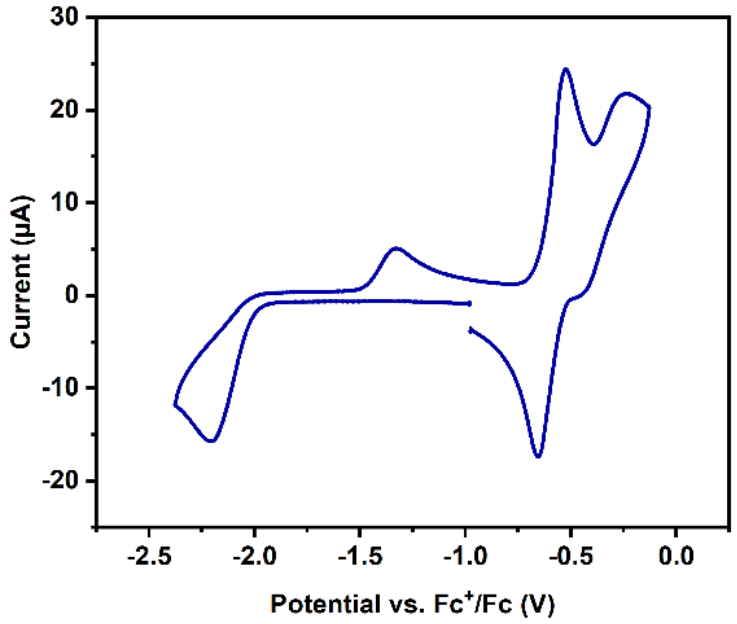

Figure 4.22. Cyclic voltammogram of 2 mM solution of **2** and 1 mM of decamethylferrocenium hexafluorophosphate in tetrahydrofuran with 0.3 M [$^{n}Bu_4N$][PF_6] supporting electrolyte. Scan rate, 100 mV/s.

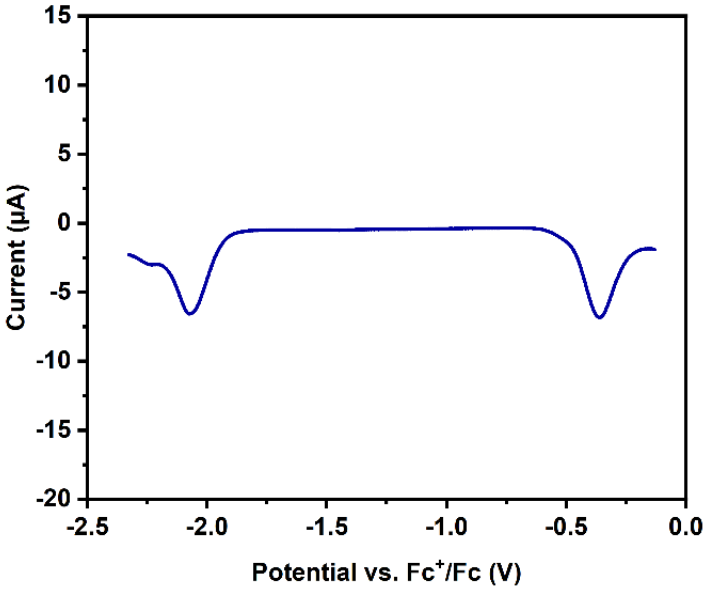

Figure 4.23. Differential pulse voltammogram (DPV) of 2 mM **2** in 0.3 M [$^{n}Bu_4N$][PF_6] THF solution. Scan rate: 50 mV/s. Reduction event = 42.0 µC, Oxidation event = 42.7 µC. The area under the curve of the two peaks is a 1:1 ratio (left to right).

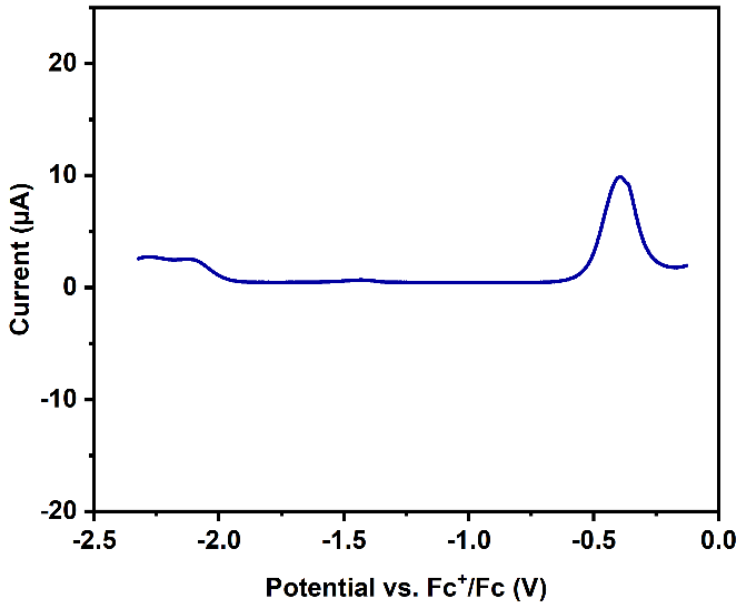

Figure 4.24. Differential pulse voltammogram (DPV) of 2 mM **2** in 0.3 M [^{n}Bu$_4$N][PF$_6$] THF solution. Scan rate: 50 mV/s. Oxidation event = 69.0 µC.

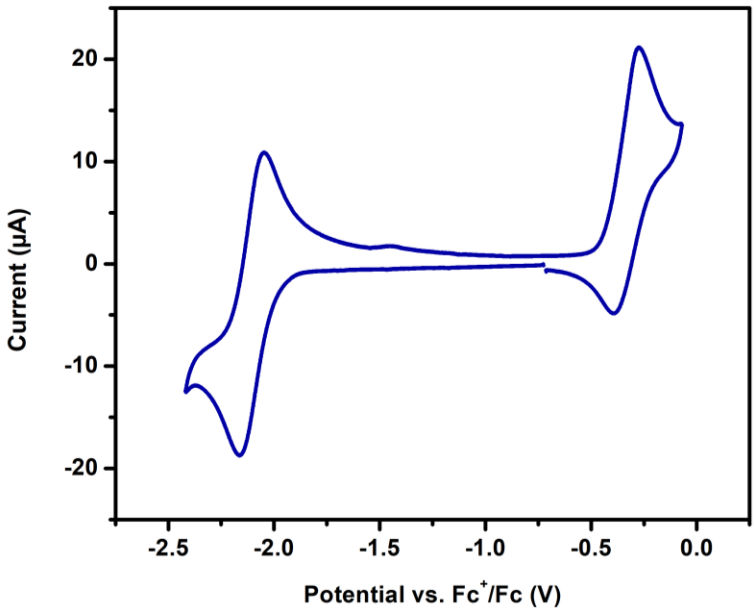

Figure 4.25. Cyclic voltammogram of 2 mM solution of **3** in THF with 0.3 M [^{n}Bu$_4$N][PF$_6$] supporting electrolyte. Scan rate: 100 mV/s.

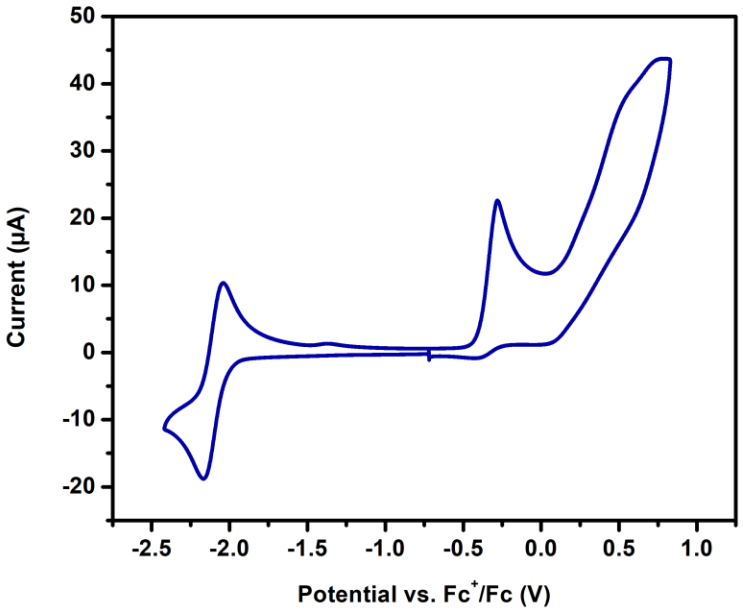

Figure 4.26. Cyclic voltammogram of 1 mM solution of **3** in THF with 0.3 M [$^{n}Bu_4N$][PF_6] supporting electrolyte. Scan rate: 100 mV/s.

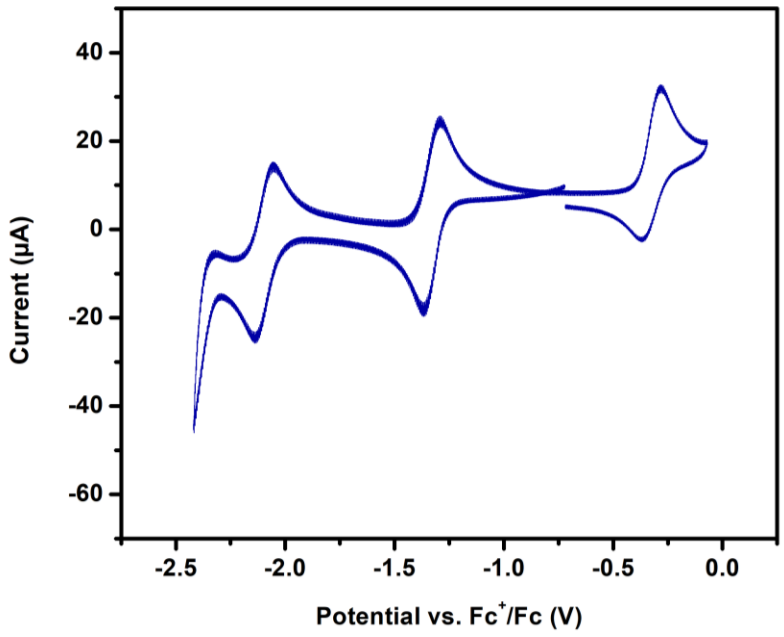

Figure 4.27. Cyclic voltammogram of 2 mM solution of **3** and 1 mM of cobaltocene in tetrahydrofuran with 0.3 M [$^{n}Bu_4N$][PF_6] supporting electrolyte. Scan rate, 100 mV/s.

4.7.3 X-Ray Crystallography

Table 4.1. X-ray Data for $[Ni_3(dppm)_3(\mu_3\text{-}Cl)(\mu_3\text{-}Sn(OEt)_3)]$ (**1**).

Empirical formula	$C_{81}H_{81}ClNi_3O_3P_6Sn$
Formula weight	1618.54
Temperature/K	100.0
Crystal system	trigonal
Space group	R-3
a/Å	21.8460(5)
b/Å	21.8460(5)
c/Å	56.1047(13)
α/°	90
β/°	90
γ/°	120
Volume/Å^3	23188.6(12)
Z	12
ρ_{calc} g/cm^3	1.391
μ/mm^{-1}	5.208
F(000)	9984.0
Crystal size/mm^3	0.05 × 0.05 × 0.05
Radiation	CuKα (λ = 1.54178)
2Θ range for data collection/°	4.724 to 133.41
Index ranges	$-26 \leq h \leq 25$, $-25 \leq k \leq 25$, $-66 \leq l \leq 66$
Reflections collected	69212
Independent reflections	9134 [R_{int} = 0.0510, R_{sigma} = 0.0270]
Data/restraints/parameters	9134/57/644
Goodness-of-fit on F^2	1.019
Final R indexes [I>=2σ (I)]	R_1 = 0.0271, wR_2 = 0.0631
Final R indexes [all data]	R_1 = 0.0360, wR_2 = 0.0664
Largest diff. peak/hole / e Å^{-3}	0.38/-0.44

Table 4.2. X-ray Data for $[Ni_3(dppm)_3(\mu_3\text{-}Cl)(\mu_3\text{-}Sn(OPh)_3)]$ (**2**).

Empirical formula	$C_{93}H_{81}ClNi_3O_3P_6Sn$
Formula weight	1762.66
Temperature/K	100.0
Crystal system	Triclinic
Space group	P-1
a/Å	14.1801(2)
b/Å	14.6922(2)
c/Å	22.0494(3)
α/°	87.4590(10)
β/°	81.5330(10)
γ/°	69.7760(10)
Volume/Å^3	4263.41(11)
Z	2
ρ_{calc} g/cm^3	1.373
μ/mm^{-1}	4.772
F(000)	1808.0
Crystal size/mm^3	0.1 × 0.1 × 0.1
Radiation	CuKα (λ = 1.54184)
2Θ range for data collection/°	4.052 to 136.654
Index ranges	$-17 \leq h \leq 17$, $-17 \leq k \leq 17$, $-26 \leq l \leq 26$
Reflections collected	134779
Independent reflections	15279 [R_{int} = 0.0374, R_{sigma} = 0.0186]
Data/restraints/parameters	15279/6/982
Goodness-of-fit on F^2	1.034
Final R indexes [I>=2σ (I)]	R_1 = 0.0250, wR_2 = 0.0643
Final R indexes [all data]	R_1 = 0.0264, wR_2 = 0.0652
Largest diff. peak/hole / e Å^{-3}	0.77/-0.38

Table 4.3. X-ray Data for $[Ni_3(dppm)_3(\mu_3\text{-}Cl)(\mu_3\text{-}Sn(C_3H_5O_3)]$ (**3**).

Empirical formula	$C_{78}H_{71}ClNi_3O_3P_6Sn$
Formula weight	1572.43
Temperature/K	100.0
Crystal system	Triclinic
Space group	P-1
a/Å	14.0247(3)
b/Å	14.3672(3)
c/Å	20.3825(4)
α/°	100.9720(10)
β/°	100.7590(10)
γ/°	110.6870(10)
Volume/Å^3	3624.93(13)
Z	2
ρ_{calc} g/cm^3	1.441
μ/mm^{-1}	5.538
F(000)	1608.0
Crystal size/mm^3	0.05 × 0.05 × 0.05
Radiation	CuKα (λ = 1.54178)
2Θ range for data collection/°	4.594 to 134.786
Index ranges	$-16 \leq h \leq 16$, $-15 \leq k \leq 16$, $-24 \leq l \leq 24$
Reflections collected	102141
Independent reflections	12565 [R_{int} = 0.0466, R_{sigma} = 0.0271]
Data/restraints/parameters	12565/66/857
Goodness-of-fit on F^2	1.018
Final R indexes [I>=2σ (I)]	R_1 = 0.0249, wR_2 = 0.0579
Final R indexes [all data]	R_1 = 0.0301, wR_2 = 0.0600
Largest diff. peak/hole / e Å^{-3}	0.46/-0.43

CHAPTER 5. Recommendations for Future Work

5.1 Introduction

One of the few downsides to graduating is leaving behind unanswered questions and unfinished ideas. My goal in this chapter is to briefly describe some projects that future researchers may find worthwhile.

5.1.1 Mössbauer Spectroscopy and computational studies of μ3-Sn capped trinuclear Nickel Clusters

To further the characterization and structural understanding of complexes: $[Ni_3(dppm)_3(\mu_3\text{-}Cl)(\mu_3\text{-}SnCl_3)]$, $[Ni_3(dppm)_3(\mu_3\text{-}H)(\mu_3\text{-}SnH)]$, $[Ni_3(dppm)_3(\mu_3\text{-}I)(\mu_3\text{-}Sn(CH_2CH_3)]$, $[Ni_3(dppm)_3(\mu_3H)(\mu_3\text{-}Sn(C_6H_{11})]$, $[Ni_3(dppm)_3(\mu_3\text{-}H)(\mu_3\text{-}Sn((Br)(H)(CH_2CH_3))]$, computation studies and attempts at obtaining Mössbauer spectroscopy are underway.[1] Through a colloboration with a tin Mössbauer spectroscopy group at University of Münster we have preliminary results that $[Ni_3(dppm)_3(\mu_3\text{-}H)(\mu_3\text{-}SnH)]$ is a formally tin (II) species, this matches with our characterization and experimental data from past reasearch. It is my hope that future generations will continue the work with Mössbauer spectroscopy for the rest of the series to further the structural and electronic understanding of these species. DFT calculations were also used to model the electronic structure of these complexes.

5.1.2 Hydrogen activation and redox chemistry of a μ3-SnEt capped trinuclear Nickel Cluster

Unfinished reactivity studies describe the H_2 activation by the μ_3-SnEt capped trinuclear nickel cluster, $[Ni_3(dppm)_3(\mu_3\text{-}I)(\mu_3\text{-}Sn(CH_2CH_3)]$, **4** (Figure 5.1). Preliminary results depict that upon addition of 4 atm H_2 to a benzene solution of **4**, complex **4** activates H_2 to form a new species and the starting material, **4**, in a 1.3:1 ratio. Upon removal of H_2 via freeze-pump-thaw and addition of N_2, the new species releases hydrogen and reforms complex **4**. It is my hope that a future

researcher may follow up on these studies to further understand the reaction product formed, reaction dynamics of this process, and elucidate a mechanism.

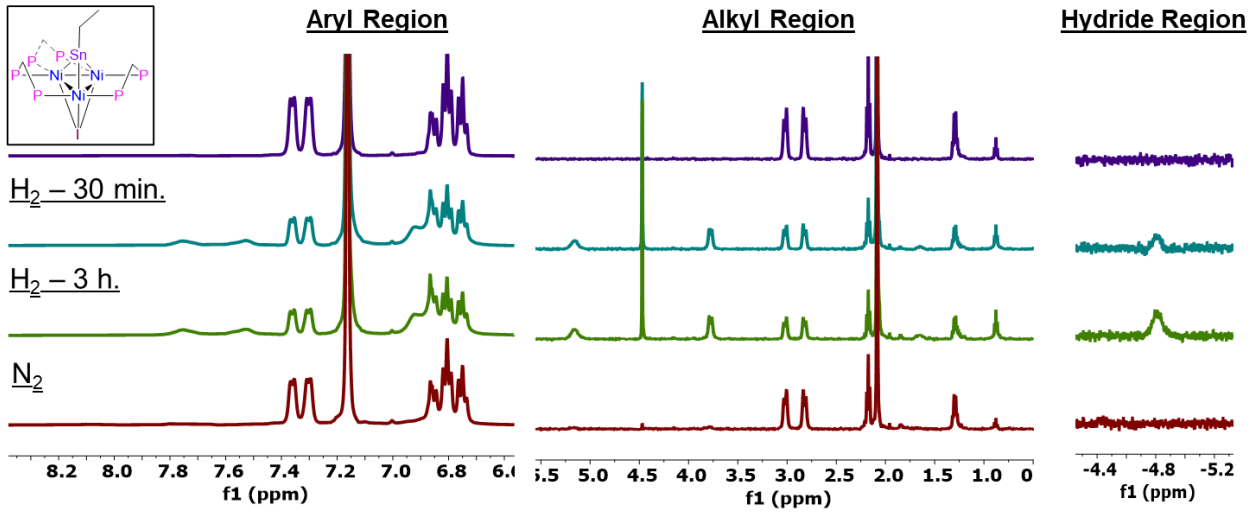

Figure 5.1. ^{1}H NMR spectra of **1** in benzene-d_6 (purple), **1** with 4 atm H_2 - 30 min. timepoint (blue), **1** with 4 atm H_2 – 3 hr. timepoint (green), **1** with 4 atm removed and N_2 reintroducted (red).

In addition, to further depict the interplay between the reactivity and electronics of complex **4**, obtaining cyclic voltammetry of this species and isolating chemical oxidation and reduction products would be of interest. Tin complexes are known for their ability to abstract halides from a variety of reagents. Therefore, care must be taken in choosing the right chemical oxidant as PF_6^- and BF_4^- can sometimes lose F atoms to these tin species. The addition of 2 eq. ferrocenium tetrakis[3,5-bis(trifluoromethyl)phenyl]borate, FcBARF, to **4** resulted in a clean ^{1}H NMR spectrum, presumably of the oxidized species, however, crystallization of the product has been elusive thus far. The reactivity profile of **4**, is relatively unknown therefore addition of a variety of small molecules to further understand the reactivity profile of the cluster coordinated stannylyne species is of interest. Preliminary work in this area has demonstrated activation of 1-hexyne, resulting in a μ_3-SnEt(I), μ_3-hexene capped trinuclear nickel cluster (Figure 5.2, 5.3). It is my hope that these studies will be expanded to other small molecules to further the reactivity profile of complexes of this class.

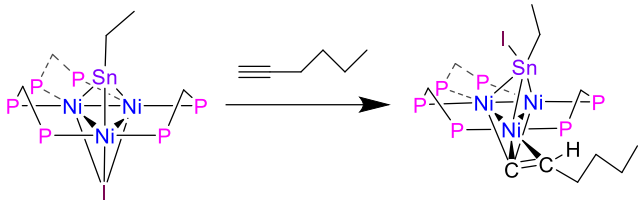

Figure 5.2. Addition of 1-hexyne to [$Ni_3(dppm)_3(\mu_3\text{-}I)(\mu_3\text{-}Sn(CH_2CH_3)$].

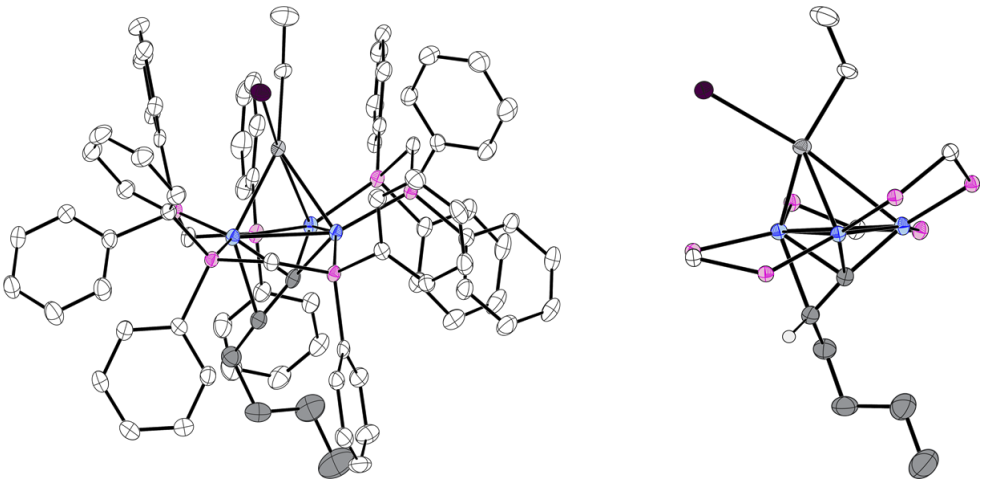

Figure 5.3. Single-crystal X-ray diffraction of a μ3-SnEt(I), μ3-hexene capped trinuclear nickel cluster. Right figure has dppm ligands removed for clarity.

5.1.3 Extending the series to other main group elements

Expanding these studies to other main group elements may allow for new modes of reactivity based on the sterics and electronics of the trinuclear nickel core. Preliminary work has demonstrated the synthesis of a $GeCl_2$ capped trinuclear nickel cluster, through the addition of 10 eq. $GeCl_2$*dioxane to the [$Ni_3(dppm)_3(\mu_3\text{-}I)_2$]. Similar synthetic methods utilizing an $SiCl_2$ precursor may allow for the isolation of an analogous $SiCl_2$ or $SiCl_3$ capped species. This would be of interest as cluster species coordinated to group 14 moieties are relatively unknown thereby providing a relatively unexplored avenue to expand the structural and reaction chemistry of tin.

5.1.4 Miscellaneous Crystal Structures

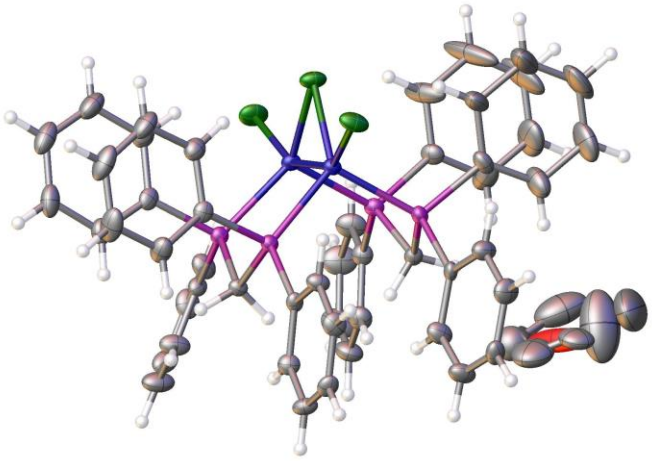

Figure 5.4. Notebook Code NAT-01-013, instrument Artemis labeled KUB_NAT_01_013, see crystallography notebook for more details. Blue is Nickel, Green is Chlorine, Pink is Phosphorous, Red is Oxygen.

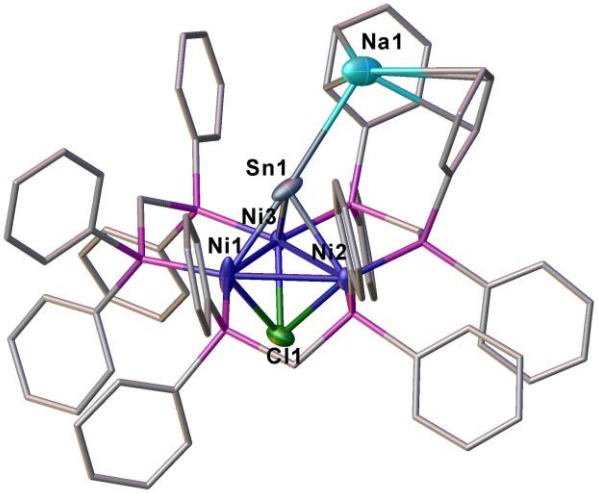

Figure 5.5. Notebook Code NAT-01-090, instrument Artemis labeled KUB_NAT01091_benzene_c5, see crystallography notebook for more details. Pink is Phosphorous.

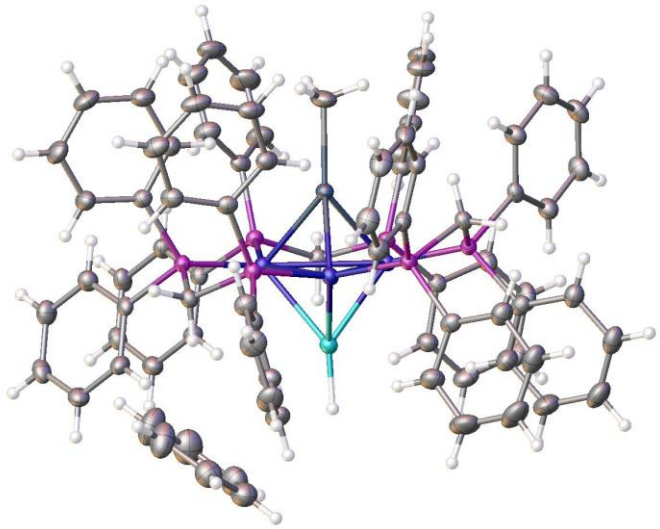

Figure 5.6. Notebook Code NAT-01-204c, instrument Artemis labeled KUB_NAT01204c, see crystallography notebook for more details. Light blue is Aluminum, dark blue is Nickel, dark gray is tin., Pink is Phosphorous.

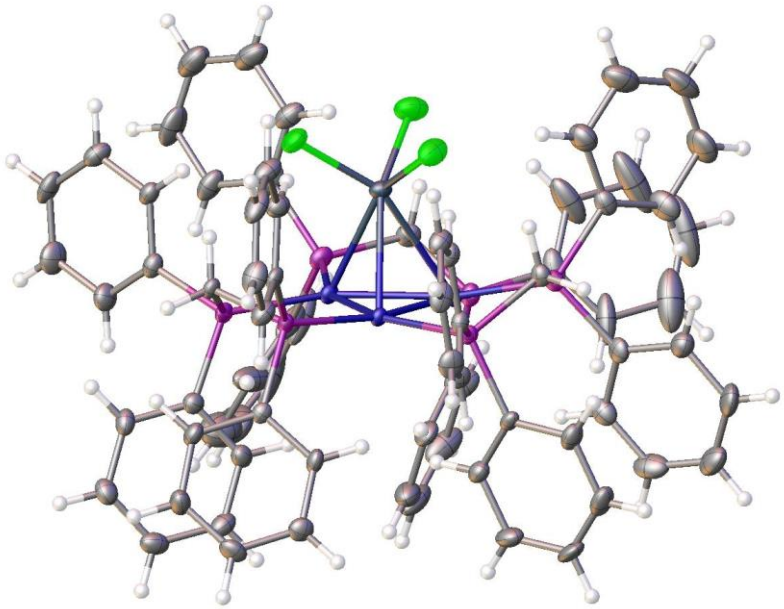

Figure 5.7. Notebook Code NAT-01-163, instrument Artemis labeled KUB_NAT01165, see crystallography notebook for more details. Bright green is fluorine, dark blue nickel, Phosphorous is pink, dark gray is tin.

5.2 Conclusions

Future project directions related to main group capped metal clusters are reported here. This remains a relatively unexplored area of research that may provide new insights on the cooperatively of bonding and reactivity between the main group elements and polynuclear transition metal complexes.

5.3 References

1. Torquato, N.A.; Palasz, J.M.; Bertrand, Q.C.; Brunner, F.M.; Chan, T; Gembicky, M.; Mrse, A.A.; Kubiak, C.P. Synthesis, structure and reactivity of μ_3-SnH capped trinuclear nickel cluster, *Chem. Sci.*, **2022**, 13, 11382-11387.